POLITECNICO DI MILANO
DEPARTMENT OF ENERGY ENGINEERING
MASTER PROGRAMME IN ENERGY FOR DEVELOPMENT

FORMULA SAE ELECTRIC: DESIGN OF A RESONANT CONVERTER FOR THE REGENERATIVE BRAKING SYSTEM APPLIED TO AN ULTRACAPS-BASED STORAGE

Master Thesis of:
Giacomo Moretti
872816

Supervisor:
Prof. Dolara Alberto

Co-supervisor:
Prof. Leva Sonia
Prof. Yales Romulo de Novaes

2019

A tutta la mia famiglia per il costante e incondizionato supporto.
A Erika per l'amore e la pazienza impareggiabili.
A tutti i miei amici, vicini e lontani, per l'immancabile affetto.
Ai professori che hanno reso possibile questa tesi.

Ao Prof. Yales Rômulo De Novaes pela inestimável oportunidade, pela imensa disponibilidade e dedicação.
Ao grupo do NPEE por sua constante ajuda e grande amizade.
A todos os meus amigos brasileiros por me proporcionarem os seis melhores meses da minha vida universitária.

This thesis was developed at the power electronics laboratory (NPEE) of the *Universidade do Estato de Santa Catarina - UDESC* (Brazil), as part of the exchange program - *bilateral agreement extra UE* -, in collaboration with the department of Energy Engineering of *Politecnico di Milano*.

Extended Summary

FORMULA SAE ELECTRIC: DESIGN OF A RESONANT CONVERTER FOR A REGENERATIVE BRAKING SYSTEM APPLIED TO AN ULTRACAPS-BASED STORAGE.

Abstract - **The electric mobility can represent the game changer technology for a long term sustainability of the transportation sector. Pursuing this objective, a model to simulate an electric vehicle (EV) for Formula SAE electric competition is created. All the systems of the EV and the hybrid storage of Li-ion batteries and ultra-capacitors are implemented. The kinetic energy of the regenerative braking is differently accumulated inside the storage systems through the Kinetic Energy Recovery System (KERS).**

A bidirectional DC-DC resonant converter, is applied to the KERS to manage the UC pack. The topological states are theoretically analyzed. The operational limits, keeping the soft-switching properties, are discussed and the results show the capability of the converter to operate under resonant mode in both boost and buck mode. The drawback is the presence of high current peaks in the resonant inductor. The use of more than one converter in interleaving and the adoption of a capability factor ensure the proper operability of the system.

Key-words: resonant converter, ultra-caps, regenerative braking, formula SAE electric, electric vehicle.

I. INTRODUCTION

Today, the awareness of environmental and climatic problems is gaining its way into social and political life. The challenge is to understand the complexity and to find the tools to face the sustainability, affordability and reliability problems of development [1]:
every human activity pays a cost in terms of environmental impact: the whole transportation sector accounts for the 20.44% of the global CO_2 emissions according to The World Bank [2] and to one fourth according to IEA (International Energy Agency) emission statistics [3].The rise of the global interest in this electric challenge is pushing the traditional automotive industry to develop the required technology. It is in this scenario that in 2013 borned, from the well known *SAE International*, the *Formula SAE Electric*.
The competition is made by static tests such as presentation, cost and design as well as by dynamic tests that

are acceleration, skip pad, autocross, efficiency and endurance.
This work presents the sizing and simulation phase. The main topics are:

- create a model of the whole vehicle linking together all the mechanical, electrical, traction, braking and storage systems (chap.2);
- deepen the efforts in the study of a resonant converter applied to the KERS to manage the energy stored in the ultracaps (UC) pack.

The limits of the resonant converter technology (high efficiency converters [12] [13]) to exploit the peculiarities of the UC are investigated. Once that the operational frontiers are set, the resonant converter configuration is adapted to the EV project considering all the converter, inverter and UC pack constraints. Then, according to that foundings, a capability factor and an interleaved solution is studied in order to ensure the proper operability of the system.

II. ELECTRIC VEHICLE MODEL

The main objective of the model is to compute, at each time step ($\triangle t$), the Power, the Voltage and the Current at the KERS output in order to correctly project and size the power converter.
The electrical connections [12] are supposed to be as in Fig.(1).

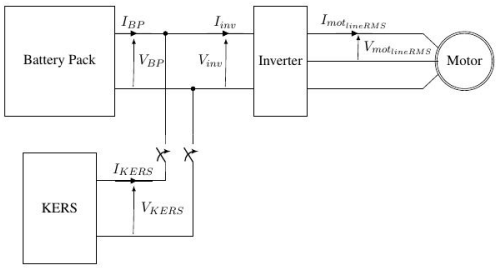

Figure 1: *Concept scheme*

Then, to organize the model, one "block" for each sub-system of the vehicle is created.
Starting from a given speed profile, the "pilot" block controls the acceleration deceleration sending signal to the motor / braking system. Through the "mechanical drivetrain" block, it arrives to the "dynamics" block where the driving variable such as acceleration (a), speed (v) and position (x) are computed. When braking is needed to slow down the EV, the signal makes the "braking system" block calculate the available regenerative energy.

Model Implementation

The model is implemented using power equations [6] [8] to relate the subsystems and regulate the driving simulation.

Drive Cycle block
The block produces a speed profile, as used in many automotive applications. It outputs displacement, velocity and acceleration, all in SI units. The drive-cycle chosen for the simulation is the "$WLTP\ class3$", reported in Fig.(2), because of the fast variability of the speed which is ideal to simulate the prototype.

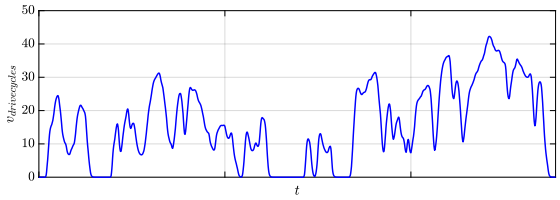

Figure 2: *Input speed profile*

"Pilot" block
In the following graph (3), the action taken by the "pilot" is shown. A PID controller compares the input speed generated by the block above with the actual speed of the vehicle and releases an acceleration/ braking signal proportional to the relative difference of the inputs.

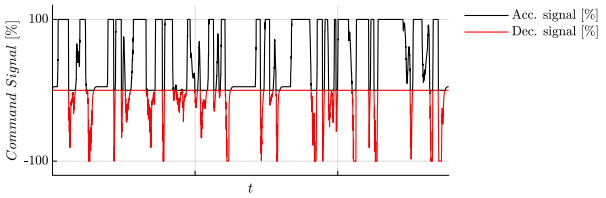

Figure 3: *Acceleration/deceleration signal intensity*

Motor block
This "motor" block uses the speed of the vehicle to deliver the allowed torque τ_{mot} to the mechanical drivetrain block.

Braking block
The block takes the braking signal, compares it with the maximum regenerative torque ($\tau_{reg_{max}}$) and computes:

- The allowed regenerative braking torque (τ_{reg});

- The additional friction braking ($\tau_{friction}$) required to properly slow down the vehicle.

Mechanical drivetrain block

This block collects the inputs from the motor, braking and "pilot" blocks and computes the power available for the traction.

The net torque to the motor is computed as:

$$\tau_{mot_{net}} = \tau_{mot} - \tau_{friction} - \tau_{reg_{braking}} \tag{1}$$

In Fig.(4) reported below, the different components of the torque at the vehicle shaft for direct (motor traction) and reverse operations (braking phase) are displayed:

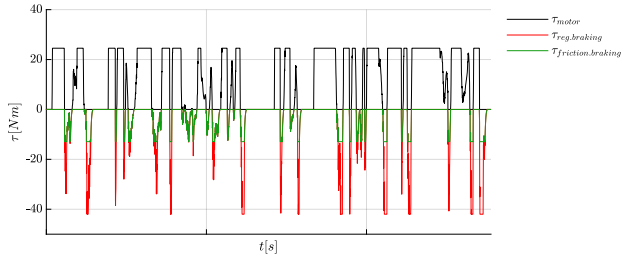

Figure 4: *Net tourque components*

Dynamics block

The power balance equation of the vehicle is implemented.

The angular acceleration ($\dot{\omega_m}$), the angular speed (ω_m) as well as the linear acceleration (a), the linear speed (v) and the position (x) per each time step are computed [6] [8]. The analysis is theoretically based and implemented in 2D. The objective is to obtain the motion equation.

The study starts from the power balance of the EV:

$$P_{motor} + P_{resistant} + P_{losses} = 0 \tag{2}$$

So:

$$\begin{aligned} P_{motor} &= \tau_m \cdot \omega_m - J_m \dot{\omega_m} \cdot \omega_m \\ P_{resistant} &= -Mgsin(\alpha) \cdot v - \tau_{res} \cdot \omega_w \\ &\quad - \frac{1}{2}\rho_{air} S_{frontal} C_D v^3 - J_r^* \dot{\omega_m} \cdot \omega_m \\ P_{losses} &= -(1-\eta)\tau_m \cdot \omega_m \end{aligned} \tag{3}$$

The inertial terms can be obtained looking for the first order derivative of the kinetics energy for both motor and user side:

$$\begin{aligned} \frac{\mathrm{d}\, E_{k_{mot}}}{\mathrm{d}\, t} &= \frac{\mathrm{d}}{\mathrm{d}\, t}\left(\frac{1}{2} J_m \omega_m^2\right) = J_m \dot{\omega_m} \cdot \omega_m \\ \frac{\mathrm{d}\, E_{k_{user}}}{\mathrm{d}\, t} &= \frac{\mathrm{d}}{\mathrm{d}\, t}\left(\frac{1}{2} J_w \omega_w^2 \cdot 4 + \frac{1}{2} M v^2\right) \\ &= \left(J_w + M R_w^2\right) tr^2 \dot{\omega_m} \omega_m \\ &= J_r^* tr^2 \dot{\omega_m} \omega_m \end{aligned}$$

The relation $v = \omega_w R_w = R_w \cdot tr \cdot \omega_m$ is used to find the motor angular speed. The second power eq.(3) can be better represented by substituting the following relations:

$$\tau_{res} = N_{4w} f_d R_w \qquad N_{4w} = Mgcos(\alpha) \tag{4}$$

The third power eq.(3) represents the power losses of the system. By substituting eq.(4) into eq.(3) and finally in eq.(2), the equation of motion is found:

$$\begin{aligned} \eta(\tau_m - J_m \dot{\omega_m})\omega_m = \\ Mg[f_d cos(\alpha) + sen(\alpha)]R_w \cdot tr \cdot \omega_m \\ +1/2 \rho_{air} S_{frontal} C_D \omega_m^3 R_w^3 tr^3 \\ +J_r^* \dot{\omega_m} \omega_m tr^2 \end{aligned} \tag{5}$$

The term before the equal represents the power at the motor side discounted by the motor inertia. The terms after the equal show respectively:

- Rolling and grading resistance;
- Aerodynamic drag;
- Inertial resistance.

So, from the eq.(5), the angular acceleration is found as well as the linear speed as shown in Fig.(5) with respect to the drive-cycle speed:

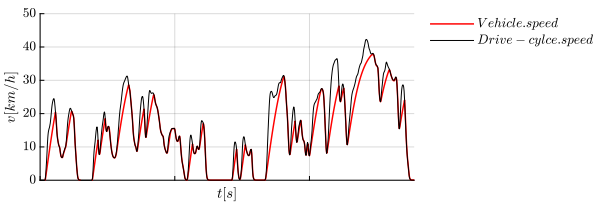

Figure 5: *Vehicle speed profile vs drive-cycle speed*

Inverter and Storage Management block

The block receives the required power as input. It computes the power at the inverter DC side through:

$$P_{inv} = \eta_{inv} P_{motor} \tag{6}$$

Dividing this value for the voltage of the battery pack (V_{BP}), the total required current (I_{tot}) is found. At this point, depending on the direct or reverse operation, an output signal is created to control the KERS. The current required from/delivered to the battery pack is calculated as the total current (I_{tot}) discounted by the KERS current (I_{KERS}).

Going through the inverter analysis, the voltage and current at the DC side are expressed as:

$$V_{inv_{DC}} = \frac{2\sqrt{2}}{\sqrt{3}} \frac{V_{mot_{NOM}}}{M_i} \qquad I_{inv_{DC}} = \frac{P_{mot}}{V_{inv_{DC}}} \eta_{inv} \tag{7}$$

Battery Pack block
This block receives the current (I_{BP}) as input , it computes the State of Charge (SOC) and the respective voltage (V_{BP}) per each time step $(\triangle t)$. It presents also a backstop function for the model below a certain level of SOC or V_{BP}, due to operational limit and technology durability. The implementation of the single cell is performed with a physical based approach. Assuming all the needed hypothesis [9], the Butler-Volmer equation, that correlate the current with the positive and the negative metal potential ($\phi = E + \eta$), can be written for the anode (negative electrode), for the cathode (positive electrode) and for the electrolyte:

$$i = n_s F \left(k_o a_o^{v_o} \exp \frac{\beta_o F(E+\eta)}{RT} - k_r a_r^{v_r} \exp \frac{-\beta_r F(E+\eta)}{RT} \right) \quad (8)$$

The overall cell voltage V_{cell} can be now written as:

$$V_{cell} = E^+ + \eta^+ - E^- - \eta^- - \eta_{el} \quad (9)$$

The BP works as the main storage source of the vehicle. The lay-out is derived from the voltage (V_{inv}) and from current (I_{inv}) requirements at the inverted DC side.
The number of cells in series (n_s) and the number of strings in parallel $(n_{//})$ are defined as:

$$n_s = \frac{V_{inv}}{V_{cell}} \qquad n_{//} = \frac{I_{tot}}{I_{cell_{NOM}}} \quad (10)$$

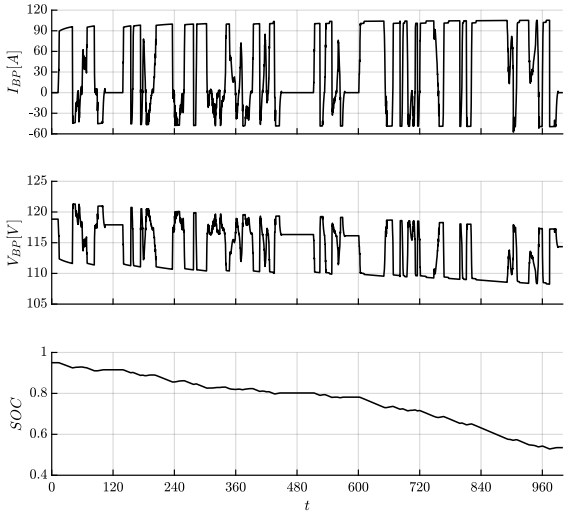

Figure 6: *Battery pack current; SOC; battery pack voltage*

The three main parameters for the analysis of the BP operation current, voltage and SOC are reported in the Fig.(6).

KERS block
This block receives the input signal from the inverter and storage management block. The output is the KERS current (I_{KERS}), which depends on the state of charge of the UC pack (SOC_{UC}) and the respective allowable charge and discharge current (I_{UC}). A relevant influencing factor on the output current is the power capability of the resonant converter (k), that will be discussed later.
The objective of this additional system is to use the UC peculiarities of high current capability, thermal stability, long ELD (Estimated Life Duration) and very fast behavior in both charge and discharge, to help the BP in the most critical driving phases.
Then, the UC pack is sized as already done for the BP. In Fig.(7) the relevant parameters of the KERS operation are displayed.

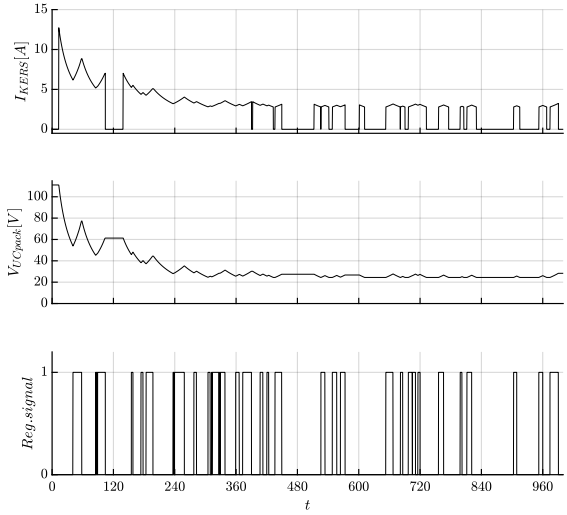

Figure 7: *KERS current; KERS voltage; regeneration signal*

As shown in the first graph, the current capability decreases proportionally to the voltage drop during discharge. In the second graph, the voltage behavior of UC pack is represented. The discharge voltage is limited by $V_{UCpack_{MIN}}$. When the voltage of the UC pack reaches the minimum value, the KERS stops to operate. In the last graph, the signal that control the regeneration during braking is displayed (1 on; 0 off).

III. KERS CONVERTER

The conception of the resonant converter comes from [12], [13] and [27]. This kind of converter is taken into analysis for this EV application mainly because of:

- high efficiency also at high switching frequency [23];
- feasible compactness and scalability [23].

By reducing the size of the passive components (such as inductors, capacitors as well as the heat sink for the semiconductor components), higher power density can be achieved. An effective way to do that is to increase the switching frequency. However, conventional PWM converters process power by interrupting the power flow by means of hard switching and thus they suffer from high switching losses [14].This loss is absent in resonant converters. [15]
They contain resonant inductor-capacitor ($L-C$) networks, also defined resonant-tank. In each switching cycle, the voltage and current waveforms vary sinusoidally in one or more sub-intervals [24] (topological steps). The commutation of the switches can be with zero-voltage switching (ZVS) or zero current switching (ZCS). In this case, the ZCS commutation is used. The resonant converter Fig.(3.6) is made bi-directional through the addition of two other switches and diodes to the boost configuration reported in [23].

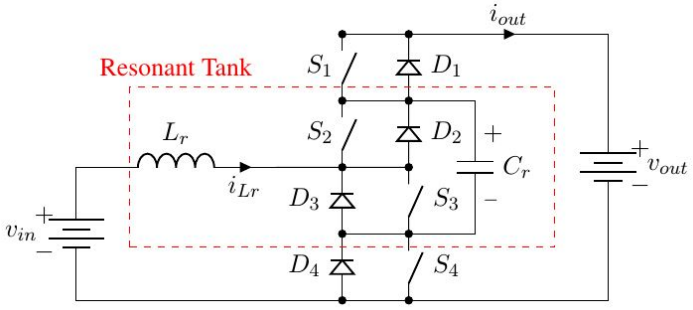

Figure 8: *Resonant buck-boost converter*

Topology

The operation topology in boost [13] [27] and buck modes as well as the characteristics of the chosen converter for the EV application are analyzed [20] [23].

Boost analysis

For the boost operation mode, the control signal of the two switches S_3 and S_4 is made of a complementary square-wave with 50% duty cycle while the switches S_1 and S_2 remain open.The two switches turn on complementary for half of the switching cycle and in each half there are three stages related to the resonant tank behavior. The operation stages of a switching cycle are illustrated in Fig.(9):

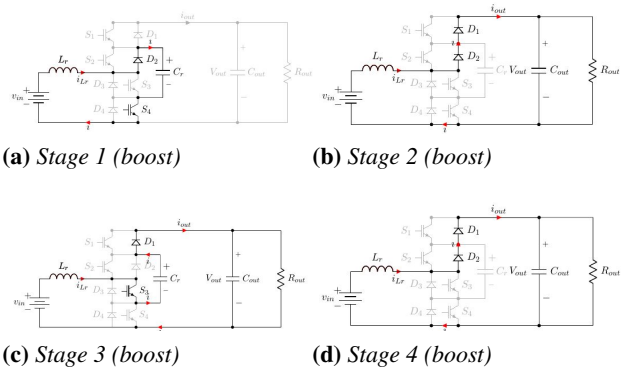

(a) *Stage 1 (boost)* **(b)** *Stage 2 (boost)*

(c) *Stage 3 (boost)* **(d)** *Stage 4 (boost)*

Figure 9: *Representation of the topological stages*

Stage 1 $[t_0, t_1]$

At t_0, S_3 turns off and S_4 turns on; D_1 is forward biased. During this stage, the resonant capacitor C_r is charged by the source as long as it reaches the voltage level in output V_{out}. Due to the resonance, the current through the resonant inductor L_r increases sinusoidally from 0 to a certain value, which is supposed to be I_1. This stage can be described by the following two equations:

$$\begin{cases} V_{in} = L_r \frac{\mathrm{d}i_{Lr}}{\mathrm{d}t} + v_{Cr}(t) \\ i_{Lr}(t) = C_r \frac{\mathrm{d}v_{Cr}(t)}{\mathrm{d}t} \end{cases} \tag{11}$$

Assuming the initial conditions for this stage:

$$\begin{cases} v_{Cr}(t_0) = 0 \\ i_{Lr}(t_0) = 0 \end{cases} \tag{12}$$

Applying the Laplace transformation [10], the following equation can be obtained:

$$\begin{cases} \frac{V_i}{s} = sL_r I_{Lr}(s) + V_{Cr} \\ I_{Lr}(s) = sC_r V_{Cr}(s) \end{cases} \tag{13}$$

And solving:

$$\begin{cases} I_{Lr}(s) = \frac{C_r}{s^2 L_r C_r + 1} V_{in} \\ V_{Cr}(s) = \frac{V_{in}/s}{1 + s^2 L_r C_r} \end{cases} \tag{14}$$

Now, considering the resonant angular frequency and the resonant impedance:

$$\omega_0 = \frac{1}{\sqrt{L_r C_r}} \qquad Z_r = \sqrt{\frac{L_r}{C_r}} \tag{15}$$

Substituting and applying the inverse Laplace transformation [10]:

$$\begin{cases} i_{Lr}(t) = \frac{sin(\omega_0 t)}{\omega_0}\frac{V_{in}}{L_r} \\ v_{Cr}(t) = V_{in}[1 - cos(\omega_0 t)] \end{cases} \quad (16)$$

Defining the following parameters:

$$\overline{i_{Lr}(t)} = \frac{i_{Lr}(t)}{V_{in}/Z_r} \qquad \overline{v_{Cr}(t)} = \frac{v_{Cr}(t)}{V_{in}} \quad (17)$$

And applying the parameterized inductor current and capacitor voltage:

$$\begin{cases} \overline{i_{Lr}(t)} = sin(\omega_0 t) \\ \overline{v_{Cr}(t)} = 1 - cos(\omega_0 t) \end{cases} \quad (18)$$

The voltage gain of the converter is $G_{boost} = \frac{V_0}{V_i}$.

At the end of this stage t_1, the following equation can be derived:

$$\begin{cases} \overline{i_{Lr}(t_1)} = \overline{I_1} \\ \overline{v_{Cr}(t)} = 1 - cos(\omega_0 t) \end{cases} \quad (19)$$

Where: $\overline{I_1} = \frac{I_1}{V_{in}/Z_r}$.

It is already known that at t_1 the resonant capacitor C_r is charged untill the output voltage V_{out}, therefore $v_{Cr}(t_1) = V_{out}$ and this imply $\overline{v_{Cr}(t_1)} = G_{boost}$. The duration of the first stage can be calculated as:

$$\omega_0 \triangle t_{10} = \pi - arcos(G_{boost} - 1) \quad (20)$$

Where $\triangle t_{10} = t_1 - t_0$. It is also possible to define a vector z in the state-plane as:

$$z = \overline{v_{Cr}(t)} + j\overline{i_{Lr}} \quad (21)$$

In conclusion the first stage can be described by the following vector:

$$z = 1 - cos(\omega_0 t) + jsin(\omega_0 t) \quad (22)$$

Stage 2 $[t_1, t_2]$

At t_1, S_4 is on and S_3 is off. The resonant capacitor voltage V_{Cr} is equal to the output voltage V_{out}, the diode D_1 turns on. So, in this stage V_{Cr} is clamped as V_{out}, while the current through the inductor i_{Lr} drops linearly to zero, since the output voltage is higher than the input voltage. By mathematical calculation, this leads to a negative voltage across Lr. The state plane vector:

$$z_2 = G + \jmath[\overline{I_1} - (G-1)\omega_0(t - t_1)] \quad (23)$$

The duration of this stage can be calculated as follow:

$$\omega_0 \triangle t_{21} = \frac{\overline{I_1}}{G-1} \quad (24)$$

Stage 3 $[t_2, t_3]$

At t_2, S_4 is on and S_3 is off. As the current becomes 0 at the end of the second stage, D_2 is reverse biased. There is no more current through L_r, and the voltage across C_r remains at V_{out} as in Stage 2. At this stage, no current is circulating in the circuit. The stage ends at half of the whole switching cycle, which means $\omega_0 t = \pi$. So:

$$\omega_0 \triangle t_{32} = \pi - \omega_0 \triangle t_{21} - \omega_0 \triangle t_{10} \qquad z_3 = G \quad (25)$$

Stage 4 $[t_3, t_4]$

At t_3, the switch S_3 turns on and S_4 turns off. At this stage, $D1$ is forward biased while $D2$ is reverse biased. The resonant capacitor is discharged, so the voltage across it drops from V_{out} to 0. At the same time, the current through the inductor increases from 0 to I_1. The operation of the converter is similar to the first stage. The duration is equal to the first stage:

$$\omega_0 \triangle t43 = \pi - arcos(G - 1) \quad (26)$$

The vector in state-plane of this stage is:

$$z_4 = G - 1 - cos(\omega_0 t) - jsin(\omega_0 t) \quad (27)$$

Stage 5 $[t_4, t_5]$

The operation of the converter in this stage is quite similar to the stage 2. The difference is that the resonant capacitor voltage keeps at zero. The duration and the state vector are :

$$\omega_0 \triangle t_{54} = \frac{\overline{I_1}}{G-1} \qquad z_5 = \jmath[\overline{I_1} - (G-1)\omega_0(t - t_4)] \quad (28)$$

Stage 6 $[t_5, t_6]$

At the end of stage 5, the current decrease until 0 and there is no voltage across the resonant capacitor. Thus, there is no current through L_r and no voltage across C_r. Therefor:

$$\omega_0 \triangle t_{65} = \pi - \omega_0 \triangle t_{43} - \omega_0 \triangle t_{54} \qquad z_6 = 0 \quad (29)$$

Summary of the boost switching behavior

The main waveforms of voltages and currents of the components are shown in Fig.10. The resonant capacitor V_{Cr} is charged to V_{out} and then clamped at this value during the first half switching cycle. Then, in the second half switching cycle, the resonant capacitor is discharged to zero. The frequency of the current through the resonant inductor i_{Lr} is twice the switching frequency. The average value of the current through diodes

is dependent on the switching frequency, then the output voltage can be regulated by the ratio between the switching frequency and the resonant frequency (μ_0).

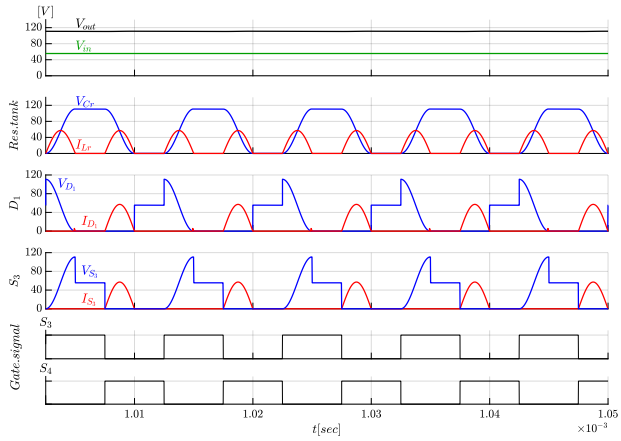

Figure 10: *Boost simulation*

Buck analysis

Due to the analysed modulation strategy, in the buck operation mode, the control signal of the two switches S_1 and S_2 is made of a complementary square-wave with 50% duty cycle while the switches S_3 and S_4 are off. The two active switches turn on complementary and each half presents three stages. The following analysis is performed in the same way of the boost one.

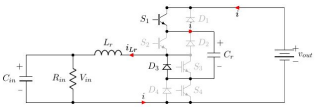

(a) *Stage 1 (buxk)*

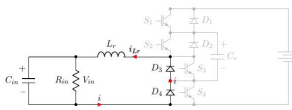

(b) *Stage 2 (buck)*

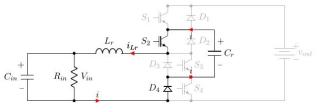

(c) *Stage 3 (buck)*

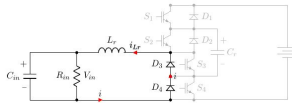

(d) *Stage 4 (buck)*

Figure 11: *Representation of the topological stages*

Stage 1 $[t_0, t_1]$

In this operation mode, at t_0, S_1 turns on and S_2 turns off, diode D_3 is forward biased. During this stage, the resonant capacitor C_r is charged by the source to the voltage level of the output voltage V_{out}. Due to the resonance, the current through the resonant inductor L_r increases sinusoidally from 0 to a certain value, defined I_1. The duration is:

$$\omega_0 \triangle t_{10} = \pi - arcos(\frac{G_{buck}}{G_{Buck} - 1}) \tag{30}$$

The state plane vector is:

$$z_1 = (G_{buck}-1)[1-cos(\omega_0 t)]+\jmath(G-1)sen(\omega_0 t) \tag{31}$$

Stage 2 $[t_1, t_2]$

At t_1, the switch S_1 is on and S_2 is off. The resonant capacitor voltage v_{Cr} is equal to the output voltage V_{out}, the diodes D_3 and D_4 are forward biased. So in this stage v_{Cr} is clamped as V_{out}, while the current through the inductor i_{Lr} decrease linearly to zero, since the output voltage is higher than the input voltage. This leads to a negative voltage across L_r. The duration is determined by $I_{Lr}(t_2) = 0$, so:

$$\omega_0 \triangle t_{21} = \overline{I_1} \qquad z_2 = \frac{1}{G_{buck}} + \jmath[\overline{I_1} - \omega_0(t - t_1)] \tag{32}$$

Stage 3 $[t_2, t_3]$

At t_2, the switch S_1 is on and S_2 is off. As the current becomes 0 at the end of the second stage, the diodes are reverse biased, so there is no current through L_r. The voltage across C_r remains as in stage 2. In this stage, no current is circulating in the circuit. So:

$$\omega_0 \triangle t_{32} = \pi - \omega_0 \triangle t_{21} - \omega_0 \triangle t_{10} \qquad z_3 = \frac{1}{G_{buck}} \tag{33}$$

Stage 4 $[t_3, t_4]$

In this stage, at time t_3 the switch S_2 turns on and S_1 turns off. The diode D_4 is forward biased while D_3 is reverse biased. The resonant capacitor is discharged, so the voltage across it drops from V_{out} to 0. At the same time, the current through the inductor increases from 0 to I_1 again. The operation of the converter is similar the first stage. It lasts:

$$\omega_0 \triangle t_{43} = \pi - arcos(\frac{G_{buck}}{G_{Buck} - 1}) \tag{34}$$

And vector:

$$z_4 = 1 + cos(\omega_0 t) - \imath \frac{sen(\omega_0 t)}{G_{buck}} \tag{35}$$

Stage 5 $[t_4, t_5]$

At t_4, the switch S_1 is off and S_2 is on. The stage 5 behaves exactly as the second stage, except for the initial conditions. The diodes are conducting. The resonant inductor is linearly discharging until 0; at this point, the

diodes D_3 and D_4 are reverse biased and the stage ends. Duration and the state plane vector are:

$$\omega_0 \triangle t_{54} = \overline{I_1} \qquad z_5 = \jmath[\overline{I_1} - \omega_0(t - t_4)] \tag{36}$$

Stage 6 $[t_5, t_6]$

At t_5, the switch S_1 is off and S_2 is on. The current in the resonant inductor is 0 and there is no voltage across the resonant capacitor. Thus, in this last stage there is no current through L_r and no voltage across C_r. The end of this last stage is the end of the whole switching cycle. So:

$$\omega_0 \triangle t_{65} = \pi - \omega_0 \triangle t_{54} - \omega_0 \triangle t_{43} \qquad z_6 = 0 \tag{37}$$

Summary of the buck switching behavior

As before, the waveforms of the voltage and current are plotted according to the switching signal. The results are shown in Fig.(12). Neither in this operation mode, at turn-on and turn-off, the voltage and current waveforms of the switches have no overlap, this means there is no switching loss. The soft switching properties are maintained. Thus, this converter is soft-switching.
The behavior of the resonant tank is exactly the same of the boost analysis.

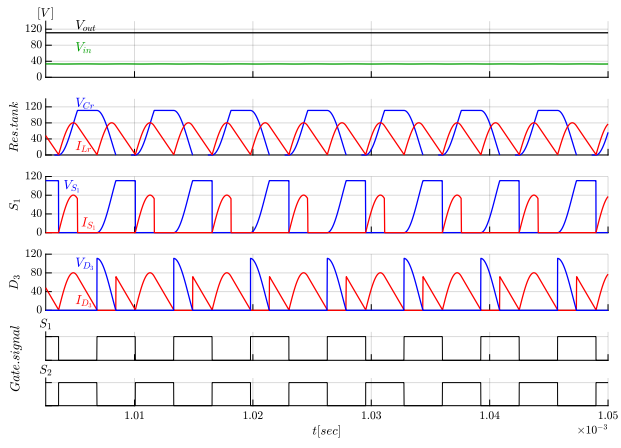

Figure 12: *Buck simulation*

Parameterized analysis

Output current and power

The average output current i_{outAVG} can be calculated [26] as the sum of the integral of the current function of the topological time steps $\triangle t_{12}$, $\triangle t_{34}$ and $\triangle t_{45}$:

$$\overline{i_{outAVG}} = \frac{1}{T_s}[\int_{t_1}^{t_2} \overline{i_{Lr}(t)}dt + \int_{t_3}^{t_4} \overline{i_{Lr}(t)}dt + \int_{t_4}^{t_5} \overline{i_{Lr}(t)}dt] \tag{38}$$

the final equation of the parameterized average output current i_{outAVE} is found:

$$\overline{i_{outAVG}} = \frac{\mu_0}{2\pi} \frac{G_{boost}}{(G_{boost} - 1)} \tag{39}$$

This equation is represented in the following Fig.(13) in order to see the dependency of $\overline{i_{outAVG}}$ on the frequency ratio μ_0 and the gain G_{boost}:

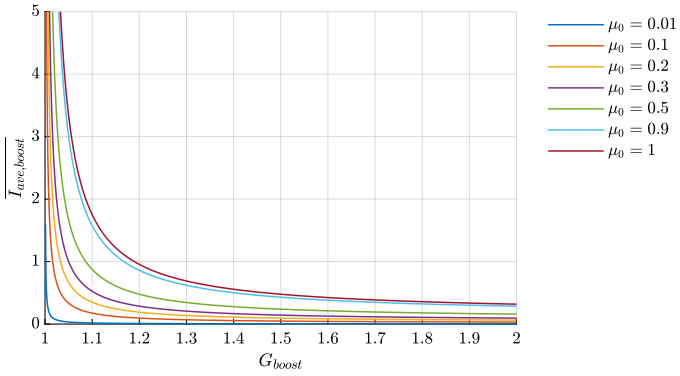

Figure 13: *Output current dependency on frequency ratio and gain*

It shows the tendency of reducing the output current while increasing the gain for a certain μ_0 value. The output power is consequently:

$$\overline{P_{outAVG}} = \frac{\mu_0}{2\pi} \frac{Gboost^2}{(Gboost - 1)} \tag{40}$$

Boost gain

The boost gain is limited to the range:

$$1 < G_{boost} < 2 \tag{41}$$

Using the resonant impedance Z_r to parameterize the output resistance (R_{out}), the following ratio can be found:

$$r_{out} = \frac{R_{out}}{Z_r} \tag{42}$$

So:

$$G = \frac{\mu_0}{2\pi} r_{out} + 1 \tag{43}$$

In addition to this, in order to keep the soft switching properties of this converter, the switching frequency should not exceed the resonant frequency, which means: $0 < \mu_0 < 1$

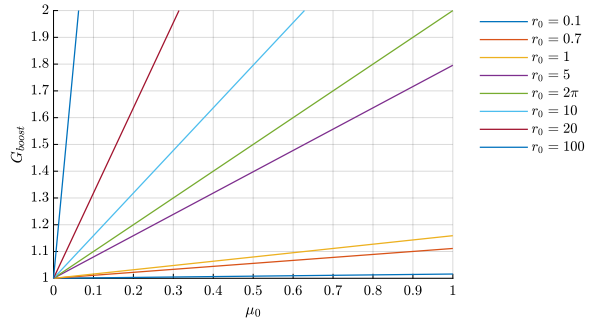

Figure 14: *Dependency of the output parameterized resistance r_{out} on frequency ratio and gain*

From the Fig.(14) is clear that, in order to reach the maximum gain $G = 2$, r_{out} should be greater than 2π.

Input current

As for the boost, the average input current i_{inAVG} can be calculated as the sum of the integral of the current function in the topological time steps $\triangle t_{10}$,$\triangle t_{21}$, $\triangle t_{43}$ and $\triangle t_{54}$:

$$\overline{i_{inAVG}} = \frac{1}{T_s}[\int_{t_0}^{t_1} \overline{i_{Lr}(t)}dt + \int_{t_1}^{t_2} \overline{i_{Lr}(t)}dt + \int_{t_3}^{t_4} \overline{i_{Lr}(t)}dt + \int_{t_4}^{t_5} \overline{i_{Lr}(t)}dt] \tag{44}$$

The final equation is found:

$$\overline{i_{inAVG}} = \frac{\mu_0}{2\pi}\frac{1}{G_{buck}} \tag{45}$$

The Fig.(15) shows the dependency of $\overline{i_{inAVG}}$ on the frequency ratio μ_0 and the gain G_{buck}:

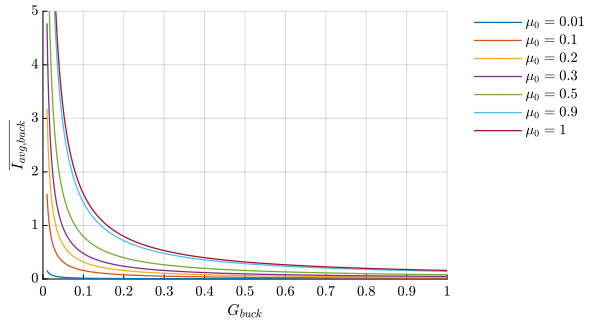

Figure 15: *Input current dependency on frequency ratio and gain*

Buck voltage gain

The buck gain range is:

$$0 < G_{buck} < 0.5 \tag{46}$$

As for the boost, considering the input voltage approximately constant, a constant load resistance R_{in}, reviewing the equation of the average input current eq.(45) and defining $r_{in} = \frac{R_{in}}{Z_r}$, the gain of the buck modulation is:

$$G_{buck} = \sqrt{r_{in}\frac{\mu_0}{2\pi}} \tag{47}$$

Considering, for the same reason as before, the maximum switching frequency equal to the resonant one, it results on: $0 < \mu_0 < 1$

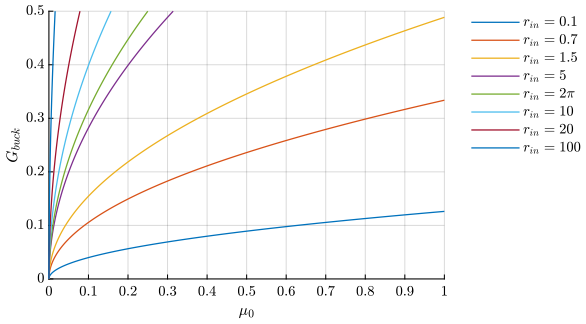

Figure 16: *Dependency of the input parameterized resistance r_{in} on frequency ratio and gain*

Clearly from the Fig.(16), in order to reach the maximum gain $G_{buck} = 0.5$, the minimum value of r_{in} is 1.5.

Design Methodology

The design process of the converter followed this main steps:

1. Definition of the optimal gain range for both boost and buck operations;
2. Identification, through the parameterized analysis, of the optimal value for the parameterized load r_0;
3. Set the maximum admittable peak current (I_{peak}) in the resonant inductor, switches and diodes;
4. Choice of the switching technology for the required resonant frequency f_0;
5. Check the UC pack current capability over all the charge / discharge operations.

As already discussed, in order to keep the soft switching properties the maximum possible gain for the boost operation mode is $1 < G(boost) < 2$ and for the buck operation mode is $0 < G(buck) < 0.5$.
So, a minimum UC pack voltage has to be set and this limits the buck resonant operation. Therefore, the optimization procedure is performed based on boost mode.

It means keeping as objective: $r_{out} > 2\pi$. The resonant frequency f_0 is set based on the choice of the switches technology. Then, defining the nominal voltage for the UC pack $\frac{V_{UCpack}}{G_{boost}}$, where the $G_{boost} = 2$, and considering the resonant frequency $f_0 = \frac{1}{2\pi\omega_0}$, the resonant impedance $Z_r = \sqrt{\frac{L_r}{C_r}}$ and the resonant angular frequency μ_0, it is possible to define:

$$L_r = \frac{Z_r}{2\pi f_0} \qquad C_r = \frac{1}{2\pi Z_r f_0} \tag{48}$$

The switching frequency for the boost operation mode is selected using (39) and (43) as:

$$f_{s_{boost}} = \frac{G-1}{R_{out}C_r} \tag{49}$$

Instead, the switching frequency for the buck operation mode is defined using (45) and (47):

$$f_{s_{buck}} = \frac{G_{buck}^2}{R_{UC_{pack}}C_r} \tag{50}$$

Where R_{UCpack} is the UC pack equivalent resistance.
Keeping under control all the component and the project constraints already mentioned, the most stringent requirement for this application is derived:

$$I_{peak_{Lr}} > \frac{2\pi V_{inv}}{R_{out}} \tag{51}$$

Since V_{inv} should be approximately constant during operation and $R_{out} = \frac{V_{inv}^2}{P_{inv}}$, is very low, the minimum possible value for $I_{peak_{Lr}}$ is very high. Moreover, it leads to a not allowed current to the input of the UC pack.
In order to solve the problem the decision is to act following simultaneously two paths:

1. Reduce the power capability of the converter;
   A capability factor k is defined setting the maximum gain of the converter $G_{boost} = 2$ and the maximum input current at the UC pack $I_{UCpack} = I_{max}$:

   $$k = \frac{I_{UCpack}\frac{V_{UCpack}}{G_{boost}}}{P_{inv}} \tag{52}$$

   So the capability of the system P_{KERS} is defined by:

   $$P_{KERS} = kP_{inv} \tag{53}$$

2. Use more than one converter in interleaving mode [21] [22];
   Assuming a reasonable number of converter ($n_{res_{conv}} = 2$), the power capability of each one becomes:

   $$P_{res_{conv}} = k\frac{P_{inv}}{n_{res_{conv}}} \tag{54}$$

   This choice can halve the power capability of each converter, so the current too, while increasing the current peak to the UC pack of just a $\sqrt{2}$ factor. The resulting peak current in the UC pack is:

   $$I_{UCpack_{peak}} = \sqrt{2}I_{peak_{Lr}} \tag{55}$$

Combining these two effects (eq.52; eq.54; eq.55), it is possible to find the whole system capability value (k) that makes each resonant converter respect all the constraints:

$$k = \frac{I_{UCpack_{max}}V_{inv}^2 n_{res_{conve}}}{2\pi\sqrt{2}V_{UCpack}P_{inv}} \tag{56}$$

The working limits of buck operation in current, gain and switching frequency are graphically displayed in the Fig.(3.24) reported below:

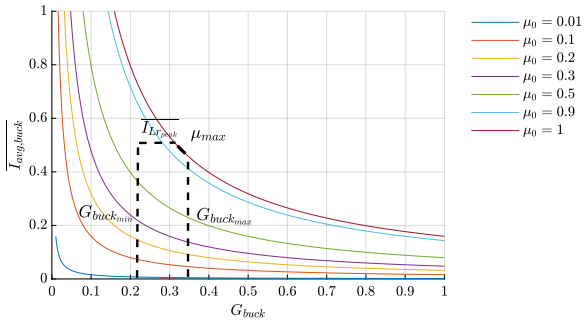

Figure 17: *Current/ Gain/ switching frequency limits in buck opertions*

Outside the boost and buck resonant areas, a change in modulation strategy from resonant to a conventional PWM operation is required (hybrid modulation).

Resonant Converter Simulation Results

In Fig.(10) the voltage and current values of the resonant tank, of one diode and one switch are reported.
In the first one, the ability of the converter to reach V_{out} and the stability of the solution at nominal operation of $G_{boost} = 2$ is reported. In the second one, the current through the resonant inductor and the voltage across

the resonant capacitor are shown. The third and the forth displays the current and voltage behavior through respectively the diode D_1 and the switch S_3. It is important to underline that there isn't overlapping of voltage and current for all the switching cycle operations. This means that in this ideal simulation the switching losses are null and that the soft switching properties of the resonant converter are kept.
Instead, Fig.(12) shows the buck simulation results. The simulation is performed at the maximum resonant gain $G_{buck} = 0.3$. As expected by theoretical limitations, the charge and discharge time of the resonant inductor is equal to the semi-period. This confirms the limitations of the resonant operations. As for the boost simulation, in the third graph there is no overlapping of voltage and current in the switches, this means that the soft switching properties are kept also in buck operation mode.

IV. CONCLUSIONS

At the end of this work, the project of the EV to compete in the FSAE electric is still in the preliminary phases. The requirements about the storage, the motor and the current / voltage parameters have been defined. The construction of the prototype, based on the results of this thesis and others research regarding the vehicle mechanical structure, is scheduled for the months ahead. The first tests of the vehicle are expected within the end of this year.

The performed analysis shows that the vehicle is able to accomplish to the requirements of the dynamical tests of the Formula SAE electric. The simulation clearly confirms the correct sizing of the storage system with a good safety margin for the real operation in witch the prototype could exploit all the motor power. As expected, the Li-ion cells charge and discharge according to the theoretical implementation, respecting the current and voltage operational constraints on the inverter DC side. Instead, the KERS operation is strongly influenced by the state of charge of the UC pack that is disconnected under a certain voltage value to ensure a proper operability of the whole system.

For what concerns the studying and sizing of the resonant converter, the theoretical analysis displays the full capability of the resonant converter to operate under soft-switching properties in both directions. Then, the limitations due to the high current EV application, pushed the analysis to correctly sizing it. The interleaved solution, combined with the introduction of the capability factor, gets the result of reducing both the peak current in the resonant inductor and the input current to the UC pack. The findings suggest that the assumptions of compactness and low weight of the converter can be achieved and that the UC can co-work with the BP. Nonetheless, the converter is not able to fully exploit the peculiarity of fast charge / discharge of the UC. Anyway, the ultra-caps technology implemented in the model remains an interesting asset to get the maximum advantage from the regenerative braking. For this reason the study of other converters technology is surely interesting for combined Li-ion and ultra-caps EV as well as the research of the best number of these resonant converter in a volume, weight, cost and capability optimization problem .

Contents

Abstract

In this work, a model to simulate an electric vehicle for Formula SAE electric competition is built. The electric motor, the vehicle dynamics, the braking system and the hybrid storage system of Li-ion batteries and ultra-capacitors are implemented. The energy of the regenerative braking is differently stored in the Battery Pack (BP) and in the Ultra-Caps (UC) pack through the Kinetic Energy Recovery System (KERS). The model provides all the current and voltage variables needed to describe the functioning of the electrical part. Thanks to the simulation results, the prototype proves to be able to accomplish the race tests.
Then, a bidirectional DC-DC resonant converter, applied to the UC pack managing, is studied and the topology states of the chosen configuration are theoretically analyzed. The operational limits, keeping the soft-switching properties, are discussed and the results show the capability of the designed converter to operate under resonant mode in both boost and buck mode. The switching losses are significantly reduced at high and low switching frequency. The drawback of this configuration is the presence of high current peaks in the resonant inductor that influence the power manageable by the converter. The use of more than one converter in interleaving and the insertion of a capability factor ensure the proper operability of the system.

Key-words: resonant converter, ultra-caps, regenerative braking, formula SAE electric, electric vehicle.

In questo lavoro, é stato costruito un modello per la simulazione di un veicolo elettrico per competere nella Formula SAE elettrica. Sono stati implementati il motore elettrico, la dinamica del veicolo, l'impianto frenante e il sistema di stoccaggio ibrido delle batterie agli ioni di litio e degli ultra-condensatori. L'energia rigenerativa della frenata é immagazzinata differenzialmente nel pacco batteria e negli ultra-capacitori (UC) attraverso il Kinetic Energy Recovery System (KERS). Il modello fornisce tutte le variabili di corrente e tensione del veicolo. Grazie ai risultati della simulazione, il prototipo dimostra di essere in grado di eseguire i test di gara.
Di seguito, é stato studiato un convertitore risonante bidirezionale DC-DC, applicato alla gestione del pacco UC, e ne sono stati analizzati gli stati topologici. Vengono discussi i limiti operativi, mantenendo le proprietá di "soft-switching" e i risultati mostrano che il convertitore é in grado di operare come da progetto sia in modalitá boost che in modalitá buck. Le perdite di commutazione sono significativamente ridotte sia ad alta frequenza che in bassa. Lo svantaggio di questa configurazione é la presenza di elevati picchi di corrente nell'induttore di risonanza che influenzano la potenza gestibile dal convertitore. L'uso di piú di un convertitore in interleaving e l'inserimento di un "capacity factor" garantiscono la corretta operativitá del sistema.

Parole chiave: convertitore risonante, ultra-caps, frenata rigenerativa, formula SAE elettrica, veicolo elettrico.

CHAPTER 1

Introduction

Nowadays, the awareness of environmental and climatic problems is gaining its way into social and political life. The scientific community and the educational institutions are working to provide answers to the growing concerns about human life impact on the planet.
In this optic, the Master Programme In Energy for Development would like to give the knowledge to understand the complexity and the tools to face the sustainability, affordability and reliability problems of development [1].
Every human activity plays a role over the environmental impact: the emissions of the traditional transportation systems, based on internal combustion engine, are a part of the climate problem. The whole sector accounts for the 20.44% of the global CO_2 emissions according to The World Bank [2] and to one fourth according to IEA (International Energy Agency) emission statistics [3].
The electric traction can represent the game changer technology for a long term sustainability of the transportation sector.
The rise of the global interest in this electric challenge is pushing the traditional automotive industry to develop the required technology. Also the European car-makers are now obligated to deal with American primacy company (Tesla) and south-Asia technology leadership in electric storage systems.
In this actual scenario of growing competition around electric mobility, also the educational institutions all over the word are forced to provide their students with new tools to properly face this technological change: it is in this condition that in 2010 borned, from the well known *SAE International*, the *Formula SAE Electric*.

1.1 Formula SAE

The Formula SAE (FSAE) was developed in 1981 as student automotive competition at University of Texas and then:*"Internationally, the expansion of Formula SAE/Formula Student has exploded to over 20 competitions currently hosted by engineering societies or private business.*

The Formula SAE program is an engineering design competition for undergraduate and graduate students. The competition provides participants with the opportunity to enhance their engineering design and project management skills by applying learned classroom theories in a challenging competition. The engineering design goal for teams is to develop and construct a single-seat racecar for the non-professional weekend autocross racer with the best overall package of design, construction, performance and cost. The concept behind Formula SAE is that a fictional manufacturing company has contracted a design team to develop a small Formula-style racecar. The prototype racecar is to be evaluated for its potential as a production item. The target marketing group for the racecar is the non-professional weekend autocross racer. Each student team designs, builds and tests a prototype based on a series of rules whose purpose is both to ensure onsite event operations and promote clever problem solving. The vehicle will be inspected in a series of tests to ensure it complies with the competition rules; in addition, the vehicle with driver will be judged in many performance tests on track. The rest of the judging is completed by experts from motorsports, automotive, aerospace and supplier industries on student design, cost and sales presentations.

Formula SAE promotes careers and excellence in engineering as it encompasses all aspects of the automotive industry including research, design, manufacturing, testing, developing, marketing, management and finances." [4]

The SAE international is hold by a foundation with the mission of *"encourage and increase student achievement and participation in science, technology, engineering and math (STEM) to build a STEM-fluent workforce. Funds raised by the SAE Foundation support SAE International's award-winning: A World In Motion (AWIM) program, Collegiate Design SeriesTM (CDS), awards and scholarships. SAE's STEM education programs enable students to develop the 21st century skills needed to succeed in real-world work environments and connect classroom learning with real life application. Overall, SAE's STEM programs have reached more than 5 million students worldwide and engaged more than 30.000 STEM industry professionals as volunteers. SAE International is a global association engaging nearly 200.000 engineers, technical experts and volunteers to advance mobility knowledge and solutions for the benefit of humanity."*

The organization plans several events in lots of locations all over the world. These

competitions are managed by the local FSAE and among the most relevant there are: Formula SAE Michigan, Formula Student, Formula Lincoln e FSAE electric, FSAE student Austria, FSAE Australia, FSAE student Germany, FSAE Italy, FSAE Japan and FSAE Brazil. In addition to the electric competitions, also hybrid events are occasionally hold together with the classical ones.

1.2 Formula SAE electric

The first electric event was hold by the Formula SAE student Germany in 2010 and from there it spread in the Italian, spanish and Brazilian organization in 2012 and then in 2013 it arrived in the FSAE Lincoln that is actually the most important in terms of partecipation. Every year the applications for FSAE grows and the performance of the participant teams improves. The *Formula SAE Electric* pursues the same objectives of the traditional FSAE but focusing on a full electric vehicle. The requirements and constraints of the EV for the contest are yearly updated on the *SAE International* website [4].
The competition is composed of several tests and to each of them a score is assigned. The winner team is defined according to the total score.
The examinations are divided in two groups: the static and the dynamic ones. Commonly, the first to be performed in the first day of competition are the static tests:

1. Presentation
   "The Presentation Event evaluates the team's ability to develop and deliver a comprehensive business, logistical, production, or technical case that will convince outside interests to invest in the team's concept."
   The score varies between 0 and 75;

2. Cost
   "Cost and Manufacturing are an integral part of any engineering project. Making trade-off decisions between content and cost based on the performance of each part and assembly and accounting for each part and process to stay within a budget is part of project management."
   The score varies between 0 and 100;

3. Design
   "The Design Event evaluates the engineering effort that went into the vehicle and how the engineering meets the intent of the market both in terms of vehicle performance and overall value."
   The score varies between 0 and 150;

than, during the second and third day of competition, the dynamic tests are faced:

1. Acceleration
   "The Acceleration event evaluates the vehicle acceleration in a straight line on flat pavement."
   The race length is 75 m from starting line to finish line. Each team has four possible attempts and only the best performance is taken into account. The record belongs to the *Massachusetts Inst of Technology* that completed the test in 4.121 sec in the Lincoln circuit in 2018. The associated score varies between 0 and 100;

2. Skid Pad
   "The Skidpad event measures the vehicle cornering ability on a flat surface while making a constant radius turn."

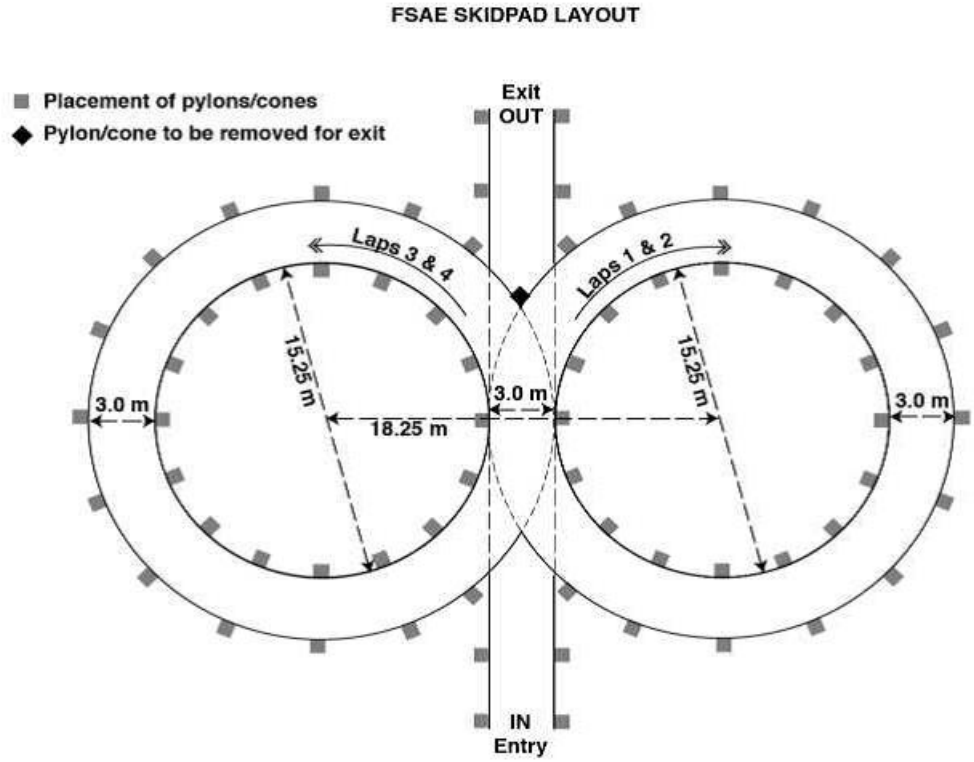

Figure 1.1: *Skip Pad layout*

The course is a pair of concentric circles in shape of the number 8 as in the figure above. Hitting a cone is a penalty. The record of 5.274 sec (of corrected time according to the regulation [4]) belongs to *Purdue University - W. Lafayette* that scored it in the same occasion of the one above (Lincoln 2018). A score from 0 to 75 is associated to this event;

3. Autocross
   "The Autocross event evaluates the vehicle maneuverability and handling qualities on a tight course"
   The objective is to evaluate the car's on a tight course without the hindrance of competing cars. The course combines the performance features of acceleration, braking and cornering into one event. The results of the Autocross scores determine the starting order for endurance. The score is calculated according to the rules [4] and the record belongs again to *Massachusetts Inst of Technology* that scored it in the Lincoln circuit in 2018 with the equivalent time of 59.813 sec. A score from 0 to 125 is associated to this event;

4. Endurance
   "The Endurance event evaluates the overall performance of the vehicle and tests the durability and reliability."

It consists of multiple laps over a closed course to a total distance of approximately 22 km. Acceleration, speed, handling, dynamics, fuel efficiency and reliability have to be proved. The winner of the last Lincoln edition is the *University of Washington* with the time of 1732.903 sec. The associated score is the most relevant one and it can go from 0 to 275;

5. Efficiency
   "The Efficiency event evaluates the fuel / energy used to complete the Endurance event"
   The Efficiency is based on a metric of the amount of consumed fuel or used energy and the lap time on the endurance course, averaged over the length of the event. The record belongs to *Montreal Polytechnique* with the equivalent rate of 108.306 sec. A score from 0 to 100 is associated to this event;

The winner team of the FSAE electric, held in Lincoln in 2018, was the *Carnegie Mellon University* with the overall score of 799.6, which is also the record to beat.

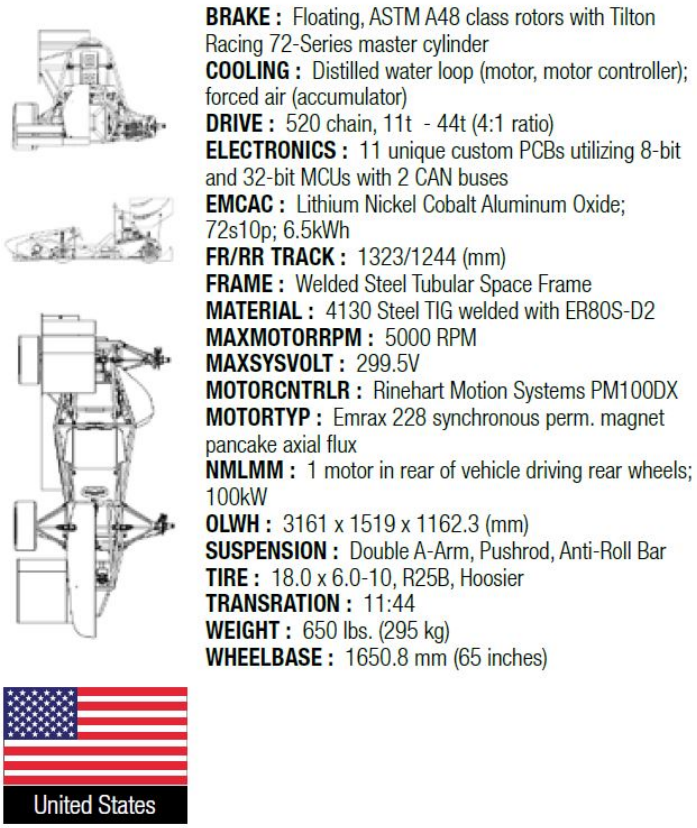

Figure 1.2: *Carnegie Mellon University vehicle specifications*

1.2.1 Brazilian FSAE

As already mentioned above, since 2012 in Brazil, in correspondance of the traditional SAE competition, also the electric events is held [5]. The Brazilian competition follows the previously typed rules. The electric event is dominated, since the very first year, by the team of the *Universidade Estadual de Campinas* that won 5 out of 6 editions.
The Brazilian electric event hasn't a large number of participants yet but it is really competitive. The scores of the best team is really similar to the most important SAE events discussed in the previous chapter.

Brazilian SAE and Lincoln SAE score comparison		
Event	"Universidade Estadual de Campinas"	Lincoln record
Presentation	70,7 [points]	75 [points]
Cost	$24069	$16758
Design	120 [points]	150 [points]
Acceleration	3,764 [s]	4.121 [s]
Skid Pad	5,65 [s]	5.274 [s]
Autocross	69,28 [s]	59.813 [s]
Endurance	1817,54 [s]	1732.903[s]
Efficiency	verified (not quantified)	0.731 (fuel efficiency factor)

The Brazilian champion team has the best acceleration event score and, as shown in the Tab. above, it is really competitive in all the different test, according to the resulting score. So, the Brazilian FSAE electric isn't just a start-up, a young experiment but it has the chance and the power to compete world-wide.

Thanks to this consideration and the ones reported at the beginning of the chapter, more and more Brazilian universities put their attention and interest over this kind of competition. One of those is the *"Universidade do estado de Santa Catarina (UDESC)"* which is also the host university of my exchange program (Bilateral agreement extra-UE). It gave me the great opportunity to participate to the project and to deepen the study and the efforts to the goal as passionate as complex of competing national wide in FSAE.

1.3 Project

The project to compete in the Brazilian FSAE electric has been developed in the Centro de Ciencias Tecnologicas (CCT) of the Universidade do Estado de Santa Catarina (UDESC, Brazil), thanks to the will of Prof. Ademir Nied and Prof. Yales Romulo de Novaes coupled with some industrial partnerships in the power electronic field (WEG, EMBRACO). The project is a double opportunity for both the students that can practice and experience over EV and for the industrial partners that, in this way, can play a role in this technological change and find well prepared workers in the labor market. Now, the project is still into the preliminary analysis and simulation phase; the aim of the heads is to be ready to compete within two years.

1.3.1 Starting point

The partners have already provided the motors and the ultra-caps implemented in this work and they are committed to provide financial and technical support for the vehicle construction phases. The other components (as batteries, wheels, etc.) will

be chosen and bought according to this preliminary study.

1.4 Objectives

This work represents the sizing and simulation phase in which the overall vehicle is analyzed and theoretically implemented. The main topics of the work are:

- create a model of the whole vehicle. Link together all the mechanical, electrical, traction, braking and storage systems to properly simulate the capability and performance of the prototype (chap.2);
- deepen the efforts in the study of a resonant converter applied to the regenerative braking system (KERS) to manage the energy stored in a ultra-caps pack (chap.3).

The second topic plays a crucial role in solving the actual limits of the electric technology and to ensure to it the long term competitiveness in the transportation sector: the importance of the energy efficiency, cost savings and storage management in the goal of increasing range and performance, is the last objective of the research. The hope is that the efforts in pushing the technology limits in racing competitions could help to increase the competitiveness on the transportation market.
In the available scientific literature the limits of Li-ion batteries and super or ultra caps coupling is someway missing. This master thesis wants to investigate these limits applying resonant converter technology (high efficiency converters [12] [13]) and exploiting the peculiarities of both batteries and capacitors with the final objective of overall efficiency. The bidirectional dc-dc resonant converter is the key component to control the energy flow between the battery and the ultra-capacitor. To reduce the internal energy loss, the operation and limitations within the soft-switching characteristics is the studied choice. Once that the operational frontiers are set, the analyzed resonant converter configuration is adapted to the EV project considering all the converter, inverter and UC pack constraints. Then, according to that foundings, a capability factor and an interleaved solution with two resonant converter is studied in order to ensure the proper operability of the system.

CHAPTER 2

Simulink Model of the Electric Vehicle (EV)

The EV model has been developed in the nPEE (Nucleo de Processamento de Engenharia Elétrica), the laboratory of power electronics of the Department of Electrical Engineering of UDESC (Brazil). It starts from the experience of the local supervisor for the exchange project Prof.Yales Romulo de Novaes, the PhD students of the laboratory and with the help of the students involved in the project.
The need of a simulation model is born to accomplish a preliminary analysis in order to develop and build the EV for the Formula SAE electric competition.
The software (Simulink, a MathWorks product) was selected because of the familiarity with the Matlab environment, the high versatility (mechanical/electrical), the well known diffusion and the online community and official support of the product [7].
It is an equation based model in which all the main systems of an EV are implemented starting from a theoretical analysis.
In this chapter the implementation steps as well as the theoretical related analysis are displayed.

2.1 Objective

The main objective of the model is to compute, for each time step ($\triangle t$), the Power, the Voltage and the Current at the KERS output in order to correctly project and size the power converter required to run the system.
For each $\triangle t$, the requirements that need to be found are in the following order:

1. Torque (τ_{mot}) and Power of the motor (P_{mot});
2. Voltage (V_{inv}) and DC current (I_{inv}) at the inverter;
3. Voltage (V_{BP}) and DC current (I_{BP}) at the battery pack;

Moreover, thanks to this analysis, the available recoverable energy of braking is computed. The electrical connections [12] are supposed to be as in Fig.(2.1) where also the names of the variables are reported.

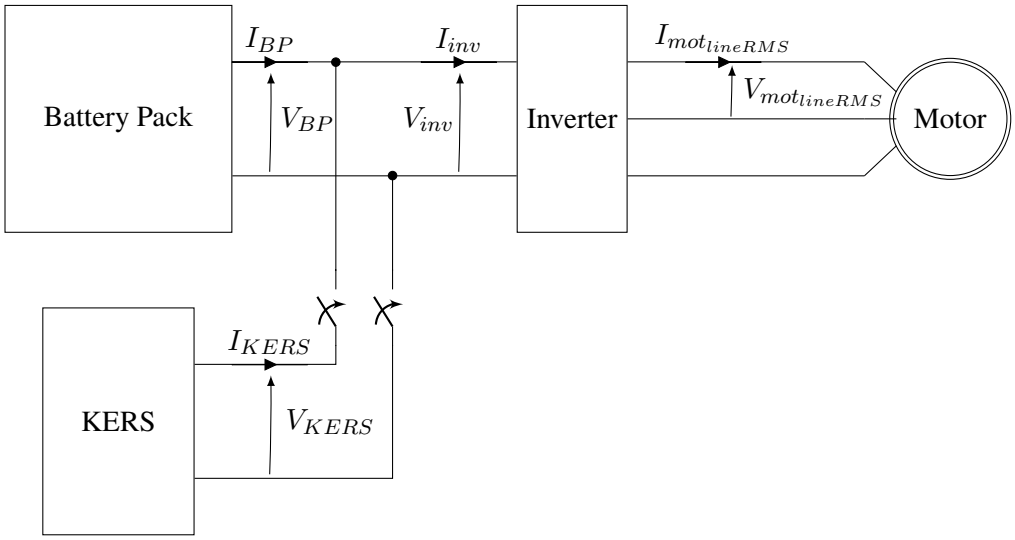

Figure 2.1: *Concept scheme*

2.1.1 Expected Output

The simulation is expected to show the capacity of the prototype in following the given speed profile, to provide the SOC (State of Charge) of the battery pack as well as the one of the UC pack and to display the current/energy flux among the implemented systems.

2.1.2 Implementation Path

In order to organize the model, one "block" for each system of the vehicle is created. Starting from a given speed profile, a "pilot" block controls the acceleration deceleration sending signal to the motor/breaking system. Though the "mechanical drivetrain" block, it arrives to the "dynamics" block where the driving variable such as acceleration (a), speed (v) and position (x) are computed. When braking is needed to slow down the EV, the signal makes the "braking system" block calculate the available regenerative energy. The simulink structure of the model is displayed in Fig.(5.2).

2.2 Model Implementation

The model is implemented using power equations [6] [8] to relate the subsystems and regulate the driving simulation. Fig.(2.2) represents the conceptual scheme that

shows the interactions among the blocks and how each subsystem is related to the whole vehicle.

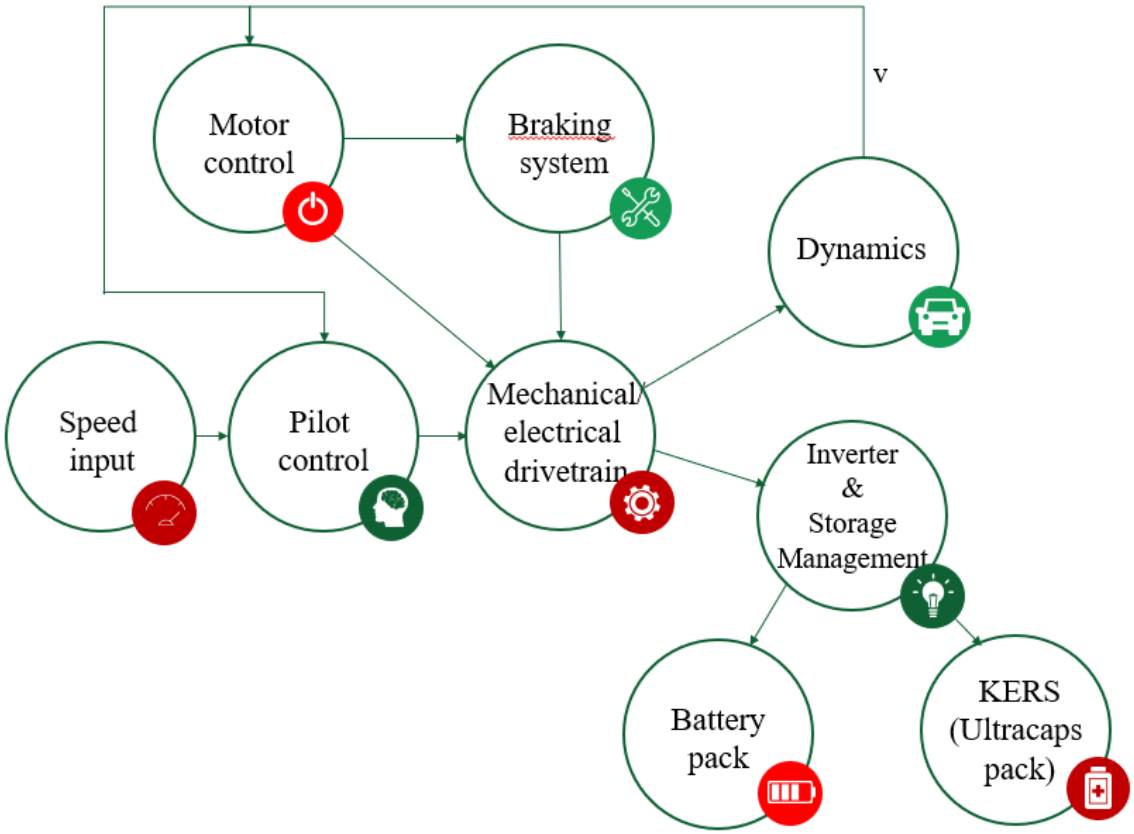

Figure 2.2: *Model conceptual scheme*

2.2.1 Input block and Pilot Speed Control

Drive Cycle

This block produces drive-cycle data, as used in many automotive applications. It outputs displacement, velocity and acceleration, all in SI units. It is possible to choose from a list of popular cycles.

The chosen one for the simulation is the "$WLTP\ class3$" because of the fast variability of the speed speed which is ideal to simulate the prototype. The frequent accelerations/decelerations that are needed to properly test the KERS.
The speed ($v_{drivecycles}$) works as input for the whole model.

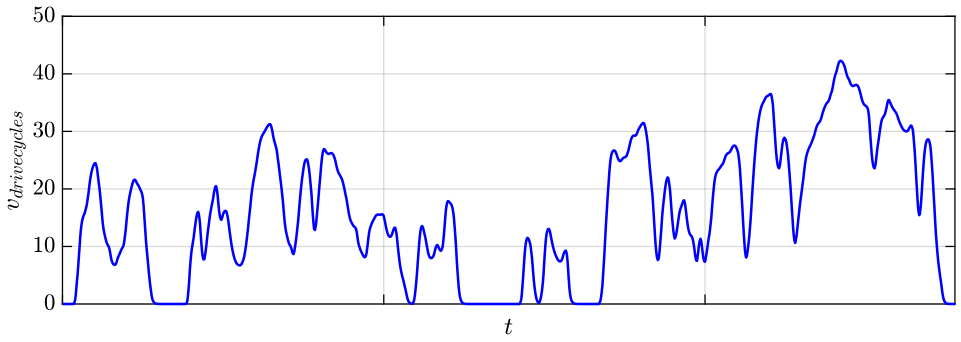

Figure 2.3: *Input speed profile*

"Pilot Control"

A PID controller compares the input speed generated by the block above with the actual speed of the vehicle and releases an acceleration/ braking signal proportional to the relative difference of the inputs.
The signal will be processed respectively by the mechanical drivetrain and the braking system blocks.

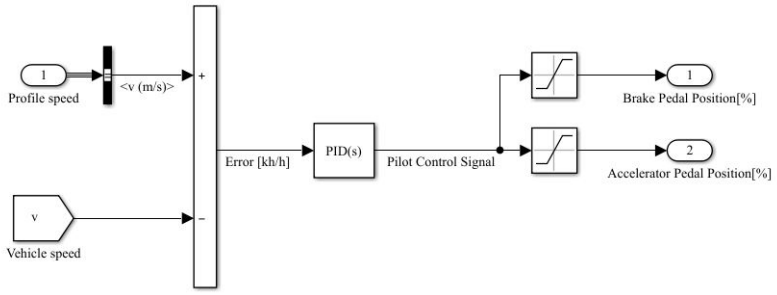

Figure 2.4: *Simulink block "Pilot Control"*

In the following graph (2.5), the action taken by the "pilot" is shown. It represents the intensity (in percentage) of the acceleration or deceleration requested in order to minimize the error between the input speed profile and the istantaneous vehicle speed.

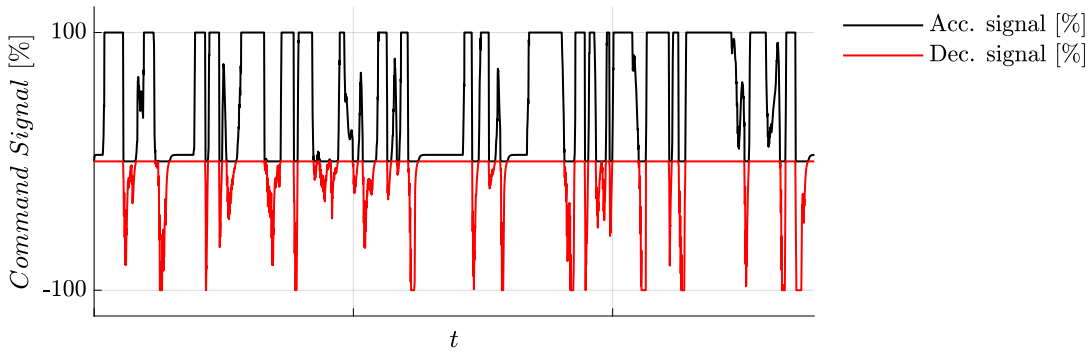

Figure 2.5: *Acceleration/deceleration signal intensity*

2.2.2 Motor

This block uses the speed of the vehicle to deliver the allowed torque τ_{mot} to the mechanical drivetrain block. The τ_{mot} is provided by the data-sheet of the motor in function of the angular speed of the motor ω_{mot}. Thanks to the relation: $\omega_{mot} = \frac{v}{r_{pneu}}$, where r_{pneu} is the radios of the wheels and according with the vehicle speed, it is possible to find the right ω_m for each time step.

Simulink implementation

In the model the motor is operated just in nominal condition. The possibility of exploiting it at full power is not implemented yet. This choice is taken to keep operational and safety margin during the prototype development and test phases.
The model is implemented on the based of the electric motor available for the project. It is a Three Phase Induction Motor of 6 [kW] of nominal Power. Then, considered the power required to move the vehicle (par.2.2.5), the model is simulated using two motors. The whole data-sheet is reported in Fig.(5.3; 5.4). The τ/ω characteristic slope of the two motors combination is reported in Fig.(2.6) :

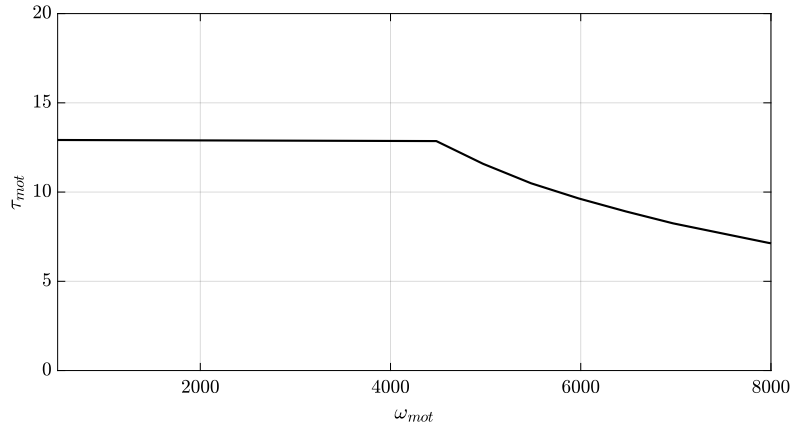

Figure 2.6: *Motor τ/ω characteristic slope*

2.2.3 Braking System

The braking block takes the braking signal, compares it with the maximum regenerative torque $(\tau_{reg_{max}})$ and computes:

- The allowed regenerative braking torque (τ_{reg});
- The additional friction braking $(\tau_{friction})$ required to properly slow down the vehicle.

The $\tau_{reg_{max}}$ value is chosen with an high margin tolerance in order to properly protect the operability and durability of the motor and the storage system.

Simulink implementation

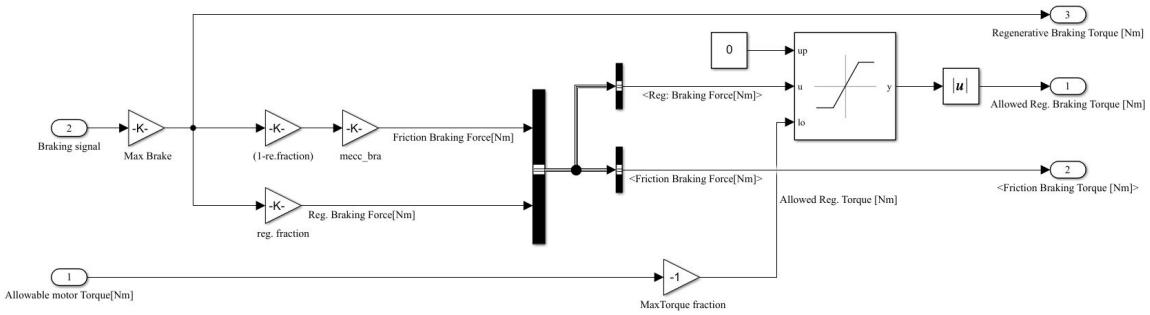

Figure 2.7: *Braking System block*

Simulation plots

2.2.4 Mechanical Drivetrain

The mechnical drivetrain block collects the inputs from the blocks (pr.2.2.3,pr.2.2.2,pr.2.2.1) and computes the power available for the traction.

The net torque to the motor is computed, each instant of time, as:

$$\tau_{mot_{net}} = \tau_{mot} - \tau_{friction} - \tau_{reg_{braking}} \tag{2.1}$$

The motor power (P_{motor}):

$$P_{motor} = \omega_m \tau_m \tag{2.2}$$

The mechanical/electrical losses are also computed trough the assumption of η_{mel}.

Simulation plot

In the graph (2.8) reported below, the different components of the torque at the vehicle shaft for direct operation (motor traction) and reverse operation(braking phase) are displayed:

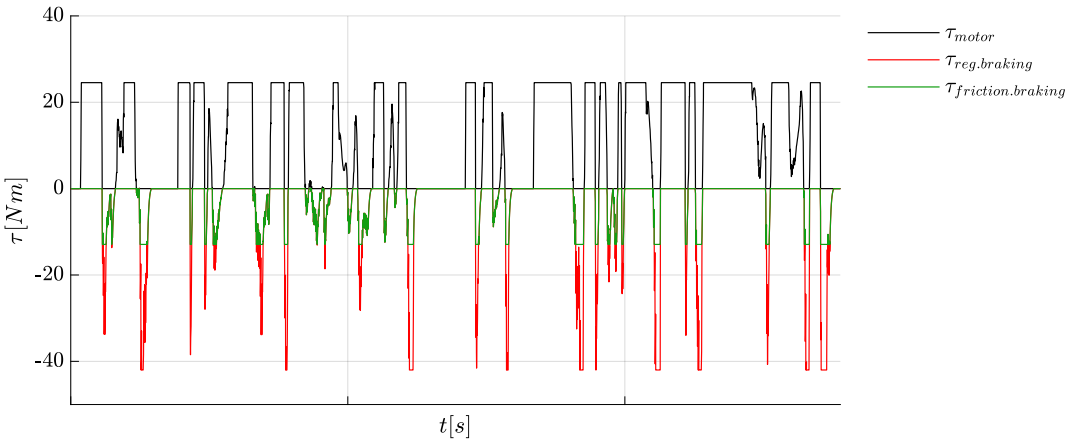

Figure 2.8: *Net tourque components*

Under acceleration condition, all the available tourque is fastly exploited. For the deceleration phases, the regenerative braking is enough just for the easiest cases. When the braking required peaks, the friction braking system supports, usually for a short time-frame, the regenerative braking.

2.2.5 Dynamics

In the dynamics block, the power balance equation of the vehicle is implemented. The angular acceleration ($\dot{\omega_m}$), the angular speed (ω_m) as well as the linear acceleration (a), the linear speed (v) and the position (x) per each time step are computed [8] [6].

Project choices

The rear-wheel drive is selected because thus configuration best enhances the performance of the vehicle. This type of traction is the most used by sports cars. The main advantages of rear-wheel drive are the better grip in acceleration and the greater possibilities of controlling the vehicle for an expert pilot.

Force scheme

The 2D forces scheme is resumed in Fig.(2.9).

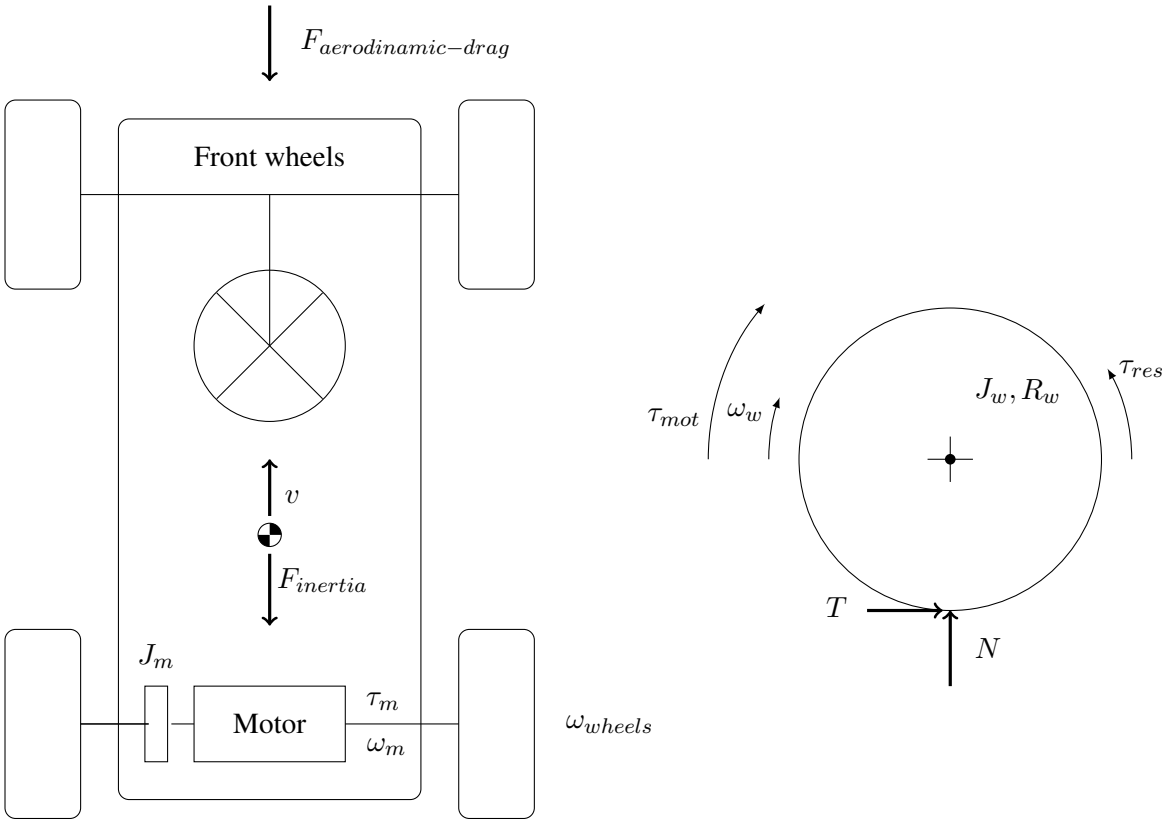

Figure 2.9: *Vehicle forces scheme*

The relation between the motor rotational speed ω_m and the wheels rotational speed ω_w is $tr = \dfrac{\omega_w}{\omega_m}$, wehere tr is the transmission (generally is it not required for an EV but is theoretically implemented in this work: $tr = 1$).
J_m represents the motor moment of inertia, J_w the wheels moment of inertia, R_w is the prenumatic radius and τ_{res} is the friction torque resistance.

Mathematical implemetation

The analysis is theoretically based and implemented in 2D. The objective of the mathematical analysis is to obtain the motion equation to describe the vehicle variables in each driving condition.
The study starts from the power balance of the EV:

$$P_{motor} + P_{resistant} + P_{losses} = 0 \tag{2.3}$$

So:

$$P_{motor} = \tau_m \cdot \omega_m - J_m \dot{\omega_{\mathbf{m}}} \cdot \omega_m$$

$$P_{resistant} = -Mgsin(\alpha) \cdot v - \tau_{res} \cdot \omega_w - \frac{1}{2}\rho_{air} S_{frontal} C_D v^3 - J_r^* \dot{\omega_{\mathbf{m}}} \cdot \omega_m \tag{2.4}$$

$$P_{losses} = -(1-\eta)\tau_m \cdot \omega_m$$

Where v is the speed of the vehicle, M is the overall weight of both vehicle and pilot, g is the gravity acceleration, η_{mel} is the mechanical and electrical efficiency, α is the tilt angle of the road (in this study $\alpha = 0$), ρ_{air} the density of the air, $S_{frontal}$ frontal surface of the vehicle, C_D the aerodinamic drag coefficient and $\dot{\omega_m}$ the angular acceleration of the motor.
The first equation in composed by the power of the motor (first term) reduced by the motor inertia. This inertial term, as well as the last term of the second equation, can be obtained looking for the first order derivative of the kinetics energy for both motor and user side:

$$\begin{aligned}
\frac{\mathrm{d}\,E_{k_{mot}}}{\mathrm{d}\,t} &= \frac{\mathrm{d}}{\mathrm{d}\,t}\left(\frac{1}{2}J_m\omega_m^2\right) = J_m\dot{\omega_{\mathbf{m}}}\cdot\omega_m \\
\frac{\mathrm{d}\,E_{k_{user}}}{\mathrm{d}\,t} &= \frac{\mathrm{d}}{\mathrm{d}\,t}\left(\frac{1}{2}J_w\omega_w^2\cdot 4 + \frac{1}{2}Mv^2\right) = \left(J_w + MR_w^2\right)tr^2\dot{\omega_{\mathbf{m}}}\omega_m \\
&= J_r^* tr^2\dot{\omega_{\mathbf{m}}}\omega_m
\end{aligned} \tag{2.5}$$

The relation $v = \omega_w R_w = R_w \cdot tr \cdot \omega_m$ is used to go from the linear speed of the vehicle to the motor angular speed. The second power equation (2.4) can be better represented by substituting the following relations:

$$\begin{aligned}
\tau_{res} &= N_{4w} f_d R_w \\
N_{4w} &= Mgcos(\alpha)
\end{aligned} \tag{2.6}$$

with N_{4w} is the vincolar reaction with the ground for all the 4 wheels and f_d the dynamic friction.
The third power equation eq.(2.4) represents the power losses of the system.
By substituting eq.(2.6) into eq.(2.4) and finally in eq.(2.3), the equation of motion is found:

$$\begin{aligned}
\eta(\tau_m - J_m\dot{\omega_{\mathbf{m}}})\omega_m =& Mg[f_d cos(\alpha) + sen(\alpha)]R_w\cdot tr\cdot\omega_m \\
&+ 1/2\rho_{air}S_{frontal}C_D\omega_m^3 R_w^3 tr^3 \\
&+ J_r^*\dot{\omega_{\mathbf{m}}}\omega_m tr^2
\end{aligned} \tag{2.7}$$

The term before the equal represents the power at the motor side discounted by the motor inertia. The terms after the equal sign show in this order:

- Rolling and grading resistance;
- Aerodynamic drag;
- Inertial resistance.

So, from the eq.(2.7), the angular acceleration results:

$$\dot{\omega_{\mathbf{m}}} = \frac{\eta\tau_{\mathbf{m}} - Mg\left[f_d cos(\alpha) + sen(\alpha)\right]R_w tr - 1/2\rho_{air}S_{frontal C_D}\omega_m^2 R_w^3 tr^3}{\eta J_m + J_r^*\tau^2} \tag{2.8}$$

According with the motion equation (2.7), the acceleration at the starting point ($\omega_m = 0$) , the available engine torque (τ_m) at full speed ($\frac{\mathrm{d}\,\omega_{mot}}{\mathrm{d}\,t} = 0$) as well as the front wheels adherence in each driving condition are preliminarily studied.

Simulink implementation

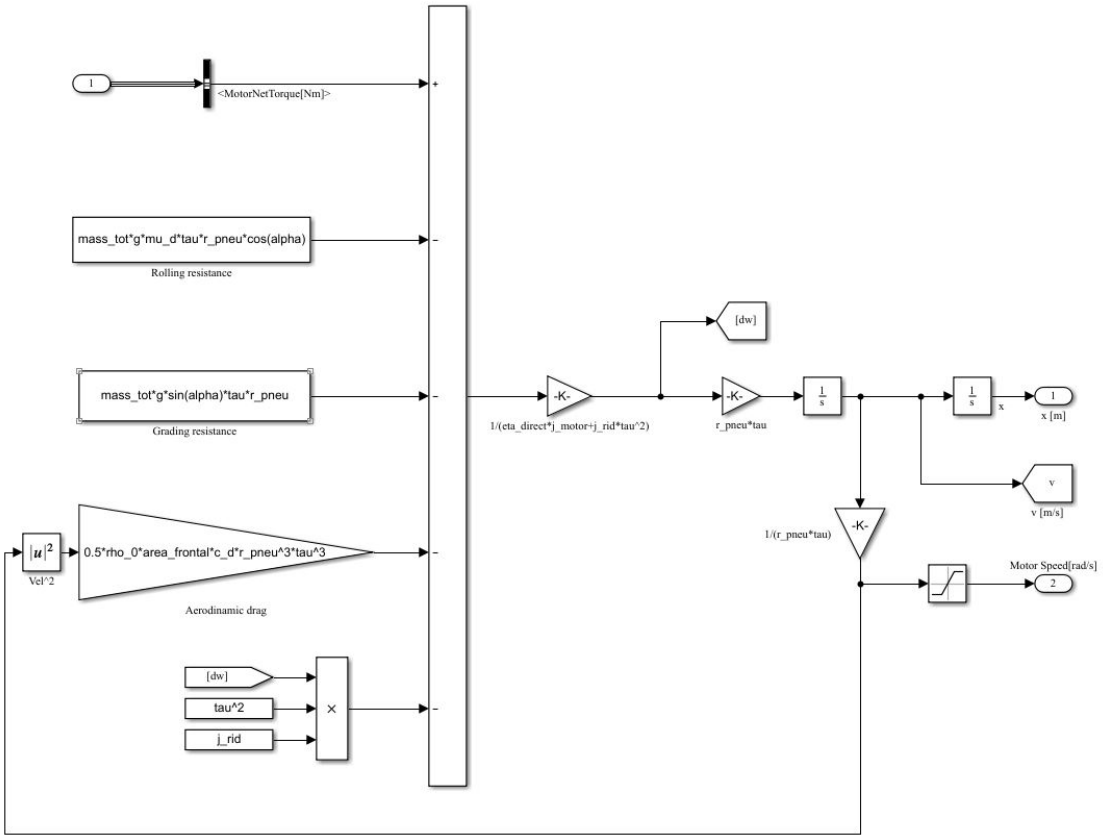

Figure 2.10: *Dynamics block*

Simulation plots

In Fig.(2.11) below the vehicle speed with the drive-cycle speed is reported.

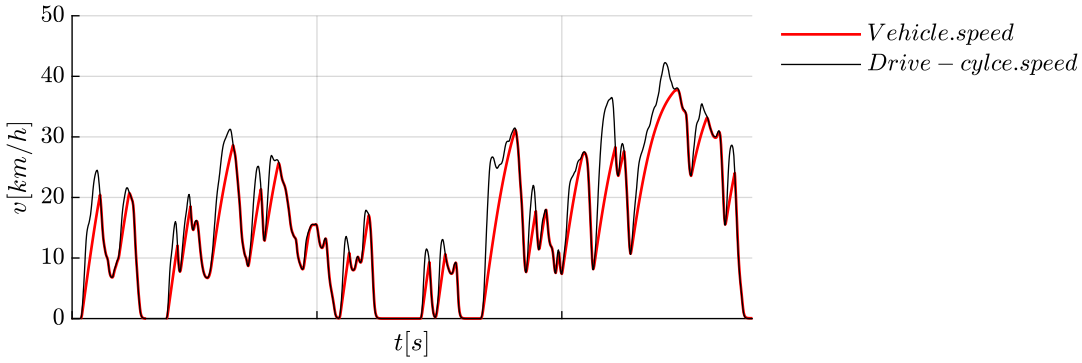

Figure 2.11: *Vehicle speed profile vs drive-cycle speed*

The vehicle (red line) is able to follow the speed profile (black line) for all the deceleration phases. It means that the friction and regenerative braking system are enough for this small speed drive test. Instead, it has not enough power to permorm the hardest acceleration required by some drive-cycle time frames (remember that the simulation is permformed at nominal motor operation but it can work, according with the data-sheet 5.3, at more than 3 times the nominal operation).

2.2.6 Inverter and Storage Management

This block receive as input the power required by the motor. It compute the power at the inverter DC side through:

$$P_{inv} = \eta_{inv} P_{motor} \tag{2.9}$$

Dividing this value for the voltage of the battery pack (V_{BP}), the total current required (I_{tot}) is found. At this point, depending on the direct or reverse operation, an output signal is created to regolate the operation of the KERS. The current required from/delivered to the battery pack is calculated as the total current (I_{tot}) discounted by the KERS current (I_{KERS}).

From the motor to the DC side of the inverter

In the Fig.(2.12) below the electrical scheme [24] of the inverter is shown:

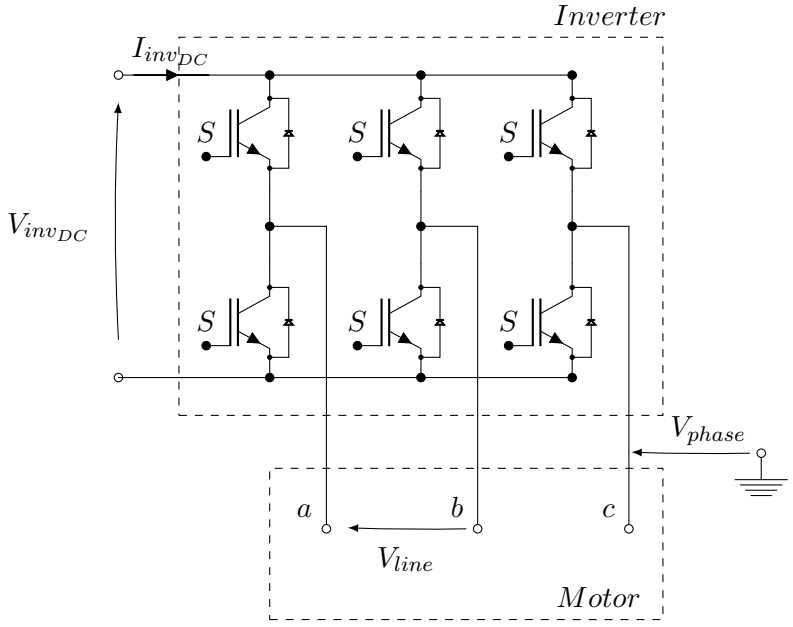

Figure 2.12: *Inverter*

it is assumed the phase voltage of the motor (V_{phase}):

$$V_{phase} = \frac{V_{inv_{DC}}}{2} M_i \tag{2.10}$$

where M_i is the modulation index. Considering the root min square of the phase voltage $V_{phase_{RMS}} = \frac{V_{phase}}{\sqrt{2}}$, the nominal voltage of the motor ($V_{mot_{NOM}}$) is eqaul to:

$$V_{mot_{NOM}} = V_{lineRMS} = \sqrt{3} V_{phase_{RMS}} \tag{2.11}$$

The inverter voltage at the DC side is expressed as:

$$V_{inv_{DC}} = \frac{2\sqrt{2}}{\sqrt{3}} \frac{V_{mot_{NOM}}}{M_i} \tag{2.12}$$

At this point, also the inverter current at the DC side ($I_{inv_{DC}}$) (thus the total current I_{tot}) can be calculated as:

$$I_{inv_{DC}} = \frac{P_{mot}}{V_{inv_{DC}}} \eta_{inv} \tag{2.13}$$

Simulink implementation

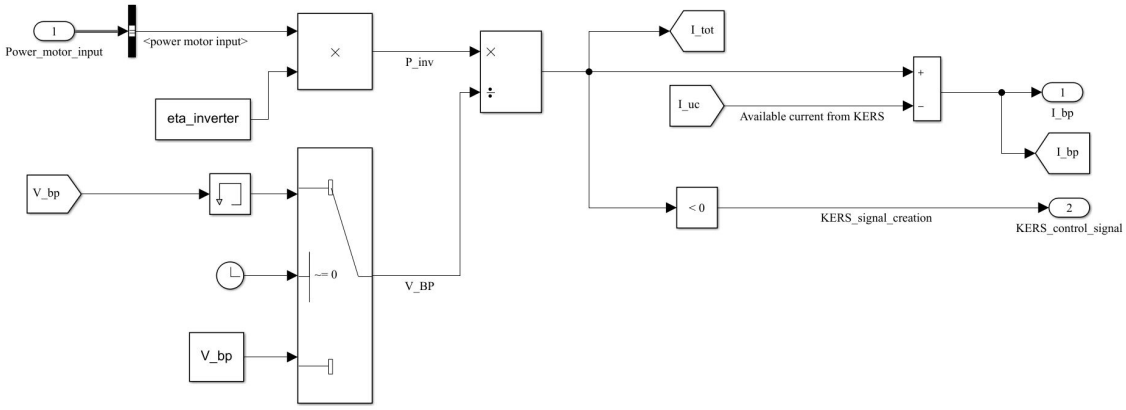

Figure 2.13: *Inverter and storage management block*

2.2.7 Battery Pack

This block receives as input the current (I_{BP}) that should be managed by the BP and it computes the State of Charge (SOC) and the respective voltage V_{BP} per each time step $(\triangle t)$. The block presents also a backstop function to stop running the model below a certain level of SOC or V_{BP} due to operational limit and technology durability.

Single Cell theoretical implementation

The implementation of the single cell is performed with a physical based approach [9].
A general designing situation in which there are no information about materials, geometry and chemistry of the cell is assumed. A closed system in which reactants and products are stored inside is defined. Due to the impossibility to locally measure the chemical activity (a) of the species, a relation with the SOC is stated:

$$\begin{aligned} \{a_{D_+}, a_{D_-}\} &\propto (1 - SOC) \\ \{a_{C_+}, a_{C_-}\} &\propto SOC \end{aligned} \tag{2.14}$$

Where the subscript D and C state respectively for discharge and charge, while $+$ and $-$ the positive and negative electrode.
Adding to these considerations the following stringent hypothesis:

- stady state operation;
- homogeneous reactions;
- Ohms law in the electrolyte;
- no mass transport effects;

The Butler-Volmer equation, that correlate the current with the positive and the negative metal potential ($\phi = E + \eta$), can be written:

$$i = n_s F \left(k_o a_o^{v_o} \exp \frac{\beta_o F(E+\eta)}{RT} - k_r a_r^{v_r} \exp \frac{-\beta_r F(E+\eta)}{RT} \right) \tag{2.15}$$

With the subscript o and r that respectively state for oxidation and reaction, n_s is the number of the electrochemical steps (excluding repetitions), k_o andk_r are the chemical equilibrium coefficients, ν_o and ν_r are the activity coefficients, β_o and β_r are the oxidation/reaction parameters, F the Faraday constant, η is the overpotential and E is the equilibrium electrode potential.
Assuming additionally $\nu_o = \nu_r = 1$ and $n_s = 1$, we can write the equation for the anode (negative electrode), for the cathode (positive electrode) and the electrolyte:

$$\text{anod } I = F \left(k_o^- SOC \exp \frac{\beta_o^- F(E^- + \eta^-)}{RT} - k_r(1 - SOC) \exp \frac{-\beta_r^- F(E^- + \eta^-)}{RT} \right)$$

$$\text{cathode } -I = F \left(k_o^+ (1 - SOC) \exp \frac{\beta_o^- + (E^- + \eta^+)}{RT} - k_r SOC \exp \frac{-\beta_r^+ F(E^- + \eta^+)}{RT} \right)$$

$$\text{electrolyte } \eta_{el} = R_{el} I$$

With R_{el} the electrolyte resistance. The overall cell voltage V_{cell} can be now written as:

$$V_{cell} = E^+ + \eta^+ - E^- - \eta^- - \eta_{el} \tag{2.16}$$

Single Cell simulation

Using the theoretical analysis reported above, the single cell operation under a constant charge/ discharge current is simulated on Matlab. The SOC variation is computed implementing:

$$\triangle C = I_{discharge} \triangle t \tag{2.17}$$

where C is the capacity of the cell. In this way the SOC_i, at each time step, can be find as:

$$SOC_i = SOC_{i-1} - \frac{\triangle C}{C_{nom}} \tag{2.18}$$

The simulation results are displayed in Fig.(2.14) above:

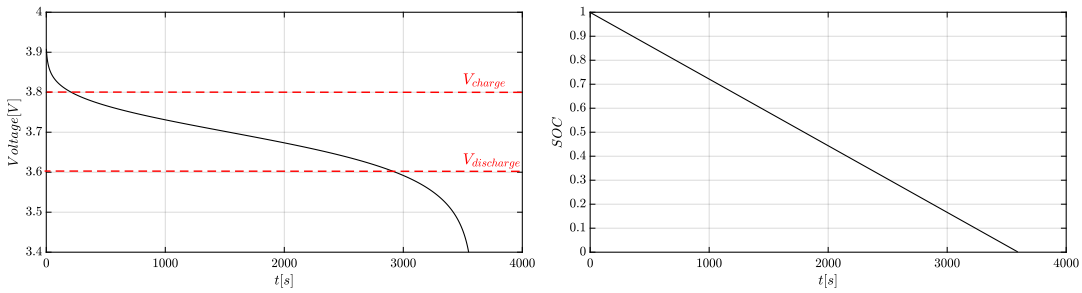

(a) **(b)**

Figure 2.14: *Single cell behavior at constant discharge current*

The charge and discharge voltage which limit the operations are shown in Fig.(2.14a). The choice is to work as far as possible inside the "linear" area of the voltage discharge curve. This is important in order to preserve the cell life-time by reduce the stress in the most critical condition that are the extreme ones (minimum and maximum SOC). Moreover, it is fundamental to have a linear behavior to correctly predict the output voltage of the device for the proper operation of the systems that are connected to it. Infact, outside of that area, the voltage drops in an quasi-exponential way that is not manageble.
As expected, in Fig.(2.14b) is shown that the SOC decrease linearly for a constant discharge current

Sizing of the Battery Pack (BP)

The correct sizing of the battery pack is crucial point in the design of the vehicle because of the energy storage needed, the voltage and current required, the mass and volumetric constraints and the thermal and control problems (the thermal and control topics are not evaluated in this work).
The BP works as the main storage source of the vehicle and the lay-out is derived from the voltage (V_{inv}) and current (I_{inv}) requirements at the inverted DC side, computed in the par.(2.2.6).
The cells are connected in series forming strings that are put in parallel in order to satisfy the application constraint. The number of cells in series (n_s) and the number of strings in parallel $(n_{//})$ is defined as:

$$\begin{aligned} n_s &= \frac{V_{inv}}{V_{cell}} \\ n_{//} &= \frac{I_{tot}}{I_{cell_{NOM}}} \end{aligned} \tag{2.19}$$

It is assumed that the charge and discharge is equal among all the cells. In this way, the resulting voltage of the battery pack (V_{BP}) is always the sum of equal cells voltage (V_{cell}): no voltage difference is considered between a string and an other. This also means, the current of the different strings is always the same.

Technology selection

The best battery choice for an high power, high current application like an EV is the lithium-ion technology (Li-ion).
Due to the lack of particular kind of batteries for the project, standard Li-ion values are assumed.

Simulink implementation

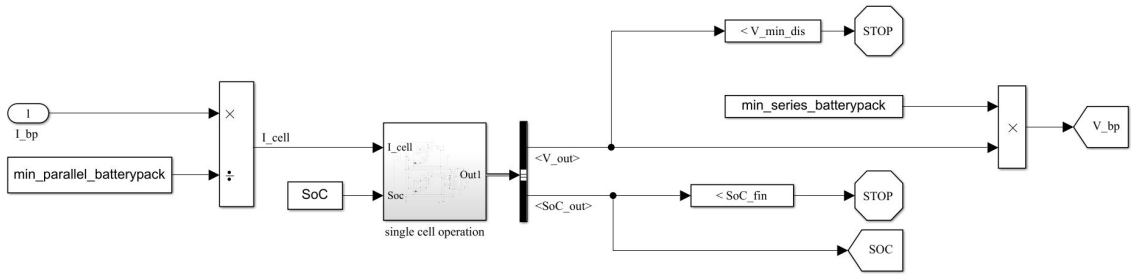

Figure 2.15: *Battery pack block*

Simulation plots

The three main parameters for the analysis of the BP operation current, voltage and SOC are reported in the Fig.(2.16) below. The first graph shows both the current (I_{BP}) drained by the motor (positive) and the one absorbed by the BP during regeneration (negative). In the second one the BP voltage (V_{BP}) is shown. The discontinuity of the voltage is due to the model used and to the absence of a filter implementation. However, the tendency of voltage decrease during discharge operation is well appreciable from the graph. The last one displays the SOC: the discharge rate is higher during the high current demand while it is appreciable the recharge during the braking time frame.

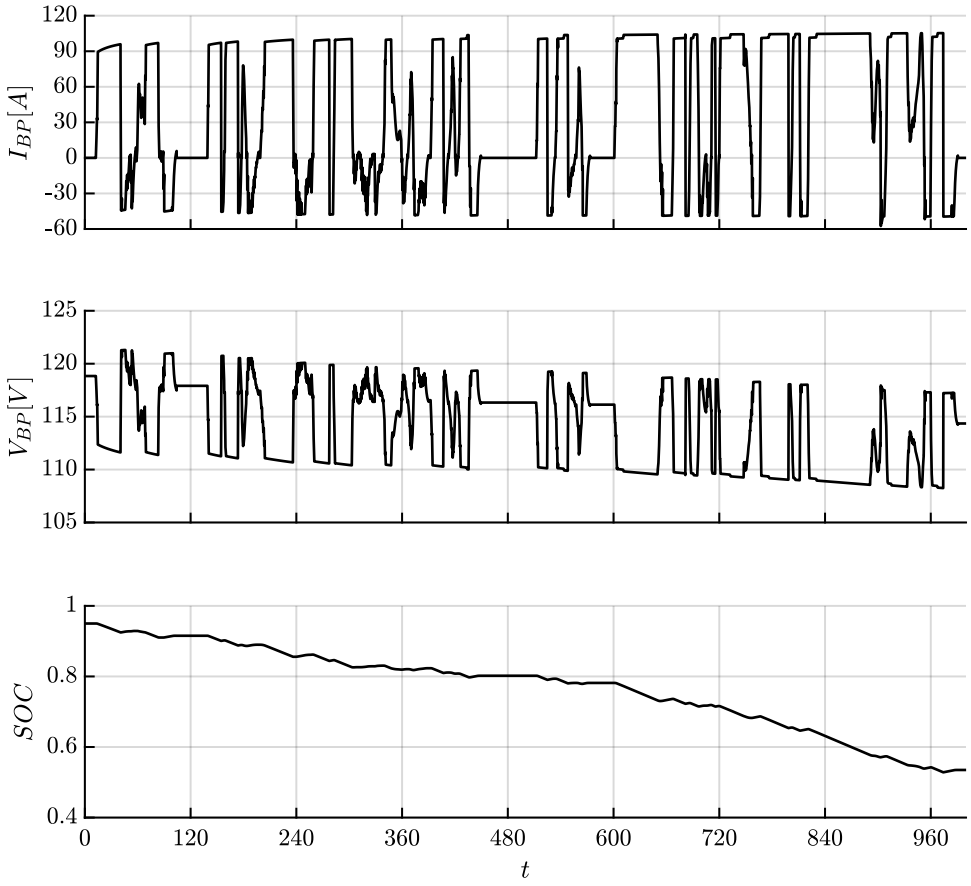

Figure 2.16: *Battery pack current; SOC; battery pack voltage*

2.2.8 KERS(Kinetics Energy Recovery System)

This block receive the input signal from the inverter and storage management block. The block output is the KERS current (I_{KERS}) which depend on the state of charge of the UC pack (SOC_{UC}) and the respective allowable charge and discharge current (I_{UC}). A relevant influencing factor on the output current is the power capability of the resonant converter (k).

System overview

A kind of Regenerative braking is called KERS [11]. To slow down a vehicle the kinetic energy of braking is commonly dissipated in the environment (lost) as thermal energy by the mechanical/hydraulic braking system. The importance of the KERS stands in the attempt of recovering as much as possible this energy lost. The KERS is an automotive system for recovering the moving vehicle's kinetic energy under braking phase. The recovered energy is stored in a reservoir for later use under when required. The electrical systems use a motor-generator incorporated in the car's transmission which converts kinetic energy into electrical energy and vice

versa.
There are different type of devices and forms in which the kinetic energy can be stored:

- Mechanical KERS
- Electric KERS
- Hydraulic KERS
- Hydro-electric KERS (HESS)

All the systems listed above have their advantages and draw backs. The most promising for the full electric automotive applications is the electric one. The well documented electrical systems utilizes batteries as the storage medium and an electric motor/generator systems as the energy transformation and control media. KERS components for battery storage systems are: electric propulsion motor/generator, power electronics-inverter, and the electrochemical storage. Pure Li-ion battery systems or combined batteries and super-caps technology can be used. Supercapacitors have special features such as long life, rapid charging and discharging, low internal resistance, high power density and simple charging method as compared to standard capacitors and batteries.
For this application, a combined system that uses concurrently battery and ultracaps is analyzed. It is designed and sized, then the functioning and limitations of this technology are studied.

Objective

The objective of this additional system is to use the UC peculiarities of high current capability, thermal stability, long ELD (Estimated Life Duration) and very fast behavior in both charge and discharge to help the BP in the most critical driving phase. The KERS is expected to absorb part of the kinetic energy recoverable during braking and to give it back during the peak demand in acceleration. It should be able to increase the performance of the EV under certain driving condition. The system should increase the overall range of the EV, improve the efficiency of the storage side and improve the life expectancy of the BP by managing the high current values in both charge and discharge. Consequently it reduces the thermal and frequency stress of the Li-ion storage system.

Concept scheme

The lay-out and the nomenclature of the KERS system is shown in Fig.(2.18) below:

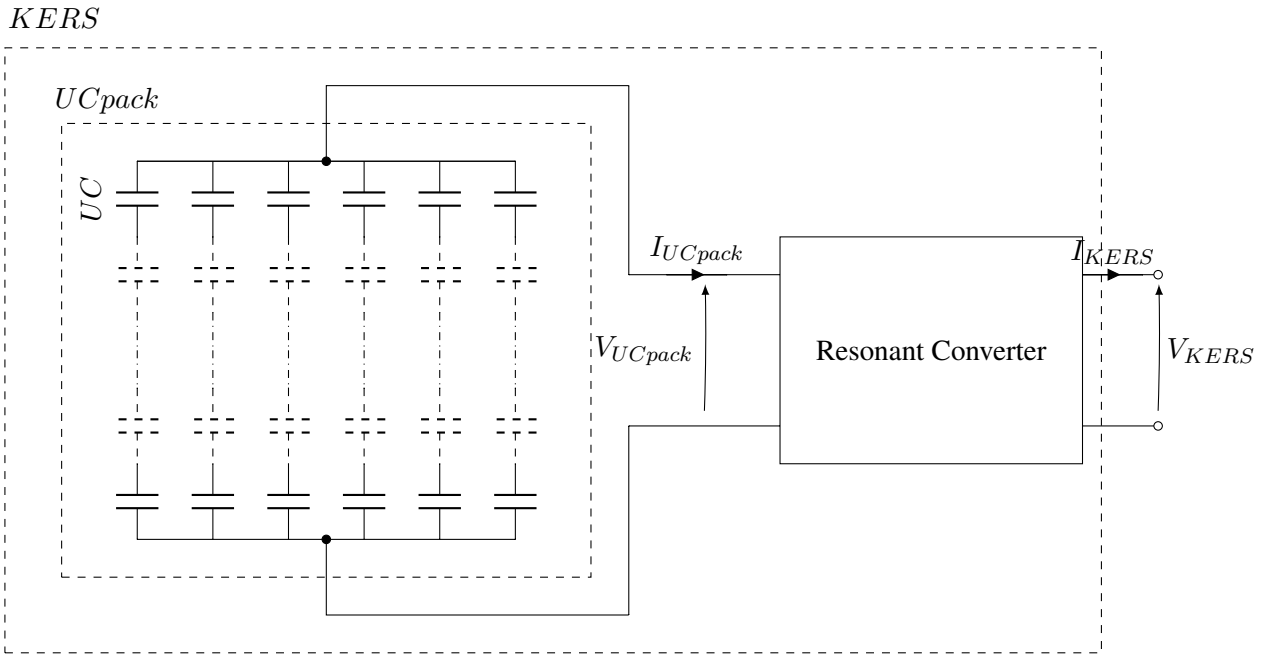

Figure 2.17: *KERS scheme*

In Chapter 3 the values of UC pack are consider the inputs to the system and "KERS" values are the outputs.

Sizing of the Ultracaps pack

The sizing process is similar to the BP one. The nominal voltage of the UC pack (V_{UCpack}) is set equal to inverter voltage (V_{inv}) and the number of UC in series is consequently chosen:

$$n_{s_{UC}} = \frac{V_{inv}}{V_{UC_{NOM}}} \tag{2.20}$$

Where $V_{UC_{NOM}}$ is the nominal voltage of each UC. Instead, the number of UC strings put in parallel is stated considering the weight and volume constraints of the vehicle ($n_{//_{UC}} = 1$).

Setting of the Minimum UC pack Voltage ($V_{UCpack_{min}}$)

The value of the minimum UC pack voltage ($V_{UCpack_{min}}$) is set in order to properly limiting the UC pack final discharge condition. The value is chosen according to the relation (2.21) as a compromize of operation between charge and discharge:

$$P_{KERS} = kP_{inv} = \eta_{res.conv} V_{UCpack_{min}} I_{UCpack_{max}} \tag{2.21}$$

So, V_{min} can be determined:

$$V_{UCpack_{min}} = \frac{kP_{inv}}{\eta_{res.conv} I_{UCpack_{max}}} \tag{2.22}$$

Simulink implementation

At each time step, the available I_{KERS} in direct/reverse operation is computed using the following eq.(2.23):

$$\eta_{res.conv} = \frac{I_{KERS} V_{inv}}{I_{UCpack} V_{UCpack}} \tag{2.23}$$

It is considered that V_{inv} is approximately fix due to the presence of a big BP and the UC pack is always working at maximum current ($I_{UCpack} = I_{UCpack_{max}}$). In this way, the I_{KERS} can be calculated for each V_{UCpack} condition:

$$I_{KERS} = \eta_{res.conv} I_{UCpack_{max}} \frac{V_{UCpack}}{V_{inv}} k \tag{2.24}$$

Where k is a capability constraint of the resonant converter that will be deeply analyzed in par.(3.6.6).
So, the UC voltage has to be computed. As input for direct (positive current) and indirect (negative current) operation the I_{KERS} is used. According with the signal control of the KERS and limitated by the min/max SOC_{UC}, the stored energy variation ($\triangle E_i$) of the UC pack is defined:

$$\triangle E_i = \frac{V_{UCpack_{(i-1)}} I_{KERS} dt}{3600} \tag{2.25}$$

Where the subscript i represent the value at this time step and $(i-1)$ the value at the time step before.
So, the actual stored energy is be defined as:

$$E_i = E_{i-1} + \triangle E_i \tag{2.26}$$

Assuming that the UC pack works at maximum constant current, the V_{UCpack_i} is:

$$V_{UCpack_i} = V_{UCpack_{NOM}} \frac{E_{UCpack_i}}{E_{UCpack_{NOM}}} \tag{2.27}$$

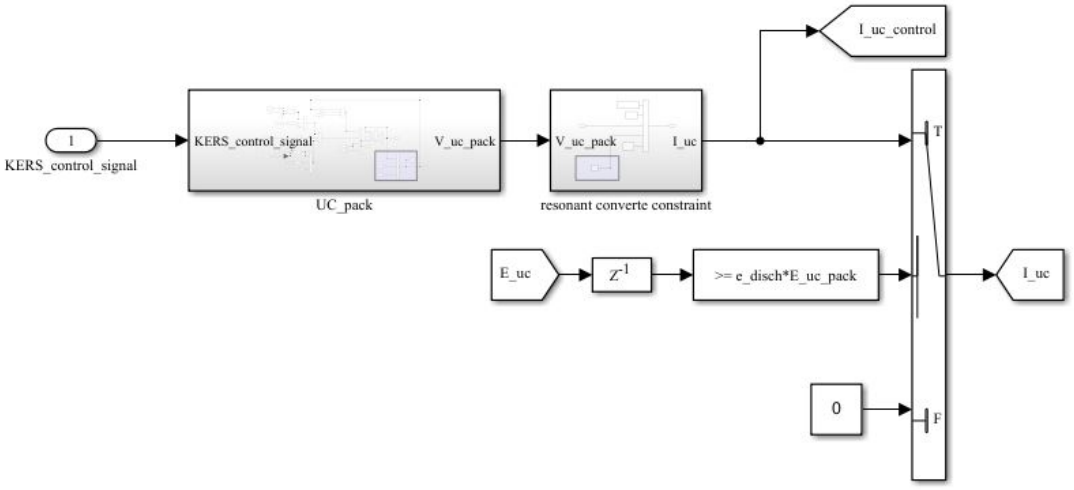

Figure 2.18: *KERS block*

Simulation plots

In the Fig.(2.19) the relevant parameters of the KERS operation are displayed.

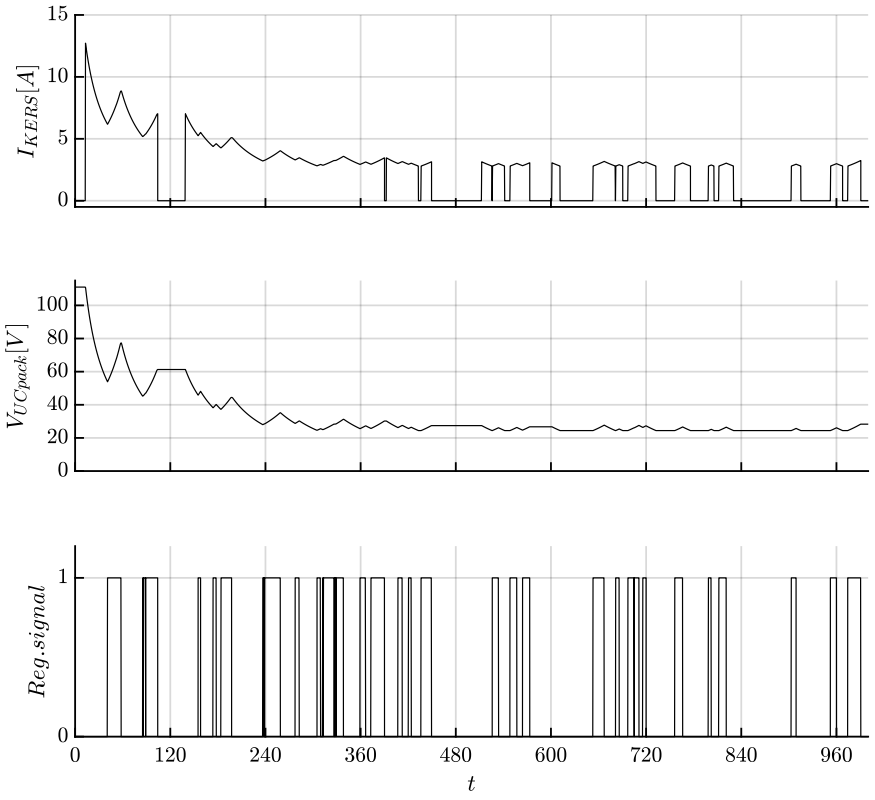

Figure 2.19: *KERS current; KERS voltage; regeneration signal*

As shown in the first graph, the current capability of the system decrease proportionally to voltage drop during discharge, according to the analysis performed at par.(2.2.8). In the second graph, the trend of UC pack is represented. The discharge voltage is limited by $V_{UCpack_{MIN}}$ discussed at par.(2.2.8). When the voltage of the UC pack reaches the minimum value, the KERS stops operate, as also confirmed by the correspondant drop to 0 of the I_{KERS}. In the last graph, the signal that control the regeneration during braking is displayed (1 on; 0 off) .

2.3 Simulation Data and Symbols

The important specification of the simulation are:

- is performed to test the formula SAE race of acceleration (d_1) and long distance (d_2);
- fixed step size with automatic solver selection;
- step size $dt = 1[ms]$.

2.3.1 Matlab workspace data

The data reported below are used to run the simulation. They came from the datasheets of the available parts (as motor and UC). The others are assumed based on theoretical assumption and referring to similar projects.

Race data			
distance 1	d_1	75	[m]
distance 2	d_2	2200	[m]
Mass data			
Pilot weight	$mass_{pilot}$	70	[kg]
Pilot car	$mass_{car}$	150	[kg]
Geometry			
Frontal area	$frontal_{area}$	1	[m^2]
Wheels radius	r_w	0.23	[m]
Wheelbase		1.2	[m]
Coefficients			
Air density	ρ_{air}	1.225	[kg/m^3]
Static friction	f_s	0.3	
Dynamic friction	f_d	0.01	
Mechanical/electrical efficiency	η_{mel}	0.97	
Aerodynamic friction coefficient	C_D	0.4	
Motor data			
Motor number	n_{motor}	2	
Wheels number	n_{wheels}	4	
Motor nominal voltage	$V_{motor_{NOM}}$	51	[V]
Motor nominal current	$I_{motor_{NOM}}$	118	[A]
Motor nominal power	$P_{motor_{NOM}}$	6	[kW]
Motor power factor	PF_{motor}	0.66	
Motor nominal frequency	$f_{motor_{NOM}}$	150	[Hz]
Inertia			
Motor inertia	J_{motor}	0.0078	[$kg \cdot m^2$]
Wheels inertia	J_{wheels}	0.155	[$kg \cdot m^2$]
Inverter			
Inverter efficiency	η_{inv}	0.95	
Resonant converter efficiency	$\eta_{res.conv}$	0.98	
Modulation index	M_{inv}	0.75	

Li-ion Battery parameters			
Ideal gas constant	R	8.314	[kJ/(kg · K)]
Faraday constant	F	96 485	[C/mol]
Bateery temperature	T	300	[K]
Negative electrode standard potential	E_{0_-}	0.7	[V]
Positive electrode standard potential	E_{0_+}	4.5	[V]
Membrane resistance	$R_{membrane}$	0.015	[Ω]
Cell mass	$mass_{cell}$	0.05	[kg]
Cell diameter	d_{cell}	0.018	[m]
Cell height	h_{cell}	0.065	[m]
Initial and final conditions for discharge or charge			
Minimum discharge voltage	$V_{cell_{min}}$	2.7	[V]
Maximum charge voltage	$V_{cell_{max}}$	4.5	[V]
Maximum current	$I_{cell_{max}}$	10	[A]
Nominal capacity	$C_{cell_{NOM}}$	2.5	[Ah]
Maximum State of charge	SOC_{max}	0.95	
Minimum State of charge	SOC_{min}	0.1	
UC parameters [LSUC 002R8S 0120F EA; Tab.(5.1)]			
Ultracaps capacity	C_{UC}	120	[F]
Nominal UC voltage	$V_{UC_{NOM}}$	2.8	[V]
Equivalent series resistance	R_{UCESC}	0.1	
Maximum UC current	$I_{UC_{max}}$	81	[A]
Leakage UC current	$I_{UC_{leak}}$	0.4	[A]
Nominal UC energy	$E_{UC_{NOM}}$	0.13	[Wh]
UC weight	$mass_{UC}$	0.023	[kg]
UC diameter	d_{UC}	0.022	[m]
UC height	h_{UC}	0.046	[m]

The following values result from the analysis reported in this chapter. They can be used to design the vehicle itself, taking care of dimensions, thermal constraints, isolating material and vehicle shape that are not studied in this work.

Inverter DC side			
Inverter current	I_{inv}	113.7	[A]
Inverter voltage	V_{inv}	111	[V]
BP sizing			
Cell nominal power	P_{cell}	38	[W]
Cell nominal energy	E_{cell}	9.5	[Wh]
Cells in series	n_s	30	
Stings in parallel	$n_{//}$	11	
Total cells	n_{BP}	330	
BP weight	$mass_{BP}$	16.5	[kg]
BP volume	Vol_{BP}	0.4	[m^3]
BP nominal voltage	V_{BP}	114	[V]
BP nominal current	V_{BP}	110	[A]
BP nominal power	P_{BP}	12.5	[kW]
BP nominal energy	E_{BP}	3.135	[kWh]
UC pack sizing			
UC pack nominal voltage	V_{UCpack}	111	[V]
UC in series	n_{UC_s}	79	
UC stings in parallel	$n_{UC_{//}}$	1	
Total UC	n_{UC}	79	
UC pack weight	$mass_{UCpack}$	1.81	[kg]
UC pack volume	Vol_{UCpack}	0.25	[m^3]
UC pack nominal power	P_{UCpack}	17.91	[kW]
UC pack nominal energy	E_{UCpack}	10.27	[Wh]
UC pack minimum voltage	$V_{UCpack_{min}}$	25.5	kHz

CHAPTER 3

KERS converter

In this chapter, a preliminary overview of the resonant converters properties is performed. The operation topology in boost [13] [27] (UC discharge) and buck (UC charge) modes as well as the characteristics of the chosen converter configuration in Fig.(3.5) for the EV application are analyzed [20] [23] .

3.1 Resonant Converters Characteristics

The resonant converter is taken into analysis for this EV application mainly because of the following characteristics:

- high efficiency also at high switching frequency [23];
- feasible compactness and scalability [23].

The passive components of the converters such as inductors, capacitors as well as the heat sink for the semiconductor components occupy a large portion of the overall size. Therefore, by reducing the size of the passive components, higher power density can be achieved. An effective way to do that is to increase the switching frequency. However, conventional PWM converters process power by interrupting the power flow by means of hard switching and thus suffer from high switching losses [14].
The switching losses are negligible in resonant converters [15]. This class of converters contains a resonant inductor-capacitor ($L-C$) network, also defined resonant-tank. In each switching cycle, the voltage and current waveforms vary sinusoidally in one or more sub-intervals [24] (topological steps). The commutation of the switches is usually with zero-voltage switching (ZVS) or zero current switching (ZCS). Due to the soft switching properties, the switching losses and stresses of

resonant converters are reduced with respect to PWM converters.
The general drawbacks of the resonant converters are generally due to the high peak values of the current in input to the resonant inductor that require a filter to be managed [15]. Then, also the control strategy is more complicated with respect to PWM converters [16].

3.1.1 Resonant Switches

To improve the switching behavior and reduce the switching losses, the zerocurrent-switching (ZCS) and zero-voltage-switching (ZVS) techniques are proposed. By incorporating an $L-C$ resonant tank, the concept of resonant switch is introduced. The resonant switches are classified in two types: zero-current (ZC) resonant switch and zero-voltage (ZV) resonant switch [20] [23] [25].
For the ZC resonant switch, an inductor is connected in series with a power switch. At turn-on, the current in the switch rises slowly in a quasi-sinusoidal from zero. Then due to the resonance of the $L-C$ tank, this current will oscillate until the zero current duration. If there is a diode connected in anti-parallel with the switch, the current is allowed to flow in both directions, this is called full-wave mode (Fig.3.1). Otherwise the current can only flow in the positive cycle and it is called half-wave mode (Fig.3.2) [20]. With this technique the current waveform of the switching device behaves in a quasi-sinusoidal manner to reach ZCS conditions during both turn-on and turn-off.

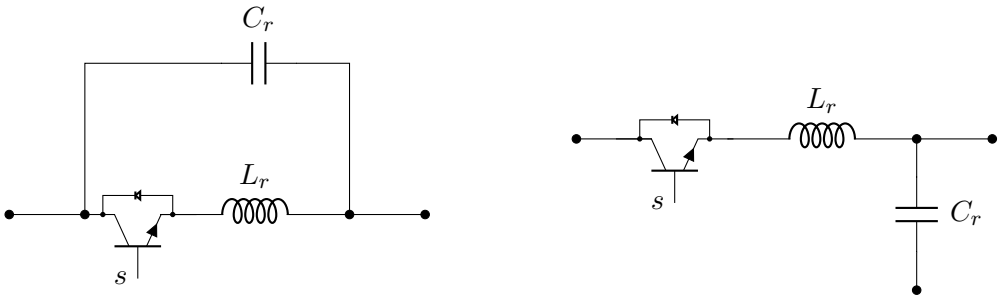

Figure 3.1: *Full wave mode zero current resonant switch (ZC)*

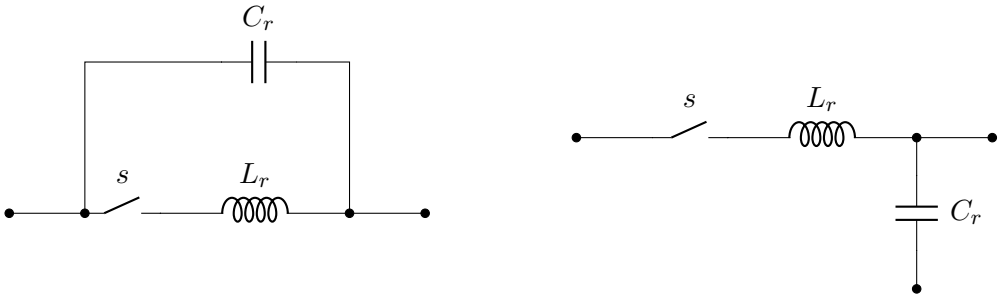

Figure 3.2: *Half wave mode zero current resonant switch (ZC)*

For the ZV resonant switch, a capacitor is connected in parallel with the switch. The voltage waveform of the switch can be shaped in a quasi-sinusoidal curve. If the switch is connected with an anti-parallel diode, the voltage will be clamped at zero

during the negative switching cycle. Similarly, this is called as half-wave mode (Fig.3.4). On the other hand, the voltage can also oscillate in negative switching cycle and is called full-wave mode (Fig.3.3). The ZVS conditions is created with this technique and the switching losses are eliminated [20].

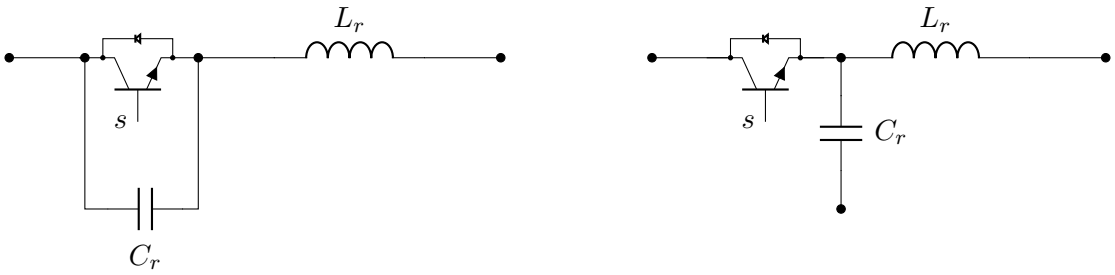

Figure 3.3: *Full wave zero voltage resonant switch (ZV)*

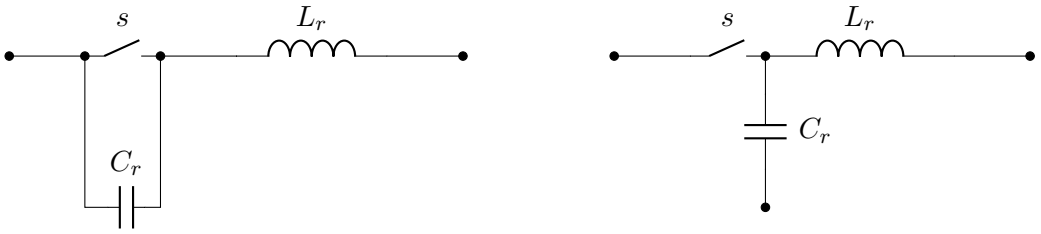

Figure 3.4: *Half way zero voltage resonant switch (ZV)*

The resonant converter is created adopting the ZV resonant switches strategy.

3.1.2 Converter conception

The conception of the converter comes from [12], [13] and [27]: the already known resonant boost converter in Fig.(3.5) where the resonant tank is underlined by the red dashed line:

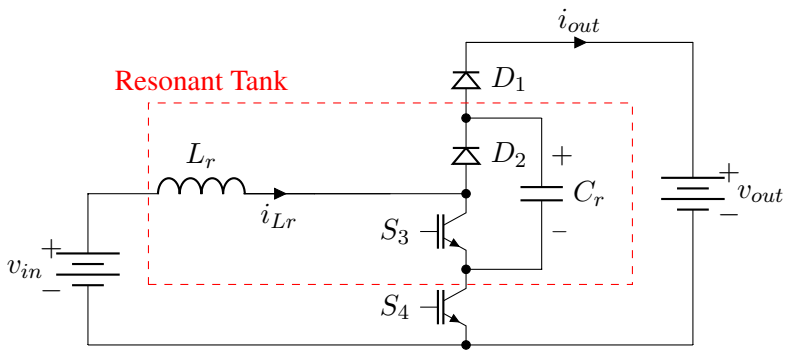

Figure 3.5: *Resonant boost converter*

Through the addition of two other switches and two other diodes [23], underlined by the green dashed line, it is made a bi-directional buck-boost converter Fig.(3.6): this means it has the peculiarity of working as a boost ($G_{boost} > 1$),

from the "left" to the "right" of the FIg. below, to discharge the UC pack; instead, it operate as a buck ($G_{buck} < 1$), from the "right" to the "left" of the Fig. below, to charge the UC pack. It is a new resonant converter configuration without literature references for an EV KERS management .

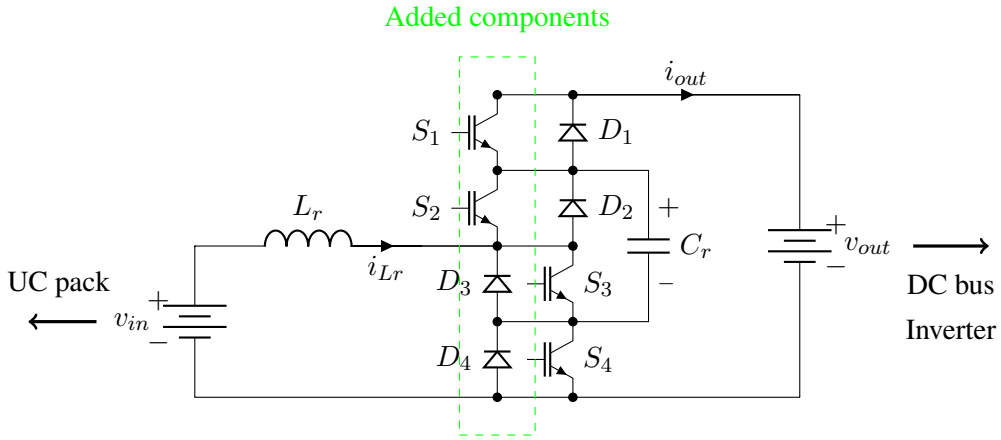

Figure 3.6: *Resonant buck-boost converter*

3.2 Investigation of converter topology

The converter topology investigated in this work is shown in Fig.(3.5). It is a buck-boost converter operating in resonant mode. The resonant tank is composed by the resonant inductor (L_r) and the resonant capacitor (C_r). Four switches (S_1, S_2, S_3, S_4) and four diodes (D_1, D_2, D_3, D_4) are used to operate the device. In this analysis, they are supposed to be ideal. It is also assumed that the output and input capacitors (C_{out} displayed in Fig.(3.7) and C_{in} displayed in Fig.(3.13)) are large enough to keep the respectives output and input voltage (V_{out} and V_{in}) constant during one switching cycle.

3.3 Boost operation

For the boost operation, the equivalent load is represented by C_{out} and R_{out} as shown in Fig.(3.7). The analysis performed in this paragraph regards the discharge phase of the UC pack: the energy is flowing from V_{in} side to the V_{out} side.

3.3.1 Switching cycle analysis(boost)

Due to the modulation strategy analysed, in the boost operation mode, the control signal of the two switches S_3 and S_4 is made of a complementary square-wave with 50% duty cycle while the switches S_1 and S_2 remain open. The two switches turn on complementary for half of the switching cycle and in each half part there are three stages related to the resonant tank behavior.

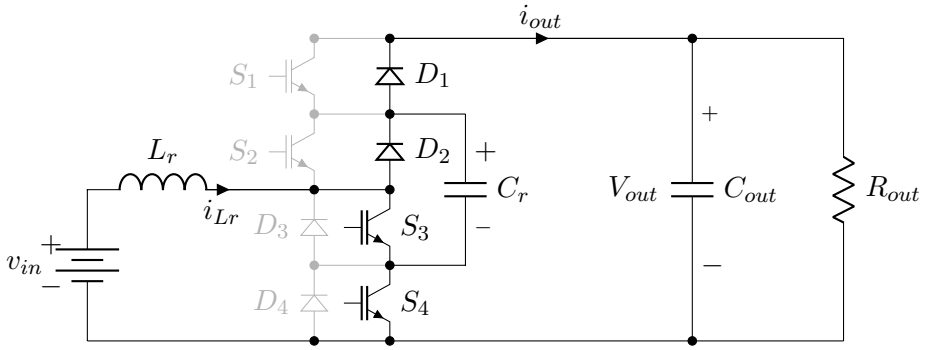

Figure 3.7: *Resonant boost*

Stage 1 [t_0, t_1]

At t_0, S_3 turns off and S_4 is turned on; D_2 is forward biased. During this stage, the resonant capacitor C_r is charged by the source as log as it reaches the voltage value in output V_{out}. Due to the resonance, the current through the resonant inductor L_r increases sinusoidally from 0 to a certain value, which is supposed to be I_1. This stage is shown in Fig.(3.8):

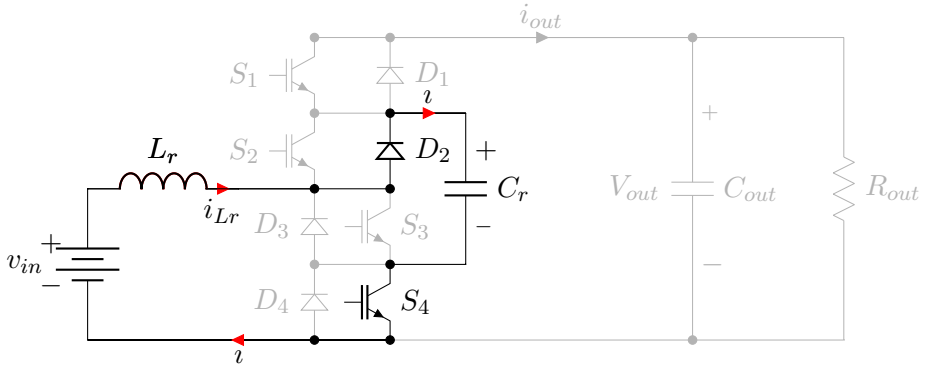

Figure 3.8: *Stage 1 (boost)*

This stage can be described by the following two equations:

$$\begin{cases} V_{in} = L_r \dfrac{\mathrm{d}i_{Lr}}{\mathrm{d}\,t} + v_{Cr}(t) \\ i_{Lr}(t) = C_r \dfrac{\mathrm{d}v_{Cr}(t)}{\mathrm{d}\,t} \end{cases} \tag{3.1}$$

Considering the regime operations, the initial conditions for the first topological stage are assumed:

$$\begin{cases} v_{Cr}(t_0) = 0 \\ i_{Lr}(t_0) = 0 \end{cases} \tag{3.2}$$

Applying the Laplace transformation [10], the following equation can be obtained:

$$\begin{cases} \dfrac{V_{in}}{s} = sL_rI_{Lr}(s) + V_{Cr} \\ I_{Lr}(s) = sC_rV_{Cr}(s) \end{cases} \tag{3.3}$$

And solving:

$$\begin{cases} I_{Lr}(s) = \dfrac{C_r}{s^2L_rC_r + 1}V_{in} \\ V_{Cr}(s) = \dfrac{V_i/s}{1 + s^2L_rC_r} \end{cases} \tag{3.4}$$

Now, considering the resonant angular frequency:

$$\omega_0 = \frac{1}{\sqrt{L_rC_r}} \tag{3.5}$$

And the resonant impedance:

$$Z_r = \sqrt{\frac{L_r}{C_r}} \tag{3.6}$$

Substituting:

$$\begin{cases} I_{Lr}(s) = \dfrac{1}{s^2 + \omega_0^2}\dfrac{V_{in}}{s} \\ V_{Cr}(s) = \dfrac{\omega_0^2}{\omega_0^2 + s^2} \end{cases} \tag{3.7}$$

At this point, the denominator of V_{Cr} has been decomposed though $Y(s) = \dfrac{A}{s} + \dfrac{Bs + C}{s^2 + \omega_0^2}$. Then, applying the inverse Laplace transformation [10] to (3.7):

$$\begin{cases} i_{Lr}(t) = \dfrac{sin(\omega_0 t)}{\omega_0}\dfrac{V_{in}}{L_r} \\ v_{Cr}(t) = V_{in}[1 - cos(\omega_0 t)] \end{cases} \tag{3.8}$$

Define the following parameters:

$$\overline{i_{Lr}(t)} = \frac{i_{Lr}(t)}{V_{in}/Z_r} \tag{3.9}$$

$$\overline{v_{Cr}(t)} = \frac{v_{Cr}(t)}{V_{in}} \tag{3.10}$$

Apply the parameterized inductor current and capacitor voltage:

$$\begin{cases} \overline{i_{Lr}(t)} = sin(\omega_0 t) \\ \\ \overline{v_{Cr}(t)} = 1 - cos(\omega_0 t) \end{cases} \tag{3.11}$$

The voltage gain of the converter is:
$G_{boost} = \dfrac{V_{out}}{V_{in}}$
At the end of this stage t_1, the following equation can be derived:

$$\begin{cases} \overline{i_{Lr}(t_1)} = \overline{I_1} \\ \\ \overline{v_{Cr}(t_1)} = 1 - cos(\omega_0 t_1) \end{cases} \tag{3.12}$$

Where:
$\overline{I_1} = \dfrac{I_1}{V_{in}/Z_r}$
It is already known that at t_1 the resonant capacitor C_r is charged untill the output voltage V_{out}, therefore:
$v_{Cr}(t_1) = V_{out}$
So:

$$\overline{v_{Cr}(t_1)} = G_{boost} \tag{3.13}$$

The duration of the first stage, which also corresponds to the charge of the resonant capacitor, can be expressed as:

$$\omega_0 \triangle t_{10} = \pi - arcos(G_{boost} - 1) \tag{3.14}$$

Where $\triangle t_{10} = t_1 - t_0$
It is also possible to define a vector Z in the state-plane as:

$$z = \overline{v_{Cr}(t)} + j\overline{i_{Lr}} \tag{3.15}$$

In conclusion the first stage can be described by the following vector:

$$z = 1 - cos(\omega_0 t) + jsin(\omega_0 t) \tag{3.16}$$

Stage 2 [t_1, t_2]

At t_1, S_4 is on and S_3 is off. The resonant capacitor voltage V_{Cr} is equal to the output voltage V_{out}, the diode D_1 turns on. So, in this stage V_{Cr} is clamped as V_{out}, while the current through the inductor i_{Lr} decrease linearly to zero, since the output voltage is higher than the input voltage. This leads to a negative voltage across Lr. This stage can be referred to Fig.(3.9):

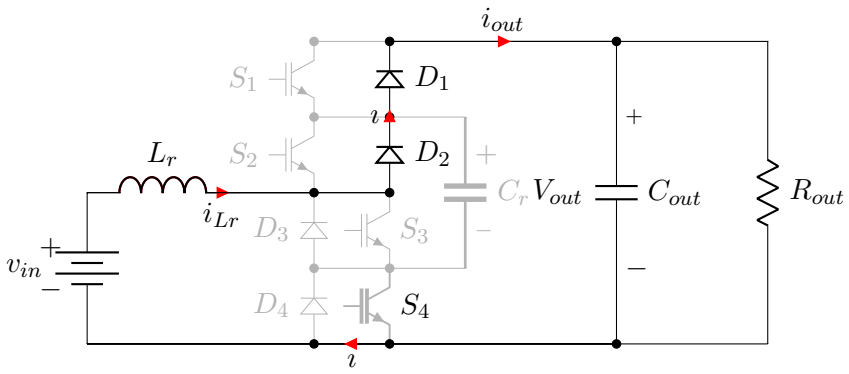

Figure 3.9: *Stage 2 (boost)*

Similarly, this stage can be described as:

$$\begin{cases} V_i + L_r \dfrac{\mathrm{d}i_{Lr}}{\mathrm{d}\,t} - V_{out} \\ \\ v_{Cr}(t) = V_{out} \end{cases} \tag{3.17}$$

With initial conditions:

$$\begin{cases} i_{Lr}(t_1) = I_1 \\ \\ v_{Cr}(t_1) = V_{out} \end{cases} \tag{3.18}$$

Applying again the Laplace trasformation as already done at step 1, the following equation can be found:

$$i_{Lr}(t1) = I_1 - \frac{V_{out} - V_{in}}{L_r}(t - t_1) \tag{3.19}$$

After the same parametrization of before:

$$\begin{cases} \overline{i_{Lr}(t)} = \overline{I_1} - (G-1)\omega_0(t - t_1) \\ \\ \overline{v_{Cr}(t)} = G \end{cases} \tag{3.20}$$

Where : $\overleftarrow{I_1} = \dfrac{I_1}{G-1}$ At the end of the stage 2 (t_2), the inductor current drop to zero:

$$I_1 - (G-1)\omega_0 \triangle t_{21} = 0 \tag{3.21}$$

The duration is:

$$\omega_0 \triangle t_{21} = \frac{\overline{I_1}}{G-1} \tag{3.22}$$

And the state plane vector:

$$z_2 = G + \jmath[\overline{I_1} - (G-1)\omega_0(t - t_1)] \tag{3.23}$$

Stage 3 [t_2, t_3]

At t_2, S_4 is on and S_3 is off. As the current becomes 0 at the end of the second stage, D_2 become reverse biased (because the V_{out} is always greater than V_{in}). There is no more current through L_r, and the voltage across C_r remains at V_{out} as in stage 2. In this stage, no current is circulating in the circuit. The equations to describe this stage are quite simple:

$$\begin{cases} i_{Lr}(t) = 0 \\ \\ v_{Cr}(t) = V_{out} \end{cases} \tag{3.24}$$

And after parametrization:

$$\begin{cases} \overline{i_{Lr}(t)} = 0 \\ \\ \overline{v_{Cr}(t)} = G \end{cases} \tag{3.25}$$

The stage ends at half of the whole switching cycle, which means $\omega_0 t = \pi$. So:

$$\omega_0 \triangle t_{32} = \pi - \omega_0 \triangle t_{21} - \omega_0 \triangle t_{10} \tag{3.26}$$

The vector is easy to obtain:

$$z_3 = G \tag{3.27}$$

Stage 4 [t_3, t_4]

At t_3, the switch S_3 turns on and S_4 turns off. In this stage, $D1$ is forward biased while $D2$ is reverse biased. The resonant capacitor is discharged, so the voltage across it drops from V_{out} to 0. At the same time, the current through the inductor increases from 0 to I_1. The operation of the converter is similar to the first stage.

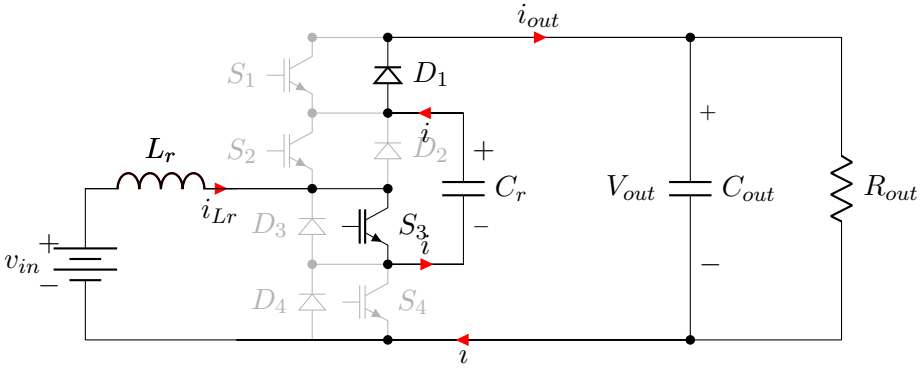

Figure 3.10: *Stage 4 (boost)*

The equations to describe this stage are:

$$\begin{cases} v_{Cr}(t) = V_{out} - V_{in} + L_r \dfrac{\mathrm{d}\, i_{Lr}(t)}{\mathrm{d}\, t} \\ \\ i_{Lr}(t) = -C_r \dfrac{\mathrm{d} v_{Cr}(t)}{\mathrm{d}\, t} \end{cases} \tag{3.28}$$

Notice that the initial conditions is different from the first stage:

$$\begin{cases} v_{Cr}(t_3) = V_{out} \\ \\ i_{Lr}(t_3) = 0 \end{cases} \tag{3.29}$$

In the same way the following equations can be obtained:

$$\begin{cases} v_{Cr}(t) = V_{out} - Vin[1 + cos(\omega_0 t)] \\ \\ i_{Lr}(t) = -\dfrac{V_{in}}{L_r}\dfrac{sin(\omega_0 t)}{\omega_0} \end{cases} \tag{3.30}$$

And after parametrization:

$$\begin{cases} \overline{v_{Cr}(t)} = G - 1 - cos(\omega_0 t) \\ \\ \overline{i_{Lr}(t)} = -sin(\omega_0 t) \end{cases} \tag{3.31}$$

The duration is equal to the first stage:

$$\omega_0 \triangle t43 = \pi - arcos(G - 1) \tag{3.32}$$

The vector in state-plane of this stage is:

$$z_4 = G - 1 - cos(\omega_0 t) - jsin(\omega_0 t) \tag{3.33}$$

Stage 5 [t_4, t_5]

At t_4, the switch S_3 is on and S_4 is off. The operation of the converter in this stage is quite similar to the stage 2. The difference is that the resonant capacitor voltage keeps at zero.

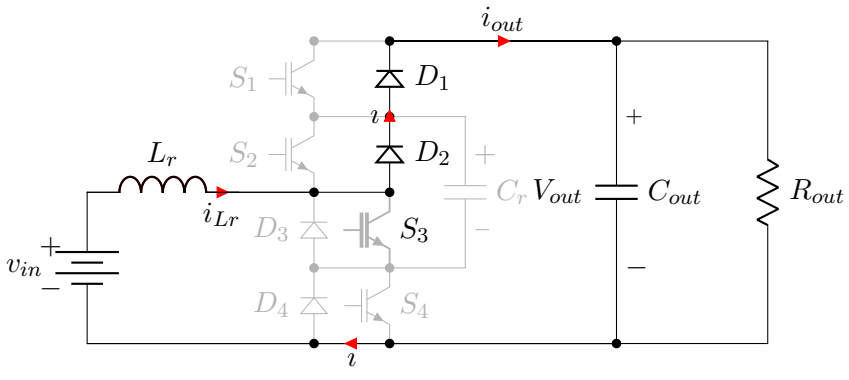

Figure 3.11: *Stage 5 (boost)*

The equations related to this stage are:

$$\begin{cases} V_{in} + L_r \dfrac{\mathrm{d}\, i_{Lr}(t)}{\mathrm{d}\, t} - V_{out} = 0 \\ \\ v_{Cr}(t) = 0 \end{cases} \tag{3.34}$$

The initial conditions is:

$$\begin{cases} i_{Lr}(t_4) = I_1 \\ \\ v_{Cr}(t_4) = V_{out} \end{cases} \tag{3.35}$$

So:

$$\begin{cases} i_{Lr}(t) = I_1 - \dfrac{V_{out} - V_{in}}{L_r}(t - t_4) \\ \\ v_{Cr}(t) = 0 \end{cases} \tag{3.36}$$

Then:

$$\begin{cases} \overline{i_{Lr}(t)} = \overline{I_1} - (G-1)\omega_0(t - t_1) \\ \\ \overline{v_{Cr}(t)} = 0 \end{cases} \tag{3.37}$$

The duration of this stage is the same of $Stage2$:

$$\omega_0 \triangle t_{54} = \frac{\overline{I_1}}{G-1} \tag{3.38}$$

And the vector:

$$z_5 = \jmath[\overline{I_1} - (G-1)\omega_0(t - t_4)] \tag{3.39}$$

Stage 6 [t_5, t_6]

At the end of stage 5, the switch S_3 is still on and S_4 is off. The current drops to 0 and there is no voltage across the resonant capacitor. Thus, in this last stage there is no current through L_r and no voltage across C_r. Therefor:

$$\begin{cases} \overline{i_{Lr}(t)} = 0 \\ \\ \overline{v_{Cr}(t)} = 0 \end{cases} \tag{3.40}$$

And:

$$\omega_0 \triangle t_{65} = \pi - \omega_0 \triangle t_{43} - \omega_0 \triangle t_{54} \tag{3.41}$$

$$z_6 = 0 \tag{3.42}$$

3.3.2 Summary of the switching strategy (boost)

From the previous analysis, the waveforms of the voltage and current of the components of the converter can be plotted according to the control signal, as shown in Fig.(3.12).

At turn-on and turn-off, the voltage and the current values at the switches terminals are zero (as shown in Fig.3.31 and Fig.3.32), this means there is no switching losses. Therefore, this converter is soft-switching.
For what concerns the resonant tank, the voltage across the resonant capacitor V_{Cr} is charged untill V_{out} and then clamped at this value during the first half switching cycle. So, in the second half switching cycle, the resonant capacitor is discharge and then v_{Cr} keeps at zero. The current through the resonant inductor varies with the switching frequency. In this way, it is possible to regulate the converter by controlling the switching frequency, according to the eq.(3.43) that will be deduced in par.(3.5.2)

$$G = \frac{f_s}{2\pi f_0} R_{out}/Z_r + 1 \tag{3.43}$$

The maximum value of the inductor current $\overline{i_{Lr}(\omega_0 t)_{max}} = 1$, happens when $\overline{v_{Cr}(\omega_0 t)} = 1$ or $\overline{v_{Cr}(\omega_0 t)} = G - 1$.

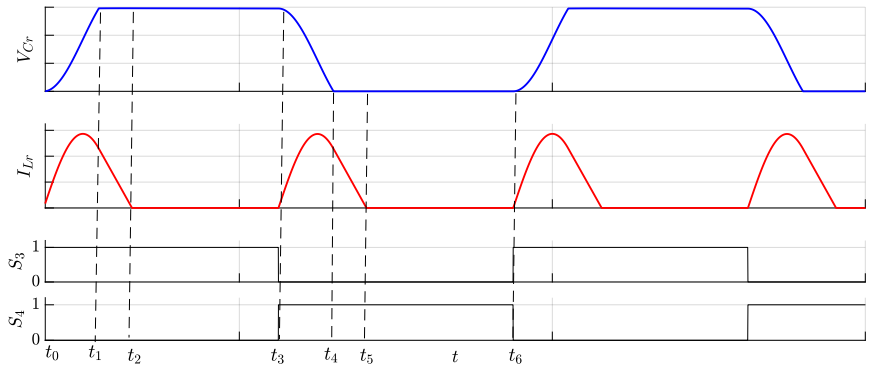

Figure 3.12: *Boost converter waveform analysed with ideal components*

3.4 Buck operation

3.4.1 Switching cycle analysis(buck)

Due to the modulation strategy analysed, in the buck operation mode, the control signal of the two switches S_1 and S_2 is made of a complementary square-wave with 50% duty cycle while the switches S_3 and S_4 are off. The two switches turn on complementary and each half part presents three stages related to the resonant tank behavior. The analysis performed in this paragraph regards the charge phase of the UC pack: the energy is flowing from V_{out} side (DC bus inverter) to the V_{in} side (UC pack).

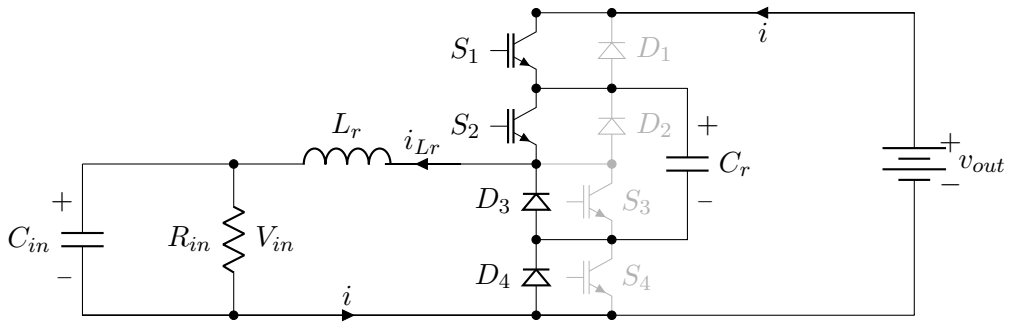

Figure 3.13: *Resonant buck*

Stage 1 [t_0, t_1]

In this operation mode, at t_0, S_1 turns on and S_2 turns off, diode D_3 is conducting. During this stage, the resonant capacitor C_r is charged by the source to the voltage level of the output voltage V_{out}. Due to the resonance, the current through the resonant inductor L_r increases sinusoidally from 0 to a certain value, defined I_1. This switching stage can be referred to Fig.(3.14)

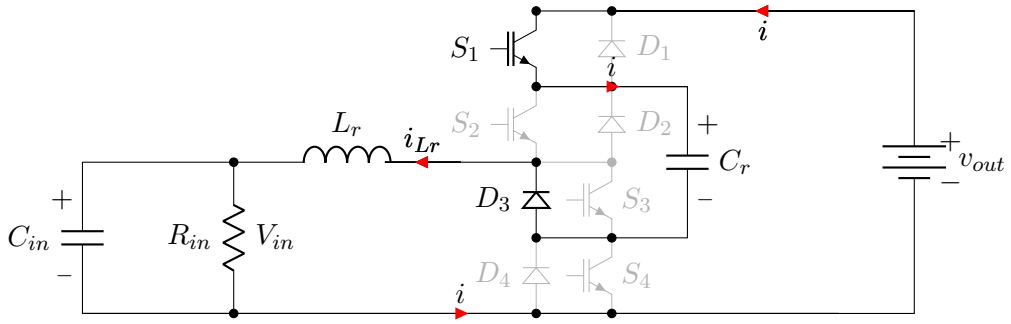

Figure 3.14: *Stage 1 (buck)*

$$\begin{cases} V_{out} - V_{Cr}(t) - L_r \dfrac{\mathrm{d}\, i_{Lr}}{\mathrm{d}\, t} - V_{in} = 0 \\ i_{Lr}(t) = C_r \dfrac{\mathrm{d}\, v_{Cr}(t)}{\mathrm{d}\, t} \end{cases} \tag{3.44}$$

At regime, the initial conditions of this topological state are:

$$\begin{cases} v_{Cr}(t_0) = 0 \\ i_{Lr}(t_0) = 0 \end{cases} \tag{3.45}$$

Defining the gain of the buck G_{buck} as:

$$G_{buck} = \frac{V_{in}}{V_{out}} \tag{3.46}$$

and remembering that V_{out} is always greater than V_{in}:

$$V_{out} > V_{in} \tag{3.47}$$

so:

$$0 < G_{buck} < 1 \tag{3.48}$$

Applying the Laplace direct and inverse transformation, following similar mathematical substitution and semplification as in the previous analysis, the showed result can be achived:

$$\begin{cases} i_{Lr}(t) = \dfrac{sen(\omega_0 t)}{\omega_0 L_r}(V_{out} - V_{in}) \\ v_{Cr}(t) = [1 - cos(\omega_0 t)](V_{out} - V_{in}) \end{cases} \tag{3.49}$$

In order to compare the two operation modes, the same parametrization strategy of the boost analysis above is used:

$$\overline{i_{Lr}(t)} = \frac{i_{Lr}(t)}{V_{in}/Z_r} \tag{3.50}$$

$$\overline{v_{Cr}(t)} = \frac{v_{Cr}(t)}{V_{in}} \tag{3.51}$$

Resulting in:

$$\begin{cases} \overline{i_{Lr}(t)} = (\dfrac{1}{G_{buck}} - 1)sen(\omega_0 t) \\ \overline{v_{Cr}(t)} = (\dfrac{1}{G_{buck}} - 1)[1 - cos(\omega_0 t)] \end{cases} \tag{3.52}$$

Considering the final condition $\overline{v_{Cr}(t)} = \dfrac{1}{G_{buck}}$ and the eq.(3.52) of the resonant capacitor voltage, the duration of this stage is:

$$\omega_0 \triangle t_{10} = \pi - arcos(\frac{G_{buck}}{G_{Buck} - 1}) \tag{3.53}$$

The state plane vector is:

$$z_1 = (G_{buck} - 1)[1 - cos(\omega_0 t)] + \jmath(G - 1)sen(\omega_0 t) \tag{3.54}$$

Stage 2 [t_1, t_2]

At t_1, the switch S_1 is on and S_2 is off. The resonant capacitor voltage $v_C r$ is equal to the output voltage V_{out}, the diodes D_3 and D_4 are forward biased. So in this stage $v_C r$ is clamped as V_{out}, while the current through the inductor i_{Lr} drops lineally to zero, since the output voltage is higher than the input voltage. This leads to a negative voltage across L_r. This stage can be referred to Fig.3.15:

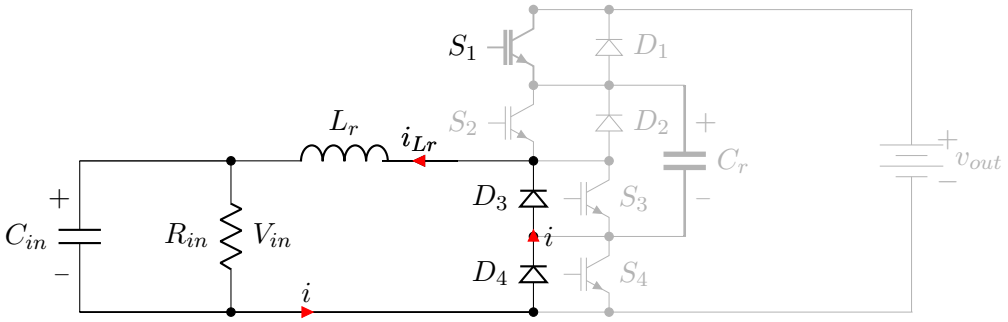

Figure 3.15: *Stage 2 (buck)*

Similarly, this stage can be described as:

$$\begin{cases} L_r \dfrac{\mathrm{d}\, i_{Lr(t)}}{\mathrm{d}\, t} = V_{in} \\ \\ v_{Cr}(t) = V_{out} \end{cases} \tag{3.55}$$

Initial conditions:

$$\begin{cases} i_{Lr}(t_1) = I_1 \\ \\ v_{Cr}(t_1) = V_{out} \end{cases} \tag{3.56}$$

As before, Laplace direct and inverse transformation,mathematical substitution and semplification are applied. The result is:

$$\begin{cases} \overline{i_{Lr}(t)} = \overline{I_1} - \omega_0(t - t_1) \\ \\ \overline{v_{Cr}(t)} = \dfrac{1}{G_{buck}} \end{cases} \tag{3.57}$$

Where $\overline{I_1} = \dfrac{I_1}{\frac{V_{in}}{Z_r}}$. The phase shift is determined by $I_{Lr}(t_2) = 0$, so:

$$\omega_0 \triangle t_{21} = \overline{I_1} \tag{3.58}$$

And the state plane vector:

$$z_2 = \frac{1}{G_{buck}} + \jmath[\overline{I_1} - \omega_0(t - t_1)] \tag{3.59}$$

Stage 3 [t_2, t_3]

At t_2, the switch S_1 is on and S_2 is off. As the current becomes 0 at the end of the second stage, the diodes D_3 and D_4 are reverse biased, so there is no current through L_r. The voltage across C_r remains as in stage2. In this stage, no current is circulating in the circuit. The equations are:

$$\begin{cases} i_{Lr}(t) = 0 \\ \\ v_{Cr}(t) = V_{out} \end{cases} \tag{3.60}$$

Resulting in:

$$\begin{cases} \overline{i_{Lr}(t)} = 0 \\ \\ \overline{v_{Cr}(t)} = \dfrac{1}{G_{buck}} \end{cases} \tag{3.61}$$

The end of this switching stage is half of the whole switching cycle, which means $\omega_0 t_3 = \pi$. So:

$$\omega_0 \triangle t_{32} = \pi - \omega_0 \triangle t_{21} - \omega_0 \triangle t_{10} \tag{3.62}$$

The vector:

$$z_3 = \frac{1}{G_{buck}} \tag{3.63}$$

Stage 4 [t_3, t_4]

In this stage, at time t_3 the switch S_2 turns on and S_1 turns off. The diode D_4 is forward biased while D_3 reverse biased. The resonant capacitor is discharged, so the voltage across it drops from V_{out} to 0. At the same time, the current through the inductor increases from 0 to I_1 another time. The operation of the converter is similar the first stage. This stage can be referred to Fig.3.16.

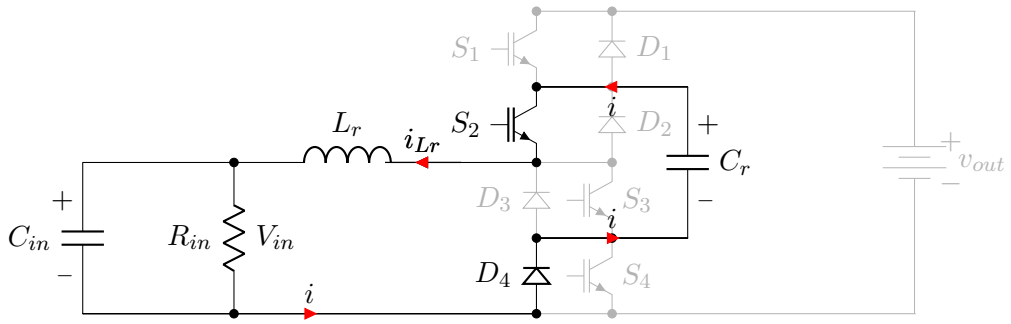

Figure 3.16: *Stage 4 (buck)*

The stage equations are:

$$\begin{cases} v_{Cr}(t) - L_r \dfrac{\mathrm{d}\, i_{Lr}(t)}{\mathrm{d}\, t} - V_{in} \\ \\ i_{Lr}(t) = -C_r \dfrac{\mathrm{d}\, v_{Cr}}{\mathrm{d}\, t} \end{cases} \tag{3.64}$$

with initial conditions:

$$\begin{cases} i_{Lr}(t_3) = 0 \\ \\ v_{Cr}(t_3) = V_{out} \end{cases} \tag{3.65}$$

Resulting:

$$\begin{cases} \overline{i_{Lr}(t)} = -\dfrac{1}{G_{buck}} sen(\omega_0 t) \\ \overline{v_{Cr}(t)} = \dfrac{1}{G_{buck}} - [1 - cos(\omega_0 t)] \end{cases} \tag{3.66}$$

Duration:

$$\omega_0 \triangle t_{43} = \pi - arcos(\frac{G_{buck}}{G_{Buck} - 1}) \tag{3.67}$$

And vector:

$$z_4 = 1 + cos(\omega_0 t) - \imath \frac{sen(\omega_0 t)}{G_{buck}} \tag{3.68}$$

Stage 5 [t_4, t_5]

At t_4, the switch S_1 is off and S_2 is on. The stage 5 behaves exactly as the second stage, except for the initial conditions (3.69). As can be seen by the Fig.(3.17), the diodes are conducting. The resonant inductor is linearly discharging until 0; at this point, the diodes D_3 and D_4 block and the stage ends.

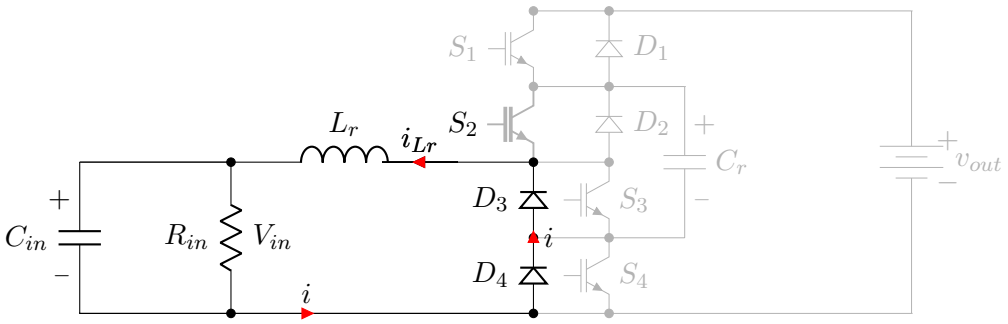

Figure 3.17: *Stage 5 (buck)*

Initial condition:

$$\begin{cases} i_{Lr}(t_5) = I_1 \\ v_{Cr}(t_5) = 0 \end{cases} \tag{3.69}$$

So:

$$\begin{cases} \overline{i_{Lr}(t)} = \overline{I_1} - \omega_0(t - t_4) \\ \overline{v_{Cr}(t)} = 0 \end{cases} \tag{3.70}$$

Duration:

$$\omega_0 \triangle t_{54} = \overline{I_1} \tag{3.71}$$

And the state plane vector:

$$z_5 = \jmath[\overline{I_1} - \omega_0(t - t_4)] \tag{3.72}$$

Stage 6 [t_5, t_6]

At t_5, the switch S_1 is off and S_2 is on. The current in the resonant inductor is 0 and there is no voltage across the resonant capacitor. Thus, in this last stage there is no current through L_r and no voltage across C_r. Therefor:

$$\begin{cases} \overline{i_{Lr}(t)} = 0 \\ \\ \overline{v_{Cr}(t)} = 0 \end{cases} \tag{3.73}$$

The end of this last stage is the end of the whole switching cycle. So:

$$\omega_0 \triangle t_{65} = \pi - \omega_0 \triangle t_{54} - \omega_0 \triangle t_{43} \tag{3.74}$$

The vector:

$$z_6 = 0 \tag{3.75}$$

3.4.2 Summary of the switching strategy (buck)

As before, the waveforms of the voltage and current are plotted according to the switching signal. The results are shown in Fig.(3.18). The relation to control the boost operation is expressed in the eq.(3.76) and it is obtained in par.(3.5.4).

$$G_{buck} = \sqrt{R_{in} \frac{f_s}{2\pi f_0 Z_r}} \tag{3.76}$$

Neither in this operation mode, at turn-on and turn-off, the voltage and current waveforms of the switches have no overlap, this means there is no switching loss. The soft switching properties are maintained. Therefore, this converter is soft-switching.
The behavior of the resonant tank is exactly the same of the boost analysis.

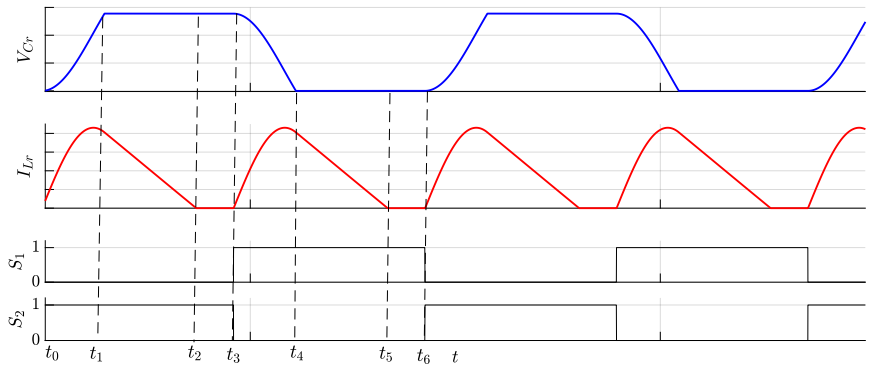

Figure 3.18: *Converter buck waveform analysed with ideal components*

3.5 Parameterized analysis

To design and size the converter, the input/output current and power should be calculated. The relative dependence of the output stage on the input stage should be analyzed since they are mandatory information for the operation of the converter.

3.5.1 Output current and output power (boost)

Output current

The average output current i_{outAVG} can be calculate [26] as the sum of the integral of the current function of the topological time steps $\triangle t_{12}$, $\triangle t_{34}$ and $\triangle t_{45}$:

$$i_{outAVG} = \frac{1}{T_s}[\int_{t_1}^{t_2} i_{Lr}(t)dt + \int_{t_3}^{t_4} i_{Lr}(t)dt + \int_{t_4}^{t_5} i_{Lr}(t)dt] \tag{3.77}$$

Then, normalizing with the same parameter of before the parameterized integral is derived:

$$\overline{i_{outAVG}} = \frac{1}{T_s}[\int_{t_1}^{t_2} \overline{i_{Lr}(t)}dt + \int_{t_3}^{t_4} \overline{i_{Lr}(t)}dt + \int_{t_4}^{t_5} \overline{i_{Lr}(t)}dt] \tag{3.78}$$

Substituting (3.20),(3.31) and (3.37) into (3.78):

$$\begin{aligned}\overline{i_{outAVG}} = \frac{1}{T_s}\{\int_{t_1}^{t_2} [\overline{I_1} - (G-1)\omega_0(t-t_1)]dt + \int_{t_3}^{t_4} [-sin(\omega_0 t)]dt + \\ + \int_{t_4}^{t_5} [\overline{I_1} - (G-1)\omega_0(t-t_4)]dt\}\end{aligned} \tag{3.79}$$

Considering the inductor current waveform (3.11) and the phase shift (3.14) at Stage 1, the parameterized maximum current value $\overline{I_1}$ can be obtained:

$$\overline{I_1} = \sqrt{1-(1-G_{boost})^2} \tag{3.80}$$

Taking the resonant capacitor voltage v_{Cr} (3.11) and the initial and final condition at Stage 1:

$$\begin{cases} \overline{v_{Cr}(t)} = 1 - cos(\omega_0 t) \\ \\ \overline{v_{Cr}(t_0)} = 0 \\ \\ \overline{v_{Cr}(t_1)} = G_{boost} \end{cases} \tag{3.81}$$

The relation $cos(\omega_0 t_{10}) = -G_{boost}$ is defined. The same can be done for Stage 4. Substituting these relations into (3.79), the final equation of the parameterized average output current i_{outAVE} is found:

$$\overline{i_{outAVG}} = \frac{\mu_0}{2\pi}\frac{G_{boost}}{(G_{boost}-1)} \tag{3.82}$$

where μ_0 is the frequency ratio:$\mu_0 = f_s/f_0$.
The current in output i_{out} is equal to the current through the diode D_1. The waveform is represented in Fig.(3.19) below:

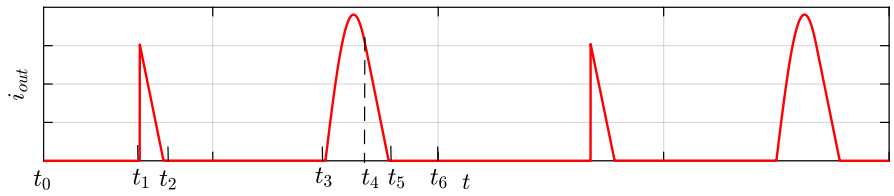

Figure 3.19: *Output current waveform*

The eq.(3.82) is represented in the following Fig.(3.20) in order to see the dependency of $\overline{i_{outAVG}}$ on the frequency ratio μ_0 and the gain G_{boost}:

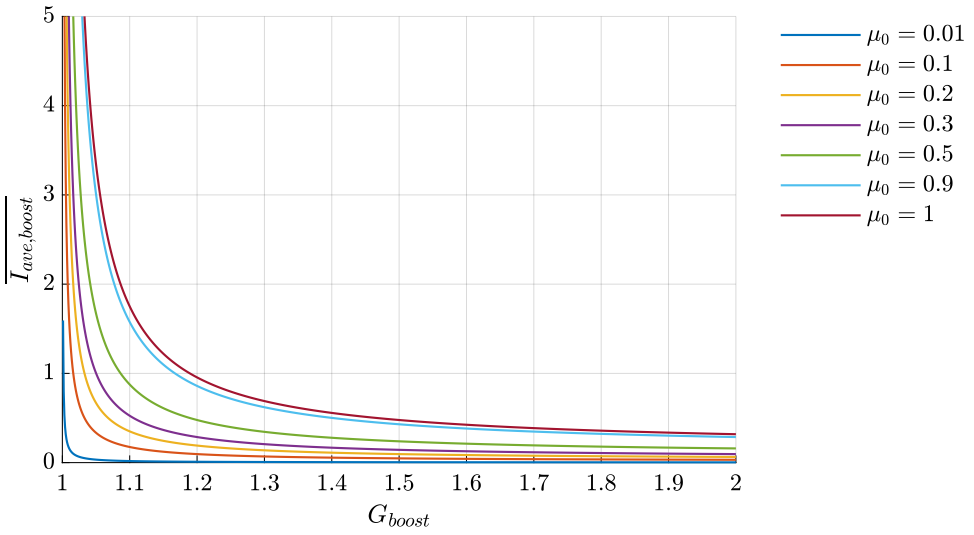

Figure 3.20: *Output current dependency on frequency ratio and gain*

It shows the tendency of reducing the output current to increase the gain for a certain μ_0 value.

Output power

Since the output voltage approximately does not change during one switching cycle, the average output power could be calculated directly by multiplying the average output current with the output voltage; this leads to the following equation:

$$\overline{P_{outAVG}} = \frac{\mu_0}{2\pi} \frac{Gboost^2}{(Gboost - 1)}$$

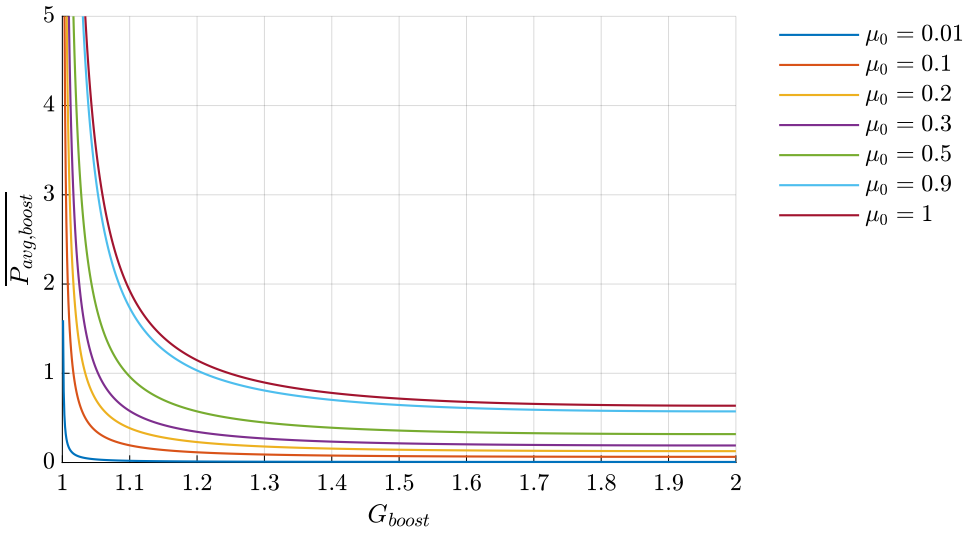

Figure 3.21: *Output power dependency on frequency ratio and gain*

Similarly, as shown in Fig.(3.21), for a certain value of μ_0, to increase the output power, the voltage gain should be reduced.

3.5.2 Converter voltage gain (boost)

To ensure the converter to work under the studied topology, some limitations should be setted. The input voltage V_i should be lower than the output voltage V_{out}, otherwise the two diodes D_1 and D_2 are forward biased. The requirement for a boost converter is also $G > 1$.
So,analyzing the duration of the first topological step, when the gain is equal to 2:

$$\omega_0 t_{10} = \pi - arcos\,(\,G - 1\,) = \pi$$

This means that the stages 2 and 3 as well as the 4 and 5 doesn't exist anymore. The converter operates in stage 1 in the first half switching cycle; the current flows through S_4 and D_2 charging the resonant capacitor and then it operates in stage 4 for the second half switching cycle; the current flows through S_3, D_1 and the load, so the resonant capacitor is discharged. In this case, the inductor current i_{Lr} behaves as a sine wave in each half of the switching cycle. It increases from 0 to a certain value I_1 and then drop to zero again when $\omega_0 t = \pi$.
At this point, the resonant capacitor has just been charged until the output voltage V_{out}, which means $V_{in} = \dfrac{V_{out}}{2}$, so this is the minimum possible value of V_{in}. Moreover, for voltage values higher than $2V_{in}$ the diode D_1 would always be in reverse bias.
Therefore the maximum gain of this converter under this operation topology is limited to 2. In conclusion, the gain is limited to the range:

$$1 < G < 2 \tag{3.83}$$

Assuming the output voltage approximately constant, a constant load resistance R_{out} and reviewing the equation of the average output current:

$$V_{out} = R_{out} i_{outAVG} \tag{3.84}$$

Using the resonant impedance Z_r to parameterize R_{out}, the following ratio can be found:

$$r_{out} = \frac{R_{out}}{Z_r} \tag{3.85}$$

So:
$G = r_{out}\overline{i_{outAVG}}$
Substituting the relation between gain and frequency to control the operation is found:

$$G = \frac{\mu_0}{2\pi} r_{out} + 1 \tag{3.86}$$

In addition to this, in order to keep the soft switching properties of this converter, the switching frequency should not exceed the resonant frequency, which means:

$$f_s \leq \frac{\omega_0}{2\pi} \tag{3.87}$$

This results in:
$0 < \mu_0 < 1$

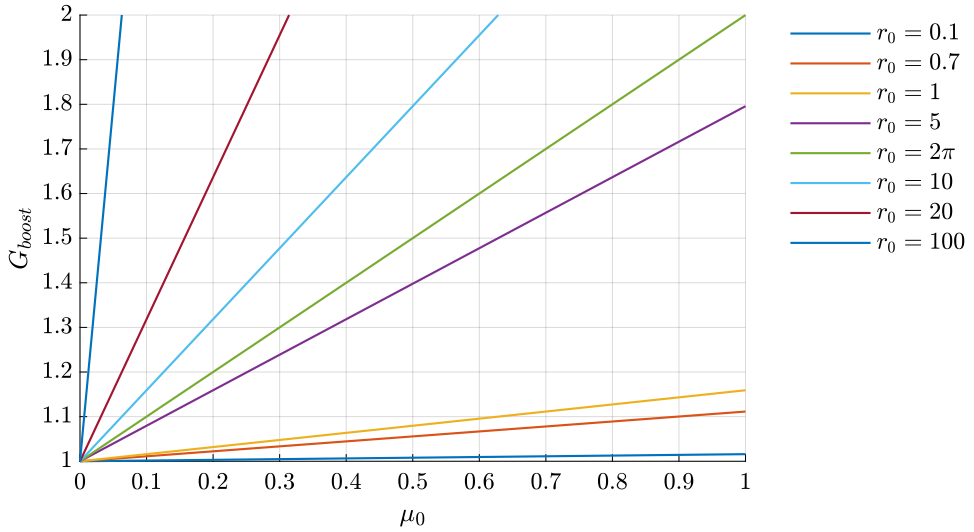

Figure 3.22: *Dependency of the output parameterized resistance r_{out} on frequency ratio and gain*

It is clear from the Fig.(3.22) that, in order to reach the maximum gain $G = 2$, the minimum value of r_{out} is 2π. So:

$$r_{out} > 2\pi$$

Underlining also that for a constant load and input voltage, the output voltage changes linearly with μ_0.

3.5.3 Input current and input power (buck)

Input current

As for the boost, the average input current i_{inAVG} can be calculate as the sum of the integral of the current function in the topological time steps $\triangle t_{10}$,$\triangle t_{21}$, $\triangle t_{43}$ and $\triangle t_{54}$:

$$i_{inAVG} = \frac{1}{T_s}[\int_{t_0}^{t_1} i_{Lr}(t)dt \int_{t_1}^{t_2} i_{Lr}(t)dt + \int_{t_3}^{t_4} i_{Lr}(t)dt + \int_{t_4}^{t_5} i_{Lr}(t)dt] \quad (3.88)$$

Then, normalizing with the same parameter of before the parameterized integral is derived:

$$\overline{i_{inAVG}} = \frac{1}{T_s}[\int_{t_0}^{t_1} \overline{i_{Lr}(t)}dt + \int_{t_1}^{t_2} \overline{i_{Lr}(t)}dt + \int_{t_3}^{t_4} \overline{i_{Lr}(t)}dt + \int_{t_4}^{t_5} \overline{i_{Lr}(t)}dt] \quad (3.89)$$

Substituting using the inductor current equations of the buck analysis of the required stages:

$$\begin{aligned}\overline{i_{inAVG}} = \frac{1}{T_s}[&\int_{t_0}^{t_1} (1-G)sen(\omega_0 t)\mathrm{d}t + \int_{t_1}^{t_2} \overline{I_1} - \omega_0 G(t-t_1)\mathrm{d}t + \\ &+ \int_{t_3}^{t_4} (-Gsen(\omega_0 t))\mathrm{d}t + \int_{t_4}^{t_5} \overline{I_1} - \omega_0 G(t-t_4)\mathrm{d}t]\end{aligned} \quad (3.90)$$

Proceding with the same analysis used for the boost resolution, the final equation is found:

$$\overline{i_{inAVG}} = \frac{\mu_0}{2\pi}\frac{1}{G_{buck}} \quad (3.91)$$

The current in input i_{in} is equal to the one through the resonant inductor. The waveform is displayed in the Fig.(3.23) below:

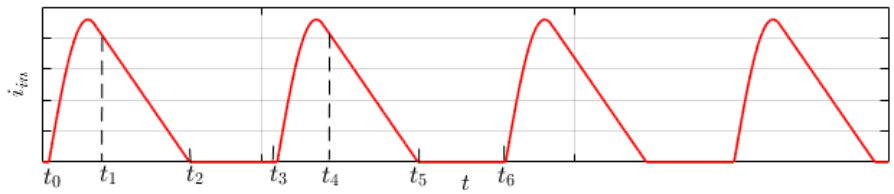

Figure 3.23: *Input current waveform*

The Fig.(3.24) shows the dependency of $\overline{i_{inAVG}}$ on the frequency ratio μ_0 and the gain G_{buck}:

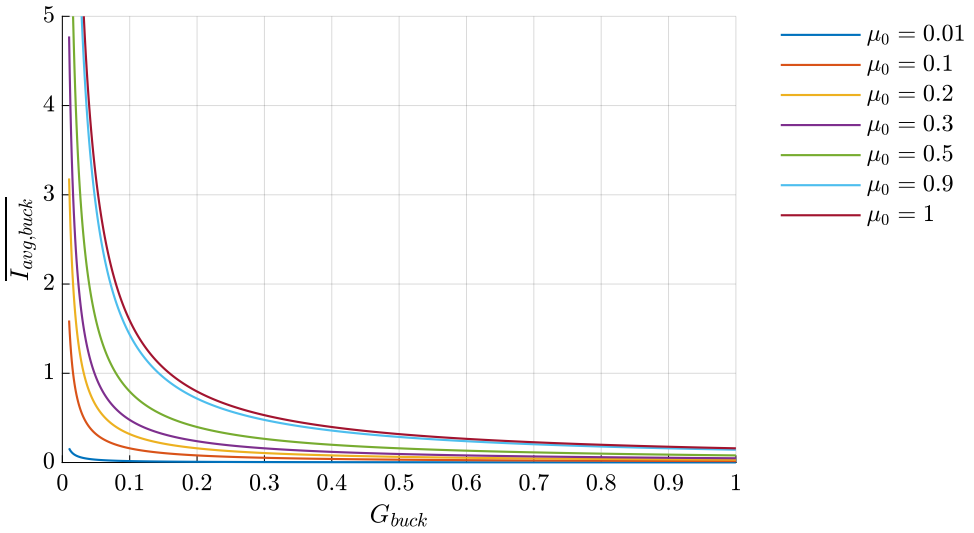

Figure 3.24: *Input current dependency on frequency ratio and gain*

As before, it shows the tendency of reducing the input current in order to increase the gain for a certain μ_0 value. The converter is able to provide a quite higher current input at low G_{buck} (it means high voltage difference).

Input power

The average input power $\overline{P_{inAVE}}$ is calculated as before; multiplying $\overline{i_{inAVG}}$ for the parameterized input voltage V_{in}. It results:

$$\overline{P_{inAVG}} = \frac{\mu_0}{2\pi}\frac{1}{G_{buck}}$$

Also in this case, the P_{inAVE} is directly proportional to μ_0 (Fig.3.24); this means that to increase the power in input, μ_0 should be increased.

3.5.4 Converter voltage gain (buck)

A similar analysis and some other limitations should be set to ensure the converter to work under the studied topology. Also under buck operation the input voltage V_{in} should be lower than the output voltage V_{out}, otherwise the resonant capacitor isn't charged. The requirement also necessary for a buck converter is $0 < G_{buck} < 1$. Analyzing the duration of the first topological step, when the gain is equal to $\frac{1}{2}$:

$$\omega_0 t_{10} = arcos\left(\frac{G_{buck}}{1-G_{buck}}\right) = \pi$$

As before, this means that the stages 2 and 3 as well as the 4 and 5 doesn't happen anymore. The converter operates in stage 1 in the first half switching cycle; the current flows through S_1 and D_3 charging the resonant capacitor and it operates as in stage 4 for the second half switching cycle; the current flows through S_2, D_4 and the input load R_{in}, so the resonant capacitor is discharged. As for the boost operation, the inductor current i_{Lr} behaves as a sine wave in each half of the switching cycle. It increases from 0 to a certain value I_1 and then drop to zero again when $\omega_0 t_= \pi$.

At this point, the resonant capacitor has just been charged until the output voltage V_{out}, which means $V_{in} = \frac{V_{out}}{2}$, so this is the minimum possible value of V_{in}, as it was for the boost analysis. Therefore the maximum gain of this converter under the buck operation topology is limited to the range:

$$0 < G_{buck} < 0.5 \tag{3.92}$$

In addition to the considerations above, the resonant operation required that the two switches S_1 and S_2 work complementary, it means with a duty cycle D equal to 0.5. Considering the gain definition for a buck converter:

$$G_{buck} = D \tag{3.93}$$

the maximum possible gain is set at the same value.
As for the boost, considering the input voltage approximately constant, a constant load resistance R_{in} and reviewing the equation of the average input current:

$$V_{in} = R_{in} i_{inAVG} \tag{3.94}$$

Use the resonant impedance Z_r to parameterize R_{in}:

$$r_{in} = \frac{R_{in}}{Z_r} \tag{3.95}$$

So:

$$G_{buck} = r_{in} \overline{i_{inAVG}} \tag{3.96}$$

Substituting (3.91) in (3.96):

$$G_{buck} = \sqrt{r_{in} \frac{\mu_0}{2\pi}} \tag{3.97}$$

Considering, for the same reason of before, the maximum switching frequency equal to the resonant one, it results: $0 < \mu_0 < 1$

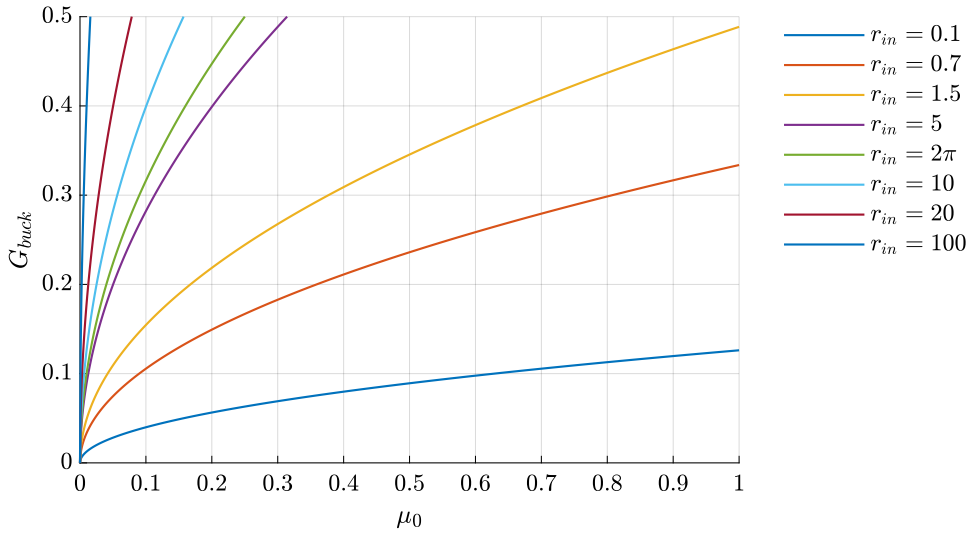

Figure 3.25: *Dependency of the input parameterized resistance r_{in} on frequency ratio and gain*

Appear clear from the Fig.(3.25) that, in order to reach the maximum gain $G_{buck} = 0.5$, the minimum value of r_{in} is 1.5. So it should be:

$$r_{in} > 1.5 \tag{3.98}$$

3.6 Design Methodology

The design process of this converter followed this main steps:

1. Definition of the optimal gain range for both boost and buck operations;
2. Identification, through the parameterized analysis, of the optimal value for the parameterized load r_0;
3. Set the maximum allowable peak current (I_{peak}) in the resonant inductor, switches and diodes;
4. Choice of the switching technology based on the required resonant frequency f_0 due to the previous points;
5. Check the UC pack current capability over all the charge/discharge operation of the system.

3.6.1 Optimal Gain Range

As already discussed, in order to keep the soft switching properties the maximum possible gain for the boost operation mode is $1 < G(boost) < 2$ and for the buck operation mode is $0 < G(buck) < 0.5$.
Taking into consideration the efficiency definition of the converter:

$$\eta_{res.conv} = \frac{P_{inverter}}{P_{UC_pack}} = \frac{I_{inv}V_{inv}}{I_{UC_pack}V_{UC_pack}}$$

Considering:

1. The V_{inv} is substantially constant thanks to the battery pack operation ;
2. The main objective of the system is absorbing/releasing as much power/current as possible in order to decrease the stress of the battery pack and guarantee all the power required in acceleration;
3. Assume that the UC pack voltage is decreasing linearly during operations;
4. The maximum I_{UCpack} is fixed by the ultra-cap limitation;

So, knowing the eq.(3.6.1)

$$V_{UCpack} = \frac{1}{\eta_{res.conv}} \frac{I_{inv}V_{inv}}{I_{UCpack}}$$

the minimum voltage value of discharge for the UC pack can be assumed. Thanks to this consideration, the V_{UCpack} should not drop under a certain level to not penalized to much the operation during charge: lower voltage means higher current at storage side and it leads to lower value of current in output in both supply/regeneration operation; in other words, at low UC voltage it is releasing/accepting less current; so, despite the UC could be ideally discharge until 0 V, this analysis that involve just the average currents is not enough to correctly state the minimum possible voltage of the UC pack.
In par. (3.6.6) an additional test about the peak current values is performed in order to properly choose $V_{UCpack_{min}}$.
In the light of these considerations and remembering the gain limits on boost eq.(3.83) and buck eq.(3.92) modes, the reasonable way to carry on an optimal dimensioning procedure is to rely on boost operation analysis because it is possible to keep the resonant advantages as far as the half of the nominal voltage of the UC pack; instead, the buck resonant advantages could cover just a smaller fraction of operation voltage: from half the nominal voltage to $V_{UCpack_{min}}$.

3.6.2 Limit value for r_0

At this point, the minimum value of r_0 in boost operation mode, in order to keep the soft switching properties of the converter, is taken. From the parameterized analysis carried on in par. (3.5.2) results:

$$r_{out} > 2\pi$$

3.6.3 Component constraints

To carry on the analysis, at this step, some simulations were performed in order to estimate the stress for the main components as switches, diodes and overall for the resonant inductor and capacitor that are the most critical ones in terms of dimensions. The UC current capability was checked as well as the current and the over-voltage in each component.
As result of this analysis the resonant frequency f_0 was set on the base of the choice of the switches technology.

3.6.4 Sizing of the Resonant Tank (L_r, C_r)

The nominal voltage $V_{UC_{nom}}$ is defined as $\frac{V_{UCpack}}{G_{boost}}$, where the $G_{boost} = 2$, that is the maximum admitted, is choosen: the reason is to allow the converter to work in a resonant way for half the voltage rate and then operate at the designed point as a normal boost converter (switching simultaneously S_3 and S_4) for the remaining usable energy. Its behavior is reported in Fig.(3.26):

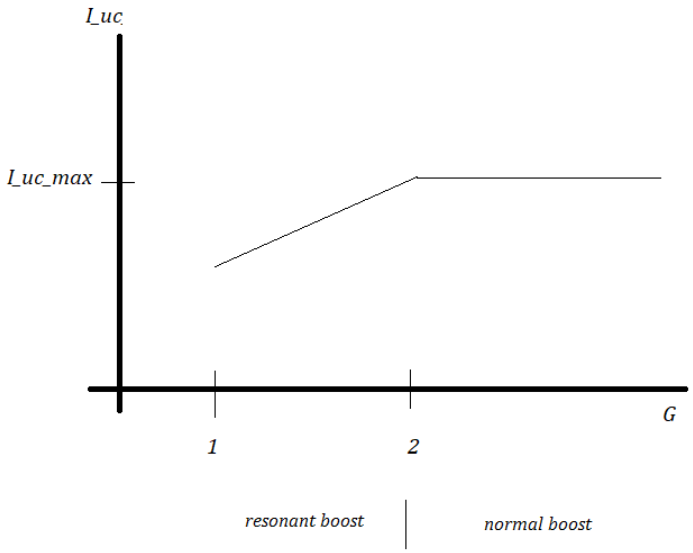

Figure 3.26: *Resonant Converter in Boost nominal operation*

Using now the following formula, the value of the resonant impedance can be found:

$$Z_r = \frac{V_{UCnom}}{I_{peak_{inductor}}} \tag{3.99}$$

Considering now the definition $f_0 = \frac{1}{2\pi\omega_0}$, the resonant impedance $Z_r = \sqrt{\frac{L_r}{C_r}}$ and the resonant angular frequency (3.5), it is possible to define:

$$L_r = \frac{Z_r}{2\pi f_0} \qquad C_r = \frac{1}{2\pi Z_r f_0} \tag{3.100}$$

3.6.5 Switching frequency (f_s) selection

The switching frequency for the boost operation mode is selected using (3.86) and (3.82) as:

$$f_{s_{boost}} = \frac{G-1}{R_{out}C_r} \tag{3.101}$$

Instead, the switching frequency for the buck operation mode is delected using (3.97) and (3.91):

$$f_{s_{buck}} = \frac{G_{buck}^2}{R_{UC_{pack}}C_r} \tag{3.102}$$

Where R_{UCpack} is the UC pack equivalent resistance.

3.6.6 Resonant Convert Limits and Sizing

Taking under control all the component and the project constraints already mentioned:

(3.6.2) $r_{out} > 2\pi$

(3.6.1) $I_{UC_{pack}} < I_{max}$ and $V_{uc} > V_{UC_{minimumfordischarge}}$

(3.99) $I_{peak_{inductor}} <$ technology allowed values

- $V_{inv} = constant$

Combining these considerations:

$$I_{peak_{Lr}} > \frac{2\pi V_{inv}}{R_{out}} \tag{3.103}$$

This eq.(3.103) represent the most stringent requirement for the EV application since $V_{inv_{DC}} = \frac{2\sqrt{2}}{3}\frac{V_{line_{RMS}}}{M_i}$ (par.2.2.6; eq.2.12) should be approximately constant during operation. $R_{out} = \frac{V_{inv_{DC}}^2}{P_{inv}}$, which represent the equivalent output resistance, is very low.
This leads to a too high (inconvenient) minimum possible value for $I_{peak_{Lr}}$ and so to a not allowed current to the input of the UC pack (from Fig.(3.5) is it possible to see that the the inductor current is the same of the one in input to the UC pack) .
In order to solve the problem the decision was to act following simultaneously two paths:

1. Reduce the power capability of the converter;
   A capability factor k is defined setting the maximum gain of the converter $G_{boost} = 2$ and the maximum input current at the UC pack $I_{UCpack} = I_{max}$ as reported in the eq.(3.104):

   $$k = \frac{I_{UCpack}\frac{V_{UCpack}}{G_{boost}}}{P_{inv}} \tag{3.104}$$

   So the capability of the system P_{KERS} is defined by:

   $$P_{KERS} = kP_{inv} \tag{3.105}$$

2. Use more than one converter in interleaving mode [21] [22];
   Assuming a reasonable number of converter ($n_{res_{conv}} = 2$), the power capability of each one become:

   $$P_{res_{conv}} = k\frac{P_{inv}}{n_{res_{conv}}} \tag{3.106}$$

   This choice can halve the power capability of each converter while increasing increasing the $I_{UCpack_{peak}}$ of a $\sqrt{2}$ factor: considering the waveform of the current in the resonant inductor I_{Lr} in topological time step 1 and 4 in both boost and buck mode (eq.3.8, eq.3.31, eq.3.52, eq.3.66), they are sinusoidal waveform. The behavior of the inductor current in time step 2 and 5 (it hows a linear shape) is approximated to a sinusoidal function because of the small

duration. A phase shift ϕ of $\pi/2$ is considered between the two converters, as shown in Fig.(3.27):

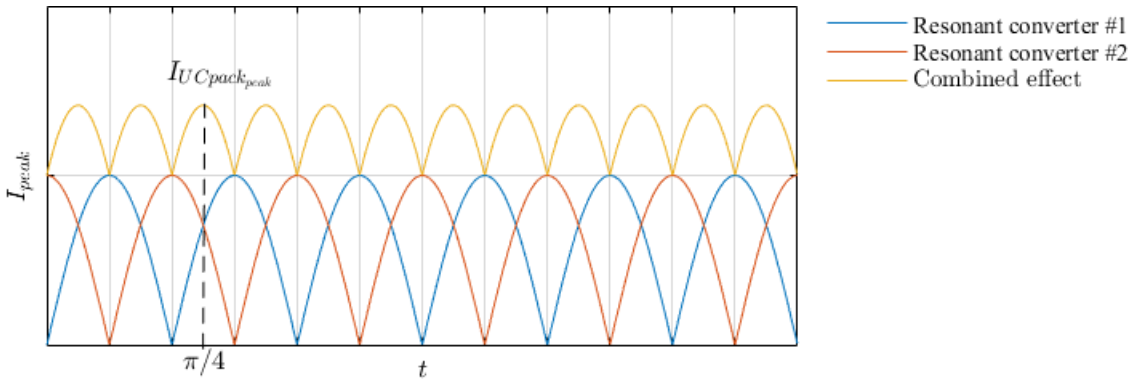

Figure 3.27: *Interleaving effect*

The following equation correctly approximate the problem:

$$I_{UCpack_{peak}} = I_{Lr_{peak}} sin(\omega_0 t) + I_{Lr_{peak}} sin(\omega_0 t + \phi) \tag{3.107}$$

Checking the maximum point at $t = \pi/4$, the resulting peak current in the UC pack is:

$$I_{UCpack_{peak}} = \sqrt{2} I_{peak_{Lr}} \tag{3.108}$$

Combining these two effects (eq.3.104; eq.3.106; eq.3.107) and considering $P = \frac{V^2}{R}$, it is possible to find the whole system capability value (k) that makes each resonant converter respect all the constraints:

$$k = \frac{I_{UCpack_{max}} V_{inv}^2 n_{res_{conve}}}{2\pi\sqrt{2} V_{UCpack} P_{inv}} \tag{3.109}$$

3.6.7 Sizing components results

Following the analysis performed above, the resulting values of resonant inductance and capacitance are needed:

L_r	7.71×10^{-7} [H]
C_r	8.21×10^{-7} [F]

3.6.8 Summary of Buck operation limits

As already mentioned in the paragraphs above, the buck operation presents resonant limits for the gain (3.92), for the maximum switching frequency ($\mu_0 = 1$) and an additional constraint due to the current capability of the UC pack. From the relation (3.103) the parameterized inductor peak current is evaluated.
Moreover, sizing the converter under the boost optimal design mode performed above, leaded to $r_{in} = 0.733$. Checking the Fig.(3.25), it means that the maximum

gain is limited to $G_{buck} = 0.34$.
The working limits of current, gain and switching frequency are graphically underlined in the Fig.(3.24) reported below:

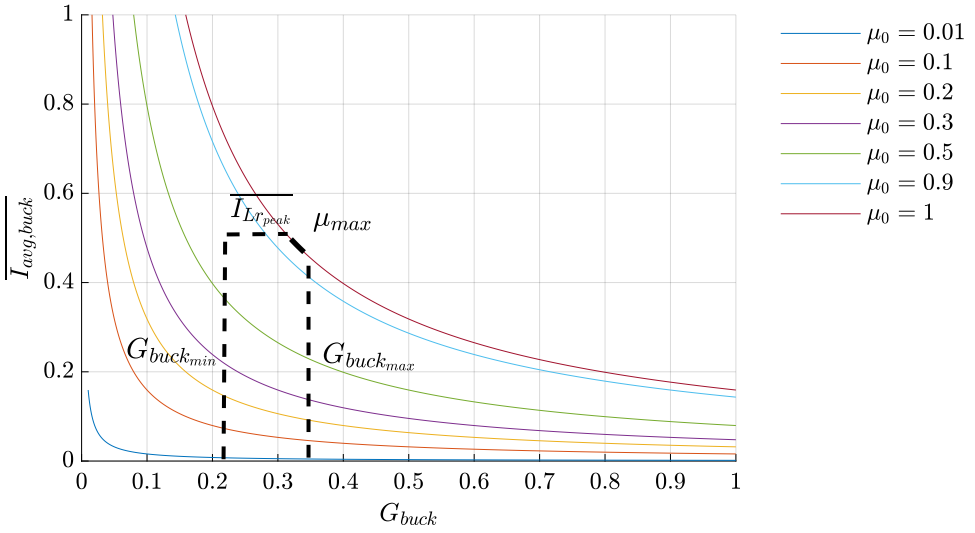

Figure 3.28: *Current/ Gain/ switching frequency limits in buck opertions*

An extra constraint can be set recalling the minimum voltage of UC pack for a proper operation of the KERS system (par.(2.2.8)). The minimum operational gain can be defined according to the eq.(2.22):

$$G_{buck_{min}} = \frac{V_{UCpack_{min}}}{V_{inv}} = 0.23 \tag{3.110}$$

3.6.9 Additional operation consideration

The constraints in both boost and buck operations are deeply analyzed in the paragraphs above. Due to those resonant limits underlined, a change in modulation strategy between resonant and conventional PWM operation is required. This double working mode, so called hybrid modulation, inevitably creates a transitory time frame that should be managed by the control system. This type of modulation required usually a deep study that is not performed in this work.
In the PWM modulation also the effect of overlapping the switching period can be analysed.

3.7 Resonant Converter Simulation

3.7.1 Model

The model for simulation is developed on Simulink using Simscape electrical modules and properties. The simulations is performed based on the data resulting from the work reported above: in the Matlab environment the computational analysis is performed and then the simulation is carried out in Simulink. The relevant information about the simulation are:

- DAE (Differential Algebric Equation) solver of Simscape;
- step size $dt = 2e - 9$ [sec];
- ideal switches, diodes, inductor and capacitors;
- tested along all the resonant gain span limits;

The lay-out used for the boost simulation is reported in Fig.(3.29). The switches and the anti-parallel diodes are simulated by an IGBT mask.

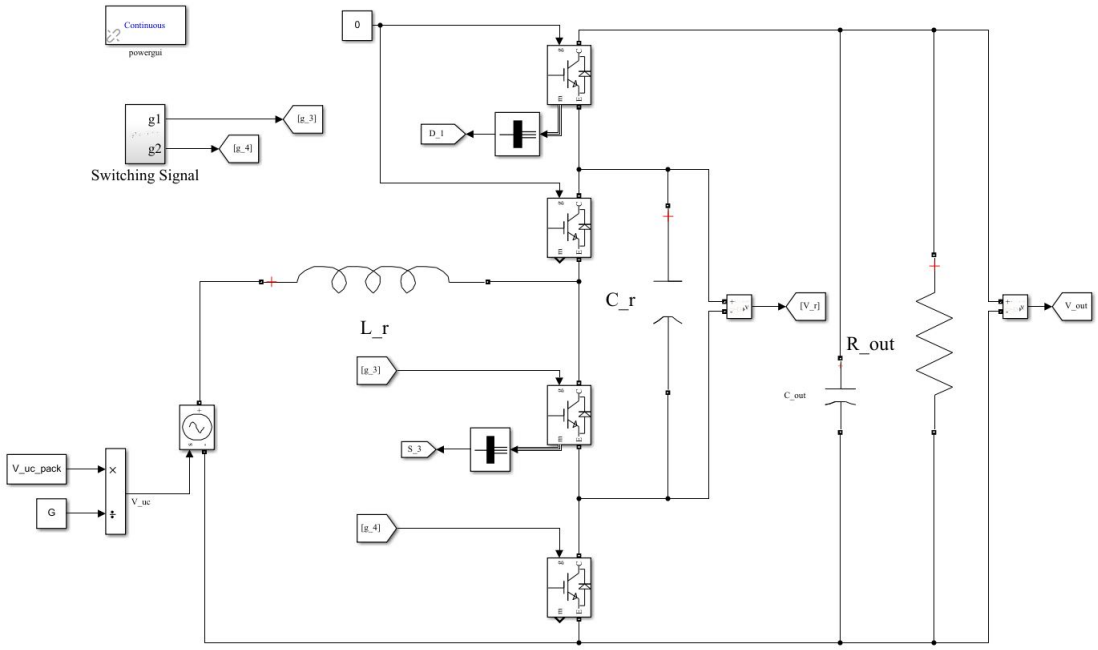

Figure 3.29: *Boost implementation on Simulink*

The switching signal is created according to the triangular form function compared to a reference signal as shown in Fig.(3.30).

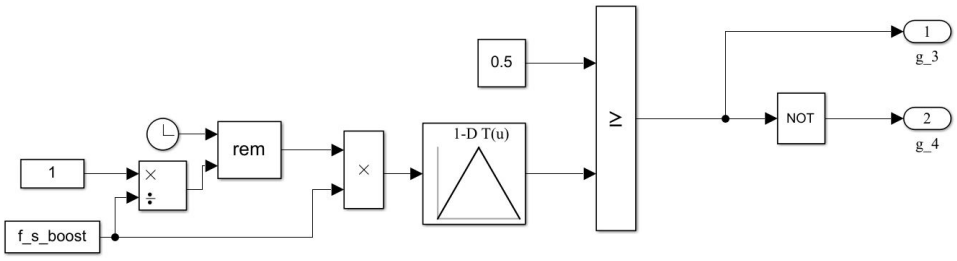

Figure 3.30: *Switching signal creation*

3.7.2 Results

The results of the simulation are aligned to the theoretical analysis and compelling with the expectation: after an high initial peak in both boost and buck simulation, that should be managed by a filter, the signals stabilizes (periodic steady state) and they show the expected behavior.
In Fig.(3.31) the voltage and current values of the resonant tank, of one diode and one switch are reported.

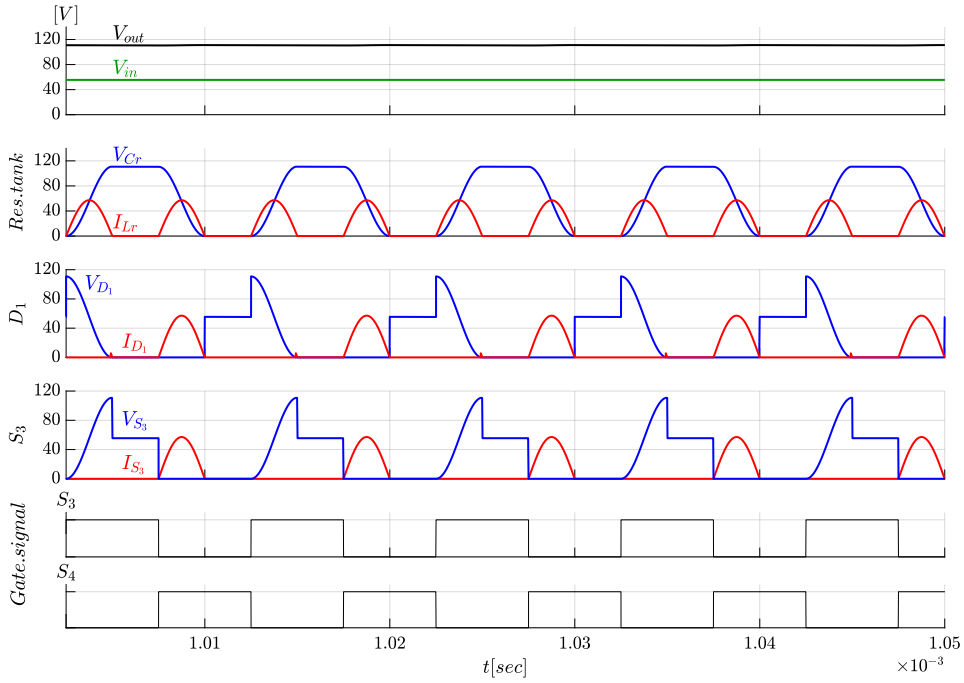

Figure 3.31: *Boost simulation*

In the first graph of Fig.(3.31), the ability of the converter to reach V_{out} and the stability of the solution at nominal operation of $G_{boost} = 2$ is reported.In the second graph of the Fig. above, the current though the resonant inductor and the voltage across the resonant capacitor are shown. The third and the forth graph of the Fig.(3.31), displays the current and voltage behavior through respectively the diode D_1 and the switch S_3. The ZCS (Zero Current Switching) can be clearly seen when looking to the instantaneous values of the voltages and currents of the active switches. This means that in this ideal simulation the switching losses are null and that the soft switching properties of the resonant converter are kept. Thanks to this consideration, for a real implementation it is reasonable to expect very low power losses (just due to conduction resistance) also at high switching frequencies.
Instead, Fig.(3.32) shows the buck simulation results. As discussed in par.(3.6.8),

the simulation is performed at the maximum resonant gain $G_{buck} = 0.3$. As expected by theoretical limitations, the charge and discharge time of the resonant inductor is equal to the semi-period. This confirms the limitations of the resonant operations. As for the boost simulation, in the third graph the commutation in soft-switching can be seen looking to the instantaneous values of the voltage and current of the represented switch S_1 that are 0: this means that the soft switching properties are kept also in buck operation mode.

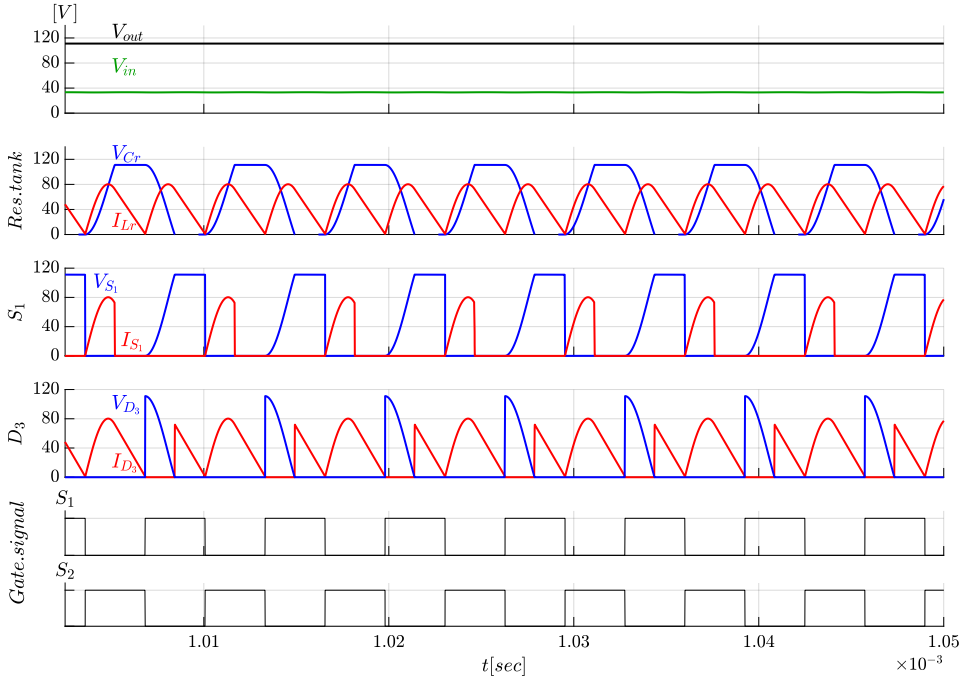

Figure 3.32: *Buck simulation*

The maximum values of the voltage and the average values of the current, applied to the switches and the diodes are displayed here:

Boost mode									
	S_1	S_2	S_3	S_4	D_1	D_2	0	0	
V_{max}	0	0	110.85	110.85	111	111	0	0	$[V]$
I_{AVE}	0	0	9.1	9.1	9.1	9.1	0	0	$[A]$

Buck mode									
	S_1	S_2	S_3	S_4	D_1	D_2	D_3	D_4	
V_{max}	111	111	0	0	0	0	111	111	$[V]$
I_{AVE}	14	14	0	0	0	0	32.7	32.7	$[A]$

This values are computed at the nominal operation of the boost mode (dicharge of UC pack) with $G_{boost} = 2$ and at the maximum conditions, for the sizing choices of the converter, for the buck mode (charge of the Uc pack) with $G_{buck} = 0.3$.

3.8 Data and Symbols

The data reported below are used to run the simulation.They are assumed based on ideal components implementation.

Switches

Resonant frequency	f_0	200	[kHz]
Snubber resistance	$R_{snubber}$	10×10^5	[Ω]
Internal resistance	R_{ons}	10×10^{-5}	[Ω]
Snubber capacitance	$C_{snubber}$	inf	[F]

Nominal set-up

Nominal boost gain	G_{boost}	2
Number of res. converter	$n_{res.conv}$	2
Parameterized output resistance	r_{out}	2π

Instead, the following values result from the analysis reported in this chapter. They can be used to properly choose the physical component needed to build the system(the components choice is not discussed yet).

System design values			
System capability	k	16	%
Res. converter power capability	$P_{res.conv}$	1.0122	[kW]
Equivalent res. converter output resistance	R_{out}	11.18	[Ω]
Inductor peak current	$I_{Lr_{peak}}$	57.27	[A]
Converter components			
Resonant impedance	Z_r	0.9694	[Ω]
Resonant inductor	L_r	7.71×10^{-7}	[H]
Resonant capacitor	C_r	8.21×10^{-7}	[F]
Resonant angular frequency	ω_0	0.1256×10^{6}	rad/s
Nominal operation			
Nominal boost switching frequency	$f_{s_{boost}}$	100	[kHz]
Equivalent res. converter input resistance	R_{in}	0.411	[Ω]
Buck operation			
Parameterized input resistance	r_{in}	0.733	
Buck gain	G_{buck}	0.3	
Buck switching frequency	f_{sbuck}	154.2	[kHz]

CHAPTER 4

Conclusions

At the end of this work, the project of the EV to compete in the FSAE electric is still in the preliminary phases. The requirements about the storage, the motor and the current / voltage parameters have been defined. The construction of the prototype, based on the results of this thesis and others research regarding the vehicle mechanical structure, is scheduled for the months ahead. The first tests of the vehicle are expected within the end of this year.

Regarding the performed analysis in Chap.2, it shows that the vehicle is able to accomplish to the requirements of the dynamical tests of the Formula SAE electric. The simulation clearly confirms the correct sizing of the storage system: the vehicle ends the endurance test with still half of the energy stored in the BP; this ensure a good safety margin for the real operation in which the prototype could exploit all the motor power and not just the nominal one as implemented in this work. As expected, the Li-ion cells charge and discharge according to the theoretical implementation, respecting the current and voltage operational constraints on the inverter DC side. Instead, the KERS operation is strongly influenced by the state of charge of the UC pack that is disconnected under a certain voltage value to ensure a proper operability of the whole system. Finally, the prototype is not able to follow the provided speed profile because of power limitation to the nominal motor values. Higher speed can easily be achieved by exploiting the full power.

The second objective of studying and sizing a resonant converter to manage the UC pack is deepen in Chap.3. The theoretical analysis displays the full capability of the resonant converter to operate under soft-switching properties in both directions. Then, the limitations due to the high current EV application, pushed the analysis to correctly sizing it. The interleaved solution combined with the introduction of the capability factor shows the expected result of reducing both the peak current in the

resonant inductor and the input current to the UC pack. The result can improve further by adding more resonant converter. The findings suggest that the assumptions of compactness and low weight of the converter can be achieved and that the UC can co-work with the BP. Nonetheless, the converter is not able to fully exploit the peculiarity of fast charge/discharge of the UC. Anyway, the ultra-caps technology implemented in the model, without the converter constraint, remains an interesting asset to get the maximum advantage from the regenerative braking. For this reason the study of other converters technology is surely interesting for combined Li-ion and ultra-caps EV as well as the research of the best number of these resonant converter in a volume, weight, cost and capability optimization problem.

CHAPTER 5

Attachments

Specifications

Series	Part No.	Capaci-tance	Rated Voltage	ESR (DC)	Max. Current	Leakage Current	Max. Stored Energy	Weight	Operating Temperature Range	Type	Dimension
Snap-in & Lug Type	LSUC 002R8S 0100F EA	100F	2.8V	9mΩ	74A	<0.3mA	0.11Wh	0.023kg	-40~65°C	Snap-in	Φ22 X L46mm
	LSUC 002R8S 0120F EA	120F	2.8V	9mΩ	81A	<0.4mA	0.13Wh	0.023kg	-40~65°C	Snap-in	Φ22 X L46mm
	LSUC 002R8L 0320F EA	320F	2.8V	2mΩ	273A	<1mA	0.35Wh	0.078kg	-40~65°C	Lug	Φ35 X L61mm
	LSUC 002R8L 0350F EA	350F	2.8V	3.2mΩ	231A	<1mA	0.38Wh	0.072kg	-40~65°C	Lug/Snap-in	Φ35 X L61mm
	LSUC 002R8L 0400F EA	400F	2.8V	3mΩ	255A	<1mA	0.44Wh	0.080kg	-40~65°C	Lug/Snap-in	Φ35 X L66mm
	LSUC 002R8L 0450F EA	450F	2.8V	3mΩ	268A	<1mA	0.49Wh	0.088kg	-40~65°C	Lug/Snap-in	Φ35 X L71mm
	LSUC 003R0L 0380F EA	380F	3.0V	3.2mΩ	257A	<1mA	0.48Wh	0.072kg	-40~65°C	Lug/Snap-in	Φ35 X L61mm
	LSUC 003R0L 0430F EA	430F	3.0V	3mΩ	282A	<1mA	0.54Wh	0.080kg	-40~65°C	Lug/Snap-in	Φ35 X L66mm
	LSUC 003R0L 0480F EA	480F	3.0V	3mΩ	295A	<1mA	0.60Wh	0.088kg	-40~65°C	Lug/Snap-in	Φ35 X L71mm

- Endurance time (65°C, VR) : 1500 hours for 2.8V / 1000 hours for 3.0V (ΔC<20% decrease, ΔESR<100% increase of initial specified value)
- Life time (25°C, VR) : 10 years (ΔC<20% decrease, ΔESR<100% increase of initial specified value)
- Cycle life time (25°C, VR) : 500,000 cycles (ΔC<20% decrease, ΔESR<100% increase of initial specified value)

Snap-in & Lug Type	LSUC 002R8L 0600F EA	600F	2.8V	3.2mΩ	288A	<1.3mA	0.65Wh	0.090kg	-40~65°C	Lug/Snap-in	Φ35 X L71mm

- Endurance time (65°C, VR) : 1500 hours (ΔC<30% decrease, ΔESR<150% increase of initial specified value)
- Life time (25°C, VR) : 10 years (ΔC<30% decrease, ΔESR<150% increase of initial specified value)
- Cycle life time (25°C, VR) : 500,000 cycles (ΔC<30% decrease, ΔESR<150% increase of initial specified value)

Prismatic Type	LSUC 002R8P 3000F EA	3000F	2.8V	0.36mΩ	2019A	<5mA	3.27Wh	0.650kg	-40~65°C	Prismatic	W55 X D55 X L155mm

- Endurance time (65°C, VR) : 1500 hours (ΔC<30% decrease, ΔESR<150% increase of initial specified value)
- Life time (25°C, VR) : 10 years (ΔC<30% decrease, ΔESR<150% increase of initial specified value)
- Cycle life time (25°C, VR) : 1,000,000 cycles (ΔC<30% decrease, ΔESR<150% increase of initial specified value)

Figure 5.1: *UC data-sheet*

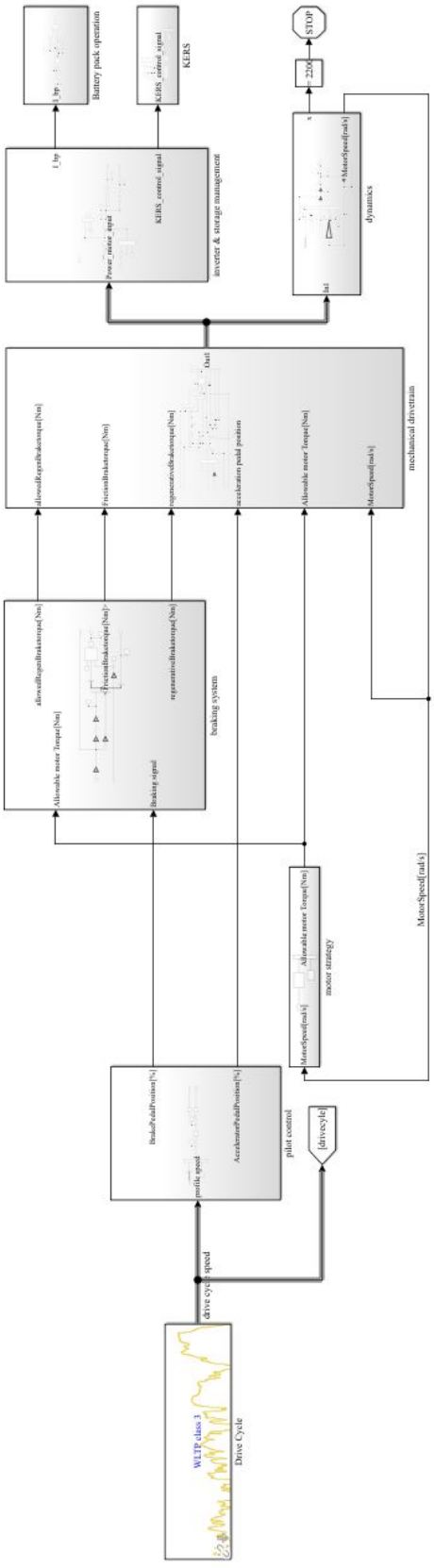

Figure 5.2: *Simulink model lay-out*

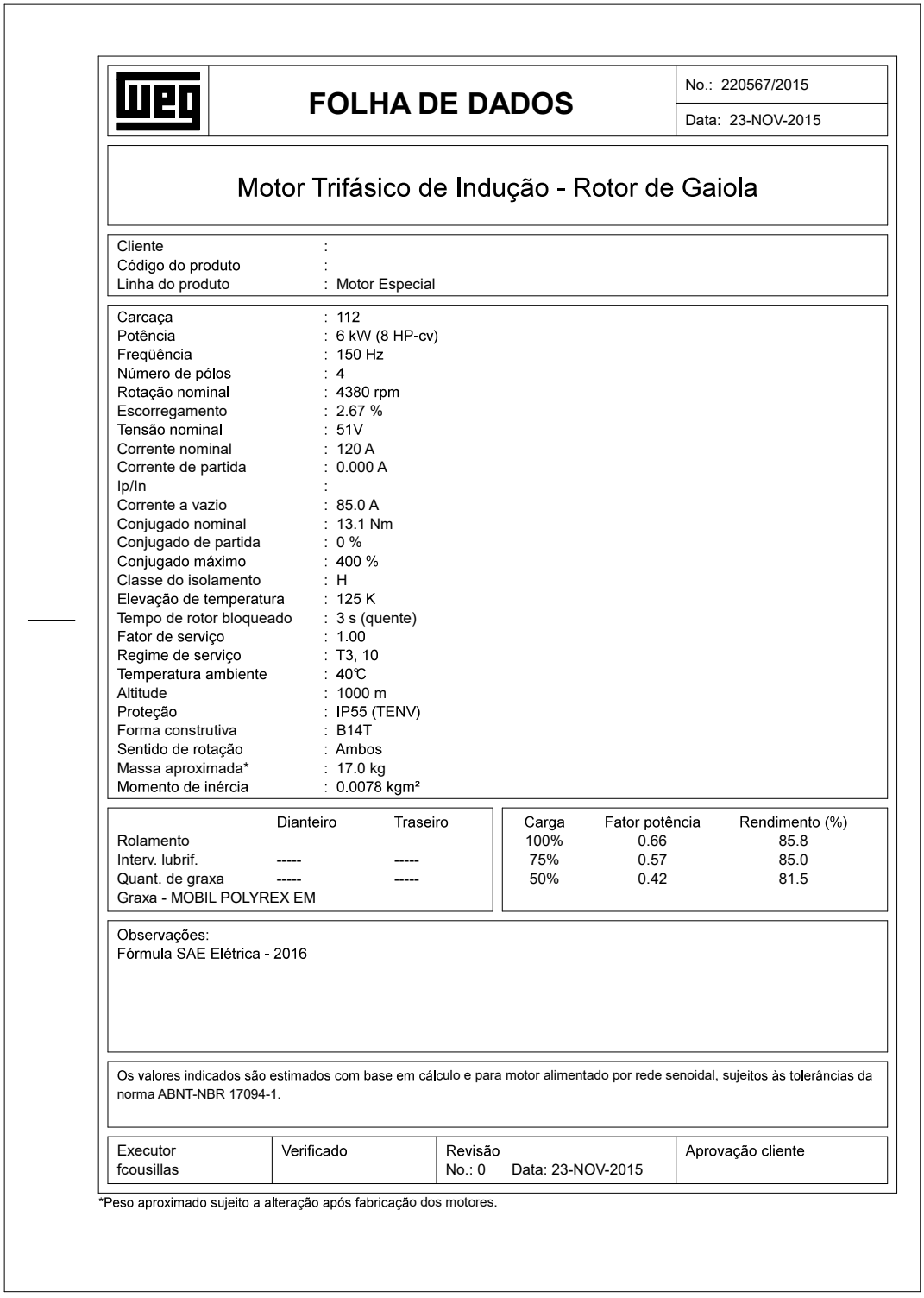

FOLHA DE DADOS

No.: 220567/2015
Data: 23-NOV-2015

Motor Trifásico de Indução - Rotor de Gaiola

Cliente	:	
Código do produto	:	
Linha do produto	:	Motor Especial

Carcaça	:	112
Potência	:	6 kW (8 HP-cv)
Freqüência	:	150 Hz
Número de pólos	:	4
Rotação nominal	:	4380 rpm
Escorregamento	:	2.67 %
Tensão nominal	:	51V
Corrente nominal	:	120 A
Corrente de partida	:	0.000 A
Ip/In	:	
Corrente a vazio	:	85.0 A
Conjugado nominal	:	13.1 Nm
Conjugado de partida	:	0 %
Conjugado máximo	:	400 %
Classe do isolamento	:	H
Elevação de temperatura	:	125 K
Tempo de rotor bloqueado	:	3 s (quente)
Fator de serviço	:	1.00
Regime de serviço	:	T3, 10
Temperatura ambiente	:	40°C
Altitude	:	1000 m
Proteção	:	IP55 (TENV)
Forma construtiva	:	B14T
Sentido de rotação	:	Ambos
Massa aproximada*	:	17.0 kg
Momento de inércia	:	0.0078 kgm²

	Dianteiro	Traseiro
Rolamento		
Interv. lubrif.	-----	-----
Quant. de graxa	-----	-----
Graxa - MOBIL POLYREX EM		

Carga	Fator potência	Rendimento (%)
100%	0.66	85.8
75%	0.57	85.0
50%	0.42	81.5

Observações:
Fórmula SAE Elétrica - 2016

Os valores indicados são estimados com base em cálculo e para motor alimentado por rede senoidal, sujeitos às tolerâncias da norma ABNT-NBR 17094-1.

Executor	Verificado	Revisão	Aprovação cliente
fcousillas		No.: 0 Data: 23-NOV-2015	

*Peso aproximado sujeito a alteração após fabricação dos motores.

Figure 5.3: *Motor data-sheet*

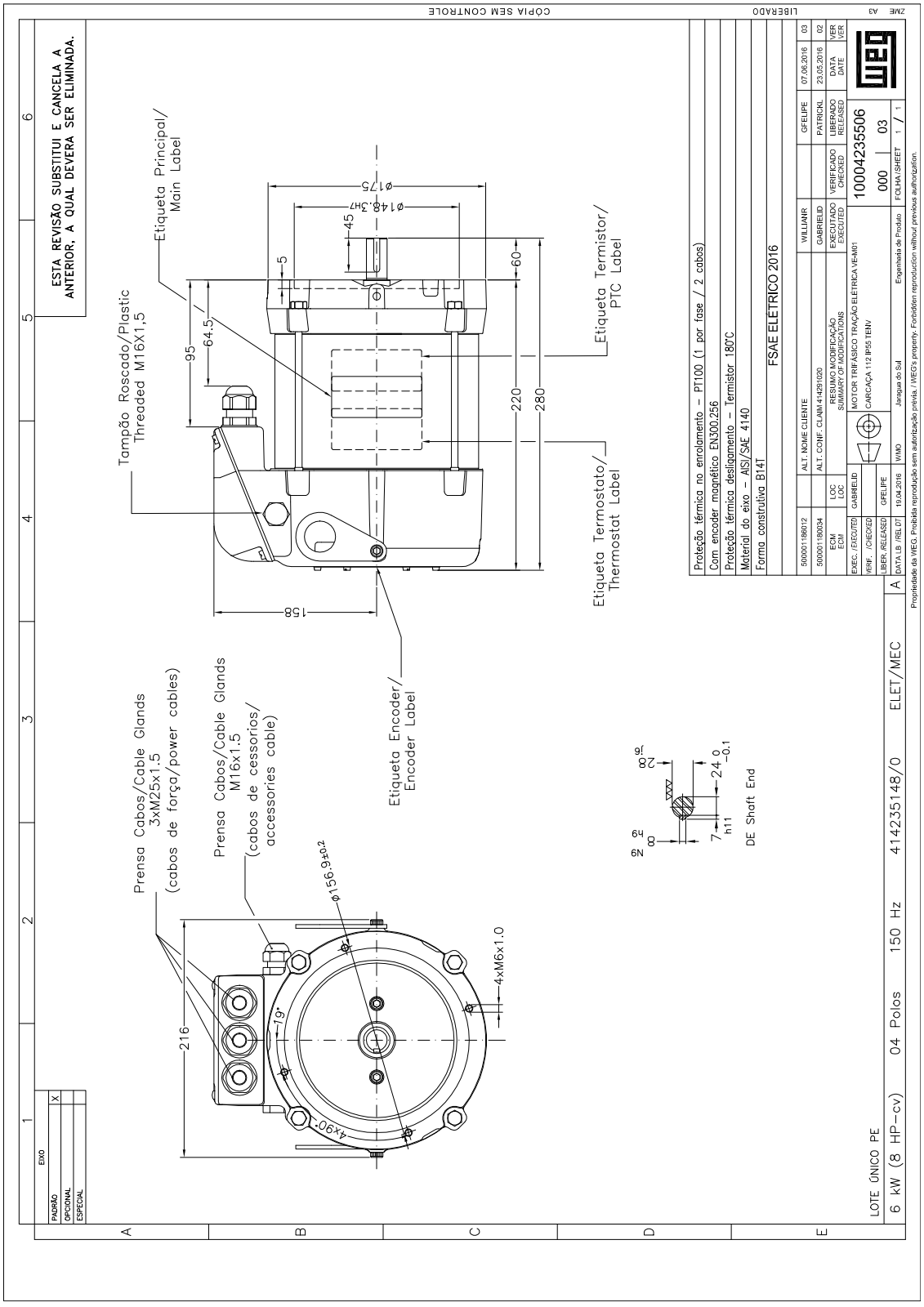

Figure 5.4: *Motor 2D*

List of Figures

Bibliography

[1] World Energy outlook 2018 (02 - 2019).
https://www.iea.org/weo2018/.

[2] World Bank data about transport emissions (02 - 2019).
https://data.worldbank.org/indicator/EN.CO2.TRAN.ZS.

[3] International Energy Agency emission statistics (02 - 2019).
https://www.iea.org/statistics/co2emissions/.

[4] Formula SAE electric regulations (02 - 2019).
https://www.fsaeonline.com/cdsweb/gen/DocumentResources.aspx.

[5] Formula SAE Brazil (02 - 2019).
http://portal.saebrasil.org.br/.

[6] Mehrdad Ehsani, Yimin Gao,Sebastien E. Gay, Ali Emadi.*"Modern Electric,Hybrid Electric, and Fuel Cell Vehicles"*.Chap.(2,4,6,10,11). CRC press.

[7] MATLAB and Simulink Racing Lounge: Vehicle Modeling.
https://it.mathworks.com/matlabcentral/fileexchange/63823-matlab-and-simulink-racing-lounge-vehicle-modeling.

[8] Prof. Pizzigoni Bruno Antonio, Dipartimento di Meccanica, Politecnico di Milano.*"Esercitazioni di dinamica di sistemi aerospaziali"*, 2015-2016.

[9] Prof. Casalegno Andrea, Dipartimento di Energia, Politecnico di Milano.*"Electrochemical energy conversion and storage system"*, 2016-2017.

[10] Prof.Luca Bascetta, Dipartimento di Elettronica, Informazione e Bioingegneria, Politecnico di Milano. *"Esercitazioni di principi di automazione per aerospaziali"*, 2014-2015.

[11] Radhika Kapoor, C. Mallika Parveen. *"Comparative Study on Various KERS"*. Proceedings of the World Congress on Engineering 2013 Vol III, WCE 2013, July 3 - 5, 2013, London, U.K.

[12] Yong Zhang , Xu-Feng Cheng , Chengliang Yin , Si Cheng. *"A Soft-Switching Bidirectional DC-DC Converter for the Battery Super-Capacitor Hybrid Energy Storage System"*. IEEE Transactions on Industrial Electronics (Volume: 65 , Issue: 10 , Oct. 2018).

[13] Peng Shuai, Yales R. De Novaes, Francisco Canales and Ivo Barbi. *"A Non-Insulated Resonant Boost Converter"*. ISEA-Institute for Power Electronics and Electrical Drives, RWTH-Aachen University, Aachen, Germany. ABB Corporate Research, Dattwil, Switzerland. INEP-Power Electronics Institute, UFSC-Federal University of Santa Catarina, Florianopolis, SC, Brazil, 2010.

[14] W.A.Tabisz, M.M.Jovanovic, and F.C.Lee, *"High-frequency multi-resonant converter technology and its applications"* in Proc. International Conference on Power Electronics and Variable Speed Drives, London, England, Jul. 17 - 19, 1990, pp. 1-8.

[15] G. Hua and F.C.Lee, *"An overview of soft-switching techniques for pwm converters"* in Proc. International Conference on Power Electronics and Motion Control, Beijing, China, Jun. 27-30, 1994, pp. 801-808.

[16] M. H.Rashid, *"Power Electronics Handbook"*. Chap.(15) San Diego, San Francisco, New York, Boston, London, Sydney, Tokyo: Acadenic Press, 2001.

[17] Lei Zhang, Zhenpo Wang, Xiaosong Hu, Fengchun Sun, David G. Dorrell.*" A comparative study of equivalent circuit models of ultracapacitors for electric vehicles"*. Journal of Power Sources Volume 274, 15 January 2015, pp. 899-906.

[18] Zhongyue Zou, JunyiCao, Binggang Cao, Wen Chen.*"Evaluation strategy of regenerative braking energy for supercapacitor vehicle"*. ISA Transactions Volume 55, March 2015, Pages 234-240.

[19] Mid-Eum Choi, Jun-Sik Lee, Seung-Woo Seo. *"Real-Time Optimization for Power Management Systems of a Battery/Supercapacitor Hybrid Energy Storage System in Electric Vehicles"*. IEEE transactions on vehicular technology, vol.63, no. 8, october 2014.

[20] F.C.Lee. *"High-frequency quasi-resonant and multi-resonant converter technologies"*. pp.(509-521) in Proc. International Conference on Industrial Electronics, Singapore, Oct. 24?28, 1988.

[21] E. Orietti, P. Mattavelli, G. Spiazzi, C. Adragna, G. Gattavari. *"Two-phase interleaved LLC resonant converter with current-controlled inductor"*.Dept. of Technology and Management

of Industrial Systems - University of Padova. ST Microelectronics. Power Electronics Conference, 2009. COBEP '09. Brazilian.

[22] Je-Hyun Yi, B. H. Cho. *Zero-Voltage-Transition Interleaved Boost Converter With an Auxiliary Coupled Inductor*. IEEE Trans. Power Electron., vol. 32, no. 8, pp. 5917?5930, Aug. 2017.

[23] Ivo Barbi,Fabiana Pottkar de Souza.*"Conversore isolados de alta frequentia com comutação soave"*. Chap.(1,2,3,4,5), Edicao especial, 1999.

[24] Robert W. Erickson, Dragan Maksimovic.*"Fundamentals of Power Electronics"*. Cap(2,5). Second edition. University of Colorado, Bulder Colorado. 2004 Kluwer Academic Publishers.

[25] Med Mohan, Tore M.Underland, William P.Robbins.*"Power electronics: Converters, Applications and Design"*. Chap.(2,9). Second edition, 1995 by John Wiley e Sons.

[26] Yales R. De Novaes.*"Estudo de um snubber para o inversor de tres niveis com neutro grampeado"*. Dissertação do grau de Mestre em Engenharia Elétrica. Universidade Federal de Santa Catarina-UFSC, 2000.

[27] Shuai Pang.*"Investigation of a Non-insulated Resonant Converter for Power Processing of Alternative Energy Sources"*. Institute for Power Electronics and Electrical Drives (ISEA) RWTH-Aachen University, 2009.